Analysis of Common Aminopolycarboxylic Acids in Low Level Radioactive Waste

A thesis submitted to The University of Manchester for the degree of Doctor of Philosophy in the Faculty of Science and Engineering

2019

James A. O'Hanlon

School of Chemistry

Blank page

Contents

Final word count: 48729

Abbreviations

AOP	Advanced oxidation process
BET	Brunauer-Emmett-Teller
BNFL	British Nuclear Fuels Ltd
CFSE	Crystal field stabilisation energy
CSH	Calcium silicate hydrate
DAD	Diode-array detector
DI	Deionised
DTPA	Diethylenetriaminepentaacetic acid
ED3A	Ethylenediaminetriacetic acid
EDDA	Ethylenediaminediacetic acid
EDMA	Ethylenediaminemonoacetic acid
EDTA	Ethylenediaminetetraacetic acid
ESC	Environmental Safety Case
ESI	Electrospray ionisation
GC	Gas chromatography
GCAS	Gram-Charlier A Series
HEDTA	*N*-(2-hydroxyethyl)ethylenediaminetriacetic acid
HIDA	*N*-(2-hydroxyethyl)iminodiacetic acid
HLW	High Level Waste
HPLC	High-performance liquid chromatography
HSAB	Hard-soft acid-base
ICP	Inductively coupled plasma
IDA	Iminodiacetic acid
ILW	Intermediate Level Waste
ISA	Isosaccharinic acid
ISO	International Standards Organisation
LC	Liquid chromatography
LLW	Low Level Waste
LLWR	Low Level Waste Repository Ltd
LMCT	Ligand-metal charge transfer
LOD	Limit of detection
LOQ	Limit of quantification
LSF	Least-squares fitting
MOD	Ministry of Defence
MS	Mass spectrometry

NDA	Nuclear Decomissioning Authority
NTA	Nitrilotriacetic acid
OPC	Ordinary Portland cement
PARAFAC	Parallel factor analysis
PCA	Principal component analysis
PFA	Pulverised fuel ash
P-XRD	Powder X-ray diffraction
RP	Reversed-phase
RSD	Relative standard deviation
TBA-Br	Tetrabutylammonium bromide
TGA	Thermogravimetric analysis
The LLWR	The Low Level Waste Repository
UKAEA	United Kingdom Atomic Energy Authority
UV	Ultraviolet
UV-Vis	Ultraviolet-Visible spectroscopy
VLLW	Very Low Level Waste
WAC	Waste Acceptance Criteria
WAMAC	Waste Monitoring and Compaction Facility
XRD	X-ray diffraction

Abstract

The aminopolycarboxylic acids (APCAs), ethylenediaminetetraacetic acid (EDTA), diethylenetriaminepentaacetic acid (DTPA) and nitrilotriacetic acid (NTA), are used throughout the nuclear industry in the decontamination agents used in the decommissioning process, therefore, are often found in radioactive waste. The Low Level Waste Repository (LLWR) impose limits on the acceptance of wastes containing APCAs because, when present in the waste, the ligands have the potential to solubilise and mobilise contaminant species, making them more available for transport to groundwater and ultimately to the bio-sphere.

A selective and sensitive methodology to detect and quantify these ligands in a range of complex matrices is advantageous in supporting waste acceptance processes and environmental monitoring at the LLWR. Therefore, a reversed-phase high-performance liquid chromatography (HPLC) procedure has been developed and validated; $r^2 > 0.999$, intra/inter-day relative standard deviation ≤ 10%, recovery = 100 ± 3%, limits of detection (LOD) = 0.31, 0.38 and 4.3 mM for Fe(III)-EDTA, Fe(III)-DTPA and Fe(III)-NTA, respectively. Two peak deconvolution methods (parallel factor analysis and least-squares fitting) were applied to resolve overlapping chromatographic peaks of Fe(III)- and Co(III)-EDTA and the performances compared. Application of the method to leachate from sampling locations around the LLWR site found EDTA in four of the six samples tested (0.4 μM < [EDTA] < 1 μM).

A solid-liquid phase extraction technique was optimised for determination of EDTA in samples of incinerated EDTA-contaminated ion-exchange resin (ion-exchange resins derived from operation and maintenance of the nuclear submarine fleet and intended for disposal at the LLWR). No EDTA was detected in incineration residue > LOD concentration (0.32 mg kg^{-1}).

The HPLC method was applied to γ-irradiated samples of APCA species to quantify the degradation and identify potential radiolysis products. It was found that G(-EDTA) = 2.5 < G(-Fe(III)-EDTA) = 3.2 < G(-Fe(III)-DTPA) = 5.4, and ethylenediaminetriacetic acid is thought to be a significant degradation product formed in the radiolysis of Fe(III)-EDTA.

Declaration

Unless otherwise stated, all work presented in this thesis was carried out by James A. O'Hanlon under the supervision of Prof. Melissa A. Denecke at The University of Manchester between July 2016 and December 2019. No portion of the work referred to in this thesis has been submitted towards the application of another qualification or degree at this or any other university or institute of learning.

Copyright Statement

Acknowledgments

I would like to thank all of my colleagues at The University of Manchester for their guidance and friendship throughout my time there. A special thank you to Melissa for putting me on this track (and keeping me on it!), and to Maria, for her unwavering support.

Chapter One: Introduction

Scope

Much of the work undertaken in this project has been tailored to suit the requirements of the industrial funding organisation (Low Level Waste Repository Ltd (LLWR)). This introductory chapter will provide an overview of the organisation to illustrate how the research presented in the remainder of the thesis is relevant.

The Low Level Waste Repository (the LLWR) is the United Kingdom's (UK) national facility for the storage and disposal of low level radioactive waste (LLW). Section 1.1 and 1.2 of this chapter describes what constitutes LLW and how it might be generated, before describing a brief history of disposal operations at the site and some of the legal framework into which the research sits.

Aminopolycarboxylic acids (APCAs) often arise in nuclear waste because of their frequent use in the decontamination agents used in the decommissioning process. They are problematic for LLWR because they have the potential to solubilise and mobilise radionuclides in the waste, making them more susceptible to transport in water out of the repository and into the environment. Section 1.3 provides an overview of the APCAs and their chemistry; Section 1.4 contains a more detailed discussion of their impact on radioactive waste and the steps that can be taken to mitigate it.

The chemical fate of the APCAs in the repository environment plays a key role in determining their overall impact; e.g. the risk associated with radionuclide mobilisation is dependent on the APCA-complex remaining intact for long enough for transportation out of the repository to occur. Section 1.5 reviews some of the principal degradation pathways available to the APCAs and the degradation products that might form.

The main aim of this research project is to develop and implement an APCA detection method on various samples of relevance to the LLWR. Section 1.6 provides a review of the existing relevant literature on the topic of APCA detection technologies. Finally,

Section 1.7 provides a short breakdown of the specific aims of this project with some of the criteria for success.

The results chapters of this thesis are presented in the form of a manuscript for submission to a journal, meaning they each have a self-contained introduction and concise literature review where the reader can find further information regarding each of the relevant topics.

1.1 Radioactive Waste

Radioactive waste is defined as any item or substance that has no further use and that contains radioactivity above certain levels defined in legislation. In the United Kingdom (UK), radioactive waste originates from a range of industries; for example, nuclear power generation, nuclear fuel reprocessing, defence related applications, medical diagnoses/treatments and research activities.[1-4]

Waste can either be contaminated or activated by radioactivity; contamination generally affects the surfaces of equipment, tools and facilities that come into contact with radioactive substances during their operational use (e.g. protective clothing, pipes and filters, needles and syringes), whereas materials can only become activated in the close proximity of a strong neutron emitter (e.g. graphite and steel from a reactor core).

Waste producers are required to characterise the chemical, physical and radiological properties of the materials they generate, which is achieved by detailed recordkeeping of all of on-site activities, stand-off measurements of the types of radiation emitted from the waste, and laboratory analyses of material collected by intrusive sampling. Characterisation data is combined with the best knowledge of the existing legacy of waste and predictions of future arisings to deliver the triennial UK Radioactive Waste and Materials Inventory (UK Inventory), the most recent of which was published in 2016.[1,3]

Solid radioactive waste in the UK Inventory is broadly split into three categories: low, intermediate and high level wastes. The classifications are dependent on the type and

quantity of radioactivity the waste contains, and whether the radioactive decay is likely to generate a significant amount of heat.

High Level Waste (HLW) is the residue produced during spent nuclear fuel reprocessing and typically arises in the form of a highly radioactive acidic liquid. HLW is converted to a stable solid by vitrification to be stored in purpose-built, highly-shielded facilities for a minimum of 50 years to allow the waste to radioactively decay and cool.[1] No long-term disposal route is currently in place for the vitrified HLW, but the preferred option is deep geological disposal, where packaged waste is sealed off in an engineered repository hundreds of metres underground.[4] HLW is distinguished by the significant quantity of decay heat it self-generates, which must be considered when designing plans for its long-term storage and disposal.

Intermediate Level Waste (ILW) can constitute a wide variety of waste forms; any item that may become radiologically contaminated or activated during operation, maintenance or dismantlement of nuclear related facilities. Major components of ILW are reactor core graphite, other metallic reactor parts and sludges produced in the treatment of liquid effluents. The defining characteristics of ILW are that its specific activity exceeds the upper-boundary of a LLW classification, but internal heat generation does not need to be factored into plans for its storage and disposal.

1.1.1 Low Level Radioactive Waste

LLW is arbitrarily defined as having a radioactive content that does not exceed four gigabecquerels per tonne (GBq t^{-1}) of alpha or 12 GBq t^{-1} of beta/gamma activity. It is less hazardous than higher activity waste and some types of non-radiological hazardous wastes.[1-4]

LLW represents a broad category that spans over a range of five orders of magnitude of specific activity; Very Low Level Waste (VLLW) is a sub-category of LLW, describing waste that is very lightly contaminated with radioactivity. Small amounts of VLLW, often derived from hospitals and universities, are often disposed alongside municipal, commercial or industrial waste. However, the bulk volume of VLLW comes from the decommissioning of nuclear sites (e.g. 90% of the VLLW in the current UK Inventory is

accounted for by lightly contaminated concrete, soil and rubble) and can be disposed of at appropriately permitted landfill facilities.[1] Reported volumes show that roughly 73% of all low activity waste falls into the VLLW sub-category or is mixed LLW/VLLW.[3]

The majority of UK LLW (not classified as VLLW) also arises at nuclear sites from activities such as: fuel fabrication and uranium enrichment, nuclear power generation, spent fuel reprocessing, decommissioning, nuclear energy research and development, Ministry of Defence (MOD) activities, manufacture of radioactive medical products and waste treatment facilities. LLW can be sub-divided into operational or decommissioning related material; operational LLW comes from routine monitoring and maintenance activities and includes protective equipment and redundant plant parts, whereas, decommissioning LLW mostly comprises building rubble and soil.

Table 1. Relationship between the total reported volume of waste and its radioactivity in the UK Inventory by 2150.[3]

Waste Type	Total Volume / m^3	Total Volume / %	Radioactivity / TBq	Radioactivity / %
HLW	1,150	0.03	3,200,000	84.4
ILW	295,000	6.55	590,000	15.6
LLW	1,350,000	30.0	93	0.002
VLLW	2,860,000	63.5	14	0.0003
Total	4,506,150		3,790,107	

In 2150, over 90% of the total volume of radioactive wastes is projected to fall into the LLW (or VLLW) classification, but this is to account for less than 0.003% of the total radioactivity (Table 1).[3] Roughly 96% of all projected radioactive waste already exists, but mostly still form part of current nuclear facilities.[1] Many of the UK's nuclear facilities are due to be decommissioned over the course of the next century having reached the end of their operational lifetimes. Approximately 84% of all forecasted future arisings of LLW are expected to originate from the decommissioning and site remediation of existing reactors and other nuclear facilities. Such activities are expected to lead to a general increase in the total annual arisings of LLW between 2040 and 2100, and a dramatic increase in the annual arisings of VLLW, shifting from a reported volume of roughly 10000 m^3 y^{-1} (present) to over 50000 m^3 y^{-1} by 2100.[3]

The large-scale decommissioning and environmental restoration required to mitigate the impact of the UK's nuclear legacy represents a significant challenge to the Nuclear Decommissioning Authority (NDA), who act on behalf of the UK Government. It was recognised that previous policy outlined for LLW management was not developed to take account of the scale of the task, precipitating the need for an optimised strategy based on three themes: the application of the Waste Hierarchy[a], to optimise the capacity and capabilities of existing LLW management assets, and to identify and implement new fit-for-purpose waste management routes.[4] Implementation of the revised strategy has had a direct impact on the management and operations at the LLWR.[4]

1.2 The Low Level Waste Repository

The LLWR is the UK's principal facility for the storage and disposal of solid LLW. The site is located on the coastal plain of West Cumbria, roughly 0.5 km from the Irish Sea coast, on the outskirts of the village of Drigg (Figure 1). The LLWR is about 8 km south of the Sellafield site and the two facilities are connected by the Carlisle to Barrow-in-Furness railway line.[5-10]

Figure 1. The LLWR site location.[11,12]

[a] The Waste Hierarchy was first introduced in 1975 in an EU directive on non-radiological waste management policy. Implementation of the Waste Hierarchy is mandated by policy and environmental regulation. The hierarchy dictates that a strategic preference should be given to waste management options in the following order: waste prevention, minimisation, reuse, recycling and, finally, disposal.

The site was originally developed as a Royal Ordnance Factory in World War II, producing over 360 tonnes of TNT per week at maximum output. The site became a nuclear facility in the late 1950s, when ownership was passed to the UK Atomic Energy Authority (UKAEA), and radioactive waste disposals began under an authorisation granted in 1959.[6] Initial disposal operations involved direct tipping (tumble-tipping) of radioactive wastes into clay-lined trenches (Figure 2). The alpha and beta activities of consigned wastes were not to exceed a daily average of 20 or 60 mCi yd^{-3}, respectively (approximately 0.97 GBq m^{-3} and 2.9 GBq m^{-3}).[5,6]

Figure 2. Operation of the LLWR trench disposal system in 1961.[6]

Responsibility for the site was later passed to British Nuclear Fuels Limited (BNFL) (1971), who oversaw considerable changes to waste management practices following a series of revised authorisations. For example, a major upgrade programme was commenced in 1987, in parallel with in-depth review by the authorising departments, leading to a host of administrative and practical changes to waste management. In 1988, the practice of tumble-tipping into trenches started to be phased out in favour of vault disposal. Trench disposals were completed in 1995 and an interim cap was finalised to protect the filled trenches until final closure of the entire repository.[6]

Capping of the trenches coincided with the opening of two new facilities designed for the production of an optimised wasteform for vault disposal: the Waste Monitoring and Compaction Facility (WAMAC) at Sellafield and the on-site LLWR Grouting Facility. Both are still operational today. Incoming waste is highly compacted at WAMAC to

produce ‘pucks’ that are loaded into half-height International Standards Organisation (ISO) shipping containers and transferred to LLWR to be in-filled with grout before final emplacement in the concrete-lined engineered vaults.

LLWR Ltd was formed in 2007 to operate the site on behalf of the NDA, this remains to be the ownership status of the LLWR. Management are tasked with ensuring optimal usage of the remaining capacity of the repository and doing so in a way that causes as little environmental impact as is reasonably possible.

Under current plans, the LLWR is expected to operate until 2130. The repository will be permanently sealed after instalment of the final cap. The cap will be a highly engineered multi-layered system designed to provide suitable long-term landform and physical cover and low-permeability surface barrier to prevent human and natural intrusion.[8] Once capped, the site will enter a Period of Authorisation, during which it will remain under active control (e.g. perimeter maintained, pumped drainage system) for a further 100 years.

1.2.1 Trenches

Between 1959 and 1995, radioactive waste disposed to LLWR was tumble-tipped into a series of seven purpose-built trenches. The dimensions range from 5-8 m in depth, 10-20 m wide, and 480-718 m long.[6] Each trench was generally excavated into a low-permeability clay-rich layer, and in regions of the site where this was not naturally available, the trench base was augmented with the addition of bentonite.[b]

Since the phasing out of trench disposal operations began in 1988, remedial engineering work has been carried out to limit the environmental impact of the legacy waste contained in the trenches. This includes the installation of an interim cap with perimeter drains, the Trench Cut-off Wall and a leachate drainage system; all of which are designed to limit and control the flow of water through the disposed wastes.

[b] Bentonite clay swells on contact with water to provide a self-sealing, low-permeability barrier. It is often used to line the base of landfill sites to prevent the migration of leachate.

The purpose of the cap, a 1:25 graded earth mound of mostly sandy-clay with an average thickness of 3.2 m and containing a low-density polyethylene geomembrane, is to limit rainwater infiltration to the waste, which prevents saturation and limits the amount of leachate generated. The low-permeability Trench Cut-off Wall surrounds the northern and eastern edges of the repository site. It is roughly 800 m in length and taken to a depth at least 2 m below the depth of the clay-lined trench bases.[8] Its purpose is to limit the lateral migration of meteoric water through the region of the site containing the trenches and vaults from the surrounding land. The leachate drainage system is designed to collect and discharge leachate into the sea via a holding tank. The leachate is routinely assessed for its volume, and radiological and non-radiological chemical composition.

Approximately 800,000 m^3 of waste was disposed to the trenches over the course of their operational lifetime, and over 75% of that waste was derived from the Sellafield or Springfields nuclear sites. Ferrous metals and stainless-steel account for over 26% of the disposed volume, rubble and soil contribute 24% and cellulose-based materials comprise roughly 18% of the trench inventory (Figure 3).[6] In terms of activity, the most abundant radionuclide in the trenches is tritium (total inventory ≈ 500 TBq), most of which is localised to a small area of one specific trench. The trenches also contain a large portion of the total LLWR inventory of ^{14}C, ^{129}I, ^{226}Ra, ^{232}Th, ^{234}U and ^{238}U.[6]

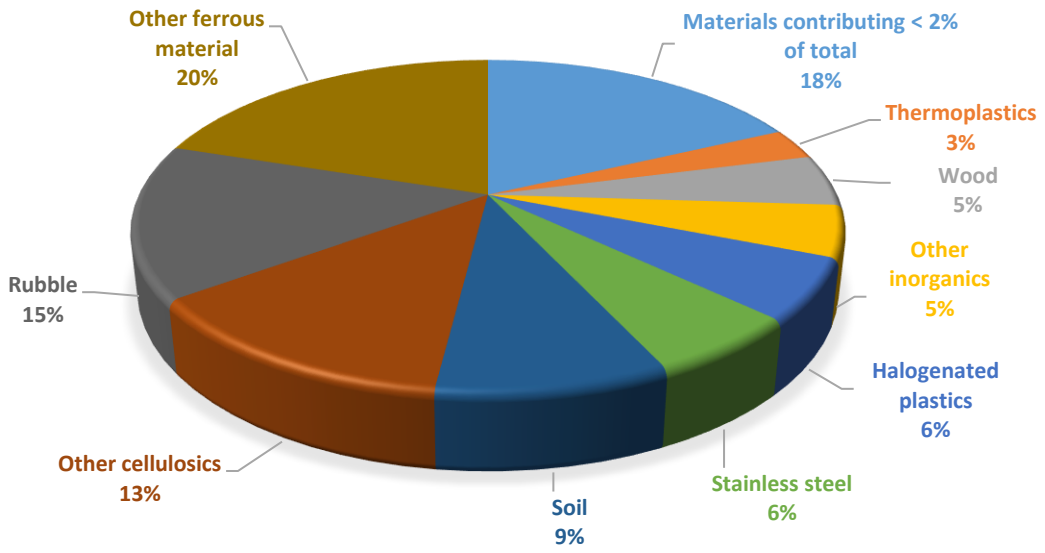

Figure 3. Inventory of waste disposed to LLWR trenches.[6]

Trench waste contains a relatively high quantity of biodegradable material, and was not compacted prior to disposal, meaning that the potential for void space and differential rates of settlement is high, which can pose a risk to the integrity of the final repository cap. Some degree of chemical degradation and physical settlement is expected 600 years into the future, far beyond the construction of the final cap in just over 100 years' time.[9] Processes of compaction and evolution are expected to influence the flow pathways and hydraulic conductivity of the waste, but the peak rates of chemo-/bio-degradation and corrosion are expected to have passed, leaving the performance of the final cap untroubled.

Degradation of cellulosic material and the corrosion of waste metal are expected to lead to reducing and mildly acidic conditions in the trenches, producing a fermentative and methanogenic environment, once the oxygen present prior to the addition of the interim cap has been consumed. Evidence for the development of such conditions has already been observed, including detection of significant methane gas generation by probes dispersed across the site of the trenches (in places, methane content > 25% of total evolved gas).[9]

Biogeochemical evolution is dynamic, and the extent and longevity of these conditions will depend on a complex set of interactions between regional factors such as the types of waste material, the rate of groundwater flow and the microbiological flora. Biogeochemical modelling is used to simulate the possible trench evolution scenarios and the influence that they might have over radionuclide or non-radiological contaminant release.

For example, uranium and technetium can exist in several oxidation states which are determined by environmental factors such as pH and redox potential (Eh). Lower oxidation state U(IV) and Tc(IV) have lower solubility in water than U(VI) and Tc(VII). Under reducing conditions, and in the pH range of interest (pH 5 to pH 11), Tc(IV) and U(IV) speciation is dominated by formation of amorphous phases of TcO_2 and UO_2, respectively.[9]

Biogeochemical modelling predicts that oxidising conditions will eventually prevail in the trench environment leading to stabilisation Tc(VII) (likely to exist as the poorly-

sorbing pertechnetate ($[TcO_4]^-$) aqueous species) and U(VI) (expected to form $UO_3 \cdot 2H_2O$ or $CaUO_4$).[9] This will impact the radionuclides' rate of dissolution, diffusive leaching, precipitation, sorption, and uptake by colloidal particles – all of which can contribute to their rate of release to the wider geo/bio-sphere.

However, the anticipated timescale for the re-oxidation of trenches varies from roughly 1000 to > 5000 years, depending on the specific region. It is expected that the facility will have been eroded by the sea after that amount of time.[9]

1.2.2 Vaults

In the mid-1980s, BNFL sought to identify a disposal system to supersede the trenches that would improve management practices, enhance containment and mitigate the visual impact of operations. This led to the development of the engineered concrete vault disposal concept.[8]

The first vault (Vault 8, following from Trenches 1-7) was commissioned in 1988. It was designed and constructed according to best practices of the time. The base slab (250-300 mm thick conventional reinforced concrete) was founded on a minimum of 1 m of low permeability clay. 350 mm thick reinforced concrete walls line the perimeter to the north, west and south, whilst a secant pile wall provides structural support along the eastern edge. The walls were not considered to provide any barrier to flow in the hydrogeological modelling of Vault 8; the main emphasis of the design was on operational aspects (e.g. optimisation of waste containerisation/conditioning versus maximisation of capacity) rather than groundwater and leachate control.[8,10]

Vault 9 was constructed between 2008 and 2010 after an extensive planning period and to a rigorous specification, designed to ensure that the new vault was compliant with a long list of UK regulations and in line with the best international practice. The secant pile wall of Vault 8 is continued southwards, to line the eastern edge of Vault 9 and to provide structural support to the retained material in the adjacent trench. The walls and base slab of Vault 9 both feature highly engineered layered systems that are designed to prevent the uncontrolled release of leachate and the ingress of groundwater. The basal liner system includes a 350 mm thick reinforced concrete slab,

on top of two 500 mm layers of bentonite enriched soil (BES), both lined with a high-density polyethylene (HDPE) geomembrane. The BES and HDPE hydraulic barriers extend up the central lining of the double-leaf 350 mm thick reinforced concrete walls, in continuity with the basal liner. A 1:200 fall is built into the base slab to ensure leachate flows in the direction of two manholes, which currently lead to a pump chamber system, but will revert to a passive drainage system once the active control period of the LLWR is over.[8,10]

As part of the update to the disposal system undertaken in the move away from tumble-tipping into the trenches, development of a new wasteform was targeted. The design outcome was that waste disposed of to the LLWR was to be grouted within steel ISO shipping containers and then neatly stacked inside the vaults. The outline of the containerised disposal model continues today, largely unchanged. The approach offers multiple benefits including enhanced containment of radionuclides, which is achieved by reducing the potential for interaction between wastes and waters passing through the facility, and a reduction in the residual void space in the repository, which reduces the potential for uneven settlement of the final cap (Figure 4).

According to the type of waste material, high-force compaction is applied to raw waste that is suitable. This is mostly undertaken at the WAMAC facility on the Sellafield site. The process results in compacted pucks which are then emplaced within half-height mild-steel ISO shipping containers along with other non-compactable wastes prior to grouting.

The cementitious grout used to backfill the containers is currently comprised of pulverised fuel ash (PFA) and ordinary Portland cement (OPC). It is specially formulated to ensure sufficient fluidity to fill irregularly distributed void space. The low viscosity also provides efficient flow properties during filling and sufficiently fast settlement to limit the need for temporary buffer storage prior to final emplacement. Chemical and physical properties of the grout formulation also contribute to the maintenance of a local environment that is conducive to radionuclide containment.[8,9] For example, the grout offers a physical substrate for radionuclide sorption; CO_2 can react directly with the hydration products of the cementitious material (e.g. $Ca(OH)_2$) to form carbonates

($CaCO_3$) to stem the migration of ^{14}C; and the grout buffers the pH of the porewater to pH 11, which promotes the formation of insoluble metal precipitates.

Figure 4 shows the LLWR site layout; i) Trenches 1-7 are in the trapezoid shaped area beneath the label towards the northern end of the site (only visible as greenery because of the interim cap); ii) the perimeter of Vault 8 can be roughly judged by the shape of the orange block (tops of ISO shipping containers) at the top-left of the trenches; iii) the grey concrete-lined base of the unfilled Vault 9 is visible; iv) the LLWR Facility is just south of the trenches; v) the railway runs along the eastern perimeter of the site; and, vi) the site entrance and offices are in the south-eastern corner.

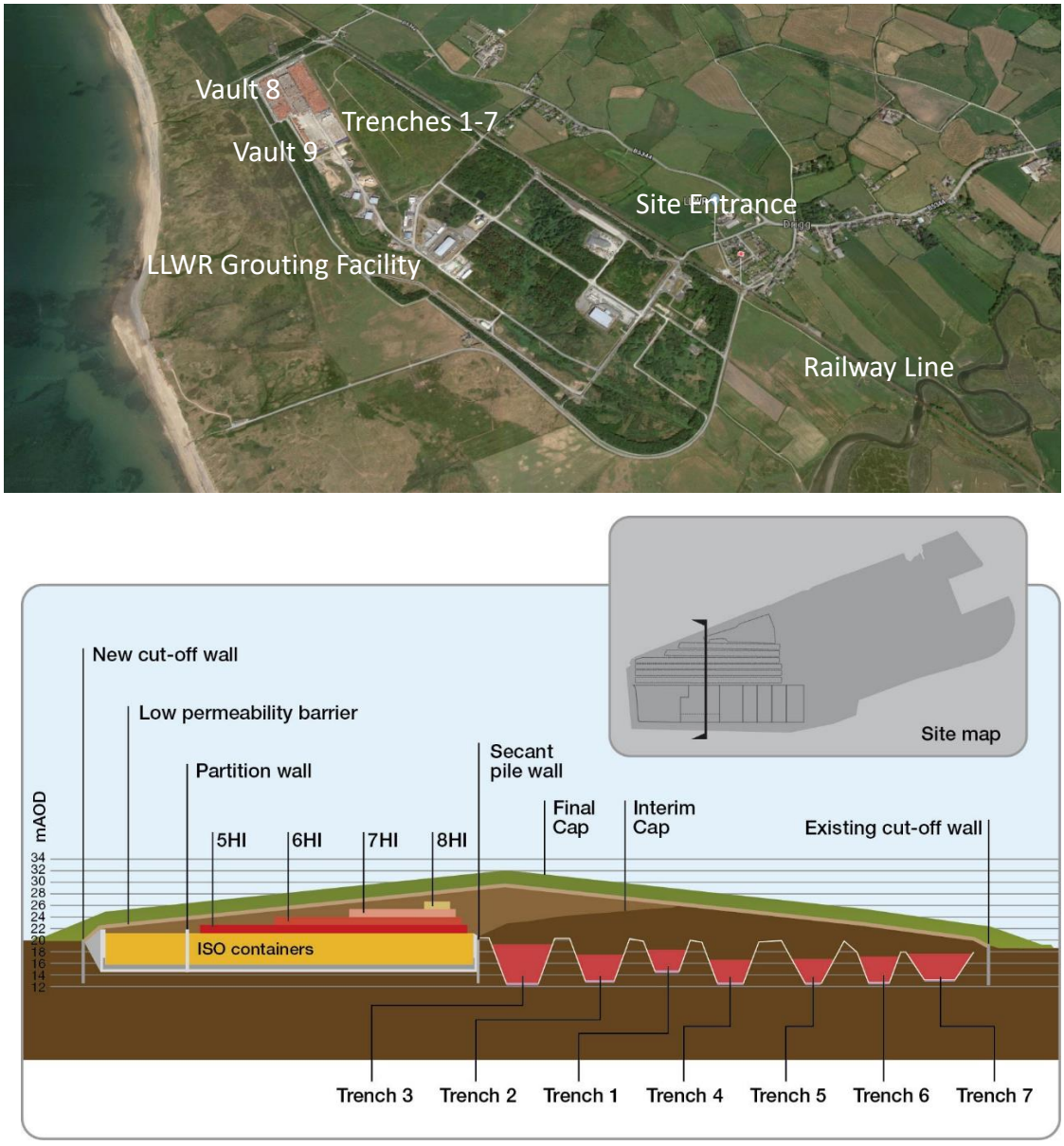

Figure 4. Top: LLWR site layout[12]; bottom: proposed design of final repository cap.[8]

A more detailed inventory of the waste disposed to the vaults has been maintained by better recordkeeping since the disposal practice was upgraded. The profile of the types of waste disposed to Vault 8 is relatively similar to that determined for the trench disposals, with cellulosic (27%), ferrous (21%) and rubble, soil and cement (19%) material making up a significant portion (Figure 5). Of the key radionuclides disposed of to LLWR, Vault 8 only contributes substantially to the facility inventory for ^{36}Cl (39%), ^{241}Am (22%) and ^{99}Tc (18%).[6]

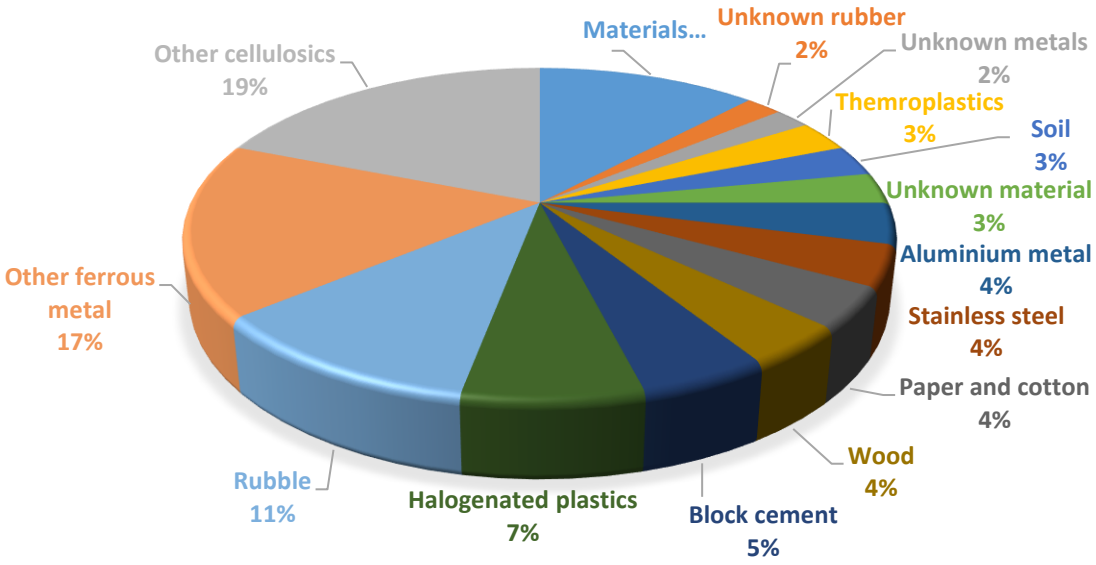

Figure 5. Inventory of wastes disposed to LLWR Vault 8 as of 31st March 2008 (unlabelled blue segment corresponds with 'Materials contributing < 2% of total: 12%').[6]

The physical evolution of the vault wasteform - the waste, cement grout and the steel container - will influence the overall structural stability and hydrogeological evolution of the disposal vault. Corrosion of the ISO containers is expected to be slow under the anaerobic conditions that develop in the repository after the final cap is added (1 μm y^{-1}). This is expected to maintain the integrity of the vault monolith for between several hundred and one thousand years.[9]

Primary controls over the physical evolution of the vault waste and cement grout are metallic corrosion of waste and degradation of organic or cellulosic materials. Corrosive processes are expected to promote waste expansion which is offset by the void space created by the degradation of the organic materials. A degree of waste compaction is expected over the course of time, though, the impact on vault integrity will be minimal given that wastes are highly compacted prior to disposal.

The chemical evolution of the vault wasteform is dominated by the effects of the cementitious grout, which provides a buffering effect through dissolution of reactive cement phases. Experimental studies have determined the LLWR grout to buffer to pH 11, and modelling studies indicate that alkaline conditions will prevail for the next 10,000 years, although, localised weakly acidic conditions may develop in the waste pucks.[9]

Biodegradation of organic material will produce CO_2.[9] A portion of the CO_2 generated in the vaults is expected to react with the calcium silicate hydrate (CSH) phases of the cement, resulting in the precipitation of calcite ($CaCO_3$). Many variables associated with the vault environment affect this process, such as the heterogeneity of the waste (localised areas of concentrated cellulosic material increases CO_2 generation), and the availability of gas release pathways and mobile water pathways. $CaCO_3$ precipitation provides a layer of armouring to the grout, which can affect the porosity, preferential flow pathways, pH buffering capacity and radionuclide surface adsorption, and a mechanism for carbon capture, which can help to limit the release of ^{14}C to the environment.

Methanogenic and fermentative Eh conditions are expected to develop in the vaults, as in the trenches. The high pH conditions, reducing environment and surface chemistry of the grout are expected to promote low solubility and mobility of radionuclides and other non-radiological contaminant to limit their release to the geo/bio-sphere.

1.2.3 The Environmental Safety Case

In roughly ten year cycles, LLWR submit a document called the Environmental Safety Case (ESC) to the Environment Agency.[5-10] The Environment Agency define an ESC as "a set of claims concerning the environmental safety of disposals of solid radioactive waste, substantiated by a structured collection of arguments and evidence." The provision of the ESC fulfils a specific requirement of the Permit that needs to be periodically granted for continued operation at the site. The ESC must contain evidence that the impacts of the LLWR on people and the environment are consistent

with regulatory guidance levels.[13] The last submission was in 2011 (2011 ESC), at which point the case was that[5]:

- LLWR have worked within a sound management framework and firm safety culture, while engaging in dialogue with stakeholders.
- LLWR have characterised and established a sufficient understanding of the site and facility, and their evolution, relevant to its environmental safety.
- On which basis, LLWR have carried out a comprehensive evaluation of options to arrive at an optimised site development plan.
- LLWR have assessed the environmental safety of the site development plan, showing that impacts are appropriately low and consistent with regulatory guidance. Using their assessments, LLWR have determined the radiological capacity of the facility and conditions under which waste may be safely accepted and disposed.

The 2011 ESC report has a tiered structure; the Level 1 Main Report summarises the main findings from all of the various topics covered in more detail in the Level 2 reports, which include the hydrogeology, waste characterisation, engineering of the vault design and potential radiological impacts.[5-10] A further 100 underpinning reports make up the Level 3 documentation. Over 80 technical experts were involved in the production of the 2011 ESC, and the Level 1 and 2 reports are made up of over 2000 pages in 17 reports.

Evidence presented in the ESC underpins the Waste Acceptance Criteria (WAC).[15] The WAC is provided by LLWR to waste consignors for them to ensure that their consignments are compliant with the Permit granted by the Environment Agency; the physical, chemical, radiological, packaging and transport requirements are all detailed in the document. The WAC is periodically updated to encapsulate the most recent amendments to the Permit, which usually run in tandem with advancements in the understanding of the risk associated with certain wastes and waste management practices.

For example, the environmental permit of LLWR originally prohibited the acceptance of wastes containing organic complexing agents (complexants); WAC Version 3.0 (April 2012) states that 'Waste shall not contain chemical complexing or chelating agents'.[16] However, evidence from geochemical modelling studies collected after the submission of the 2011 ESC indicated that complexants could be safely disposed in waste, providing certain control measures were in place.[17-20] In 2015, a successful application was made to the Environment Agency to vary the permit 'to remove current restrictions on the disposal of any complexing or chelating agents', alongside other improvements.[14]

Subsequently, WAC Version 5.0 (July 2016) was published containing a categorised approach to chemical complexants in the waste; Category 1 complexants include carboxylic acids (e.g. citric acid, picolinic acid, oxalic acid and formic acid) and inorganic compounds (e.g. tri-polyphosphates), and Category 2 species, which are the APCAs, ethylenediaminetetraacetic acid (EDTA), diethylenetriaminepentaacetic acid (DTPA) and nitrilotriacetic acid (NTA). Category 1 complexants are controlled but do not require a specific allocation, whereas Category 2 APCAs are only accepted for disposal subject to there being sufficient capacity available, and wastes containing APCAs are assessed to ensure that the usage of APCA capacity is not grossly disproportionate to the volume of the waste. A total site-wide capacity of 1000 kg for all Category 2 materials is maintained.[15]

1.3 Aminopolycarboxylic Acids

The APCAs are a class of chemical compound that contain one or more nitrogen atoms connected through carbon atoms to two or more carboxyl groups. The carboxyl groups can lose their acidic proton to form negatively charged aminopolycarboxlates which are widely used as complexants for a range of applications.

1.3.1 Structure

The parent structure of the APCA family is the proteinogenic amino acid glycine (Figure 6A), in which a primary amino group ($-NH_2$) is bonded to a carboxyl group ($-CO_2H$) via a single methyl-bridging unit ($-CH_2-$). Substitution of a hydrogen atom of the amino

group with an identical carboxyl R-group gives rise to a secondary amine called iminodiacetic acid (IDA) (Figure 6B). Further substitution to the tertiary amine gives NTA (Figure 6C); both IDA and NTA are APCAs.

Glycine and IDA units can be linked to obtain larger APCA molecules. For example, EDTA contains two IDA units linked between their tertiary amino groups by an ethyl-bridge (-CH_2-CH_2-) (Figure 6D). Similarly, DTPA links two IDA units to a central glycine unit via two ethyl-bridges that connect the three tertiary amino groups (Figure 6E). The 'ethylene-' and 'diethylene-' found in the common pre-IUPAC names of EDTA and DTPA refer to the doubly-bonded ethylene precursor used in the syntheses.

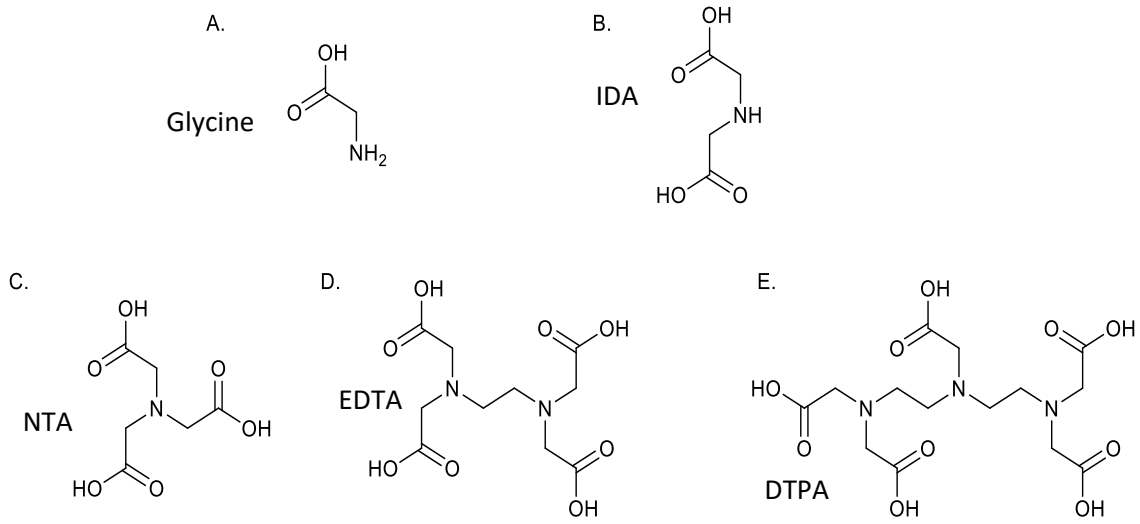

Figure 6. Chemical structures of A) glycine, B) IDA), C) NTA, D) EDTA, and E) DTPA.

1.3.2 Chemistry

The chemistry of the APCAs is dominated by their ability to form stable complexes with a range of metals. The parent molecule, glycine, forms a bi-dentate ligand when the carboxyl group is deprotonated to form glycinate, allowing it to bind to a metal centre through donation of its nitrogen lone pair and mono-dentate coordination of the carboxylate anion. More of these bonding modes are available as larger APCA structures contain greater numbers of bridging nitrogen atoms and carboxyl groups. Therefore, larger APCAs generally have greater denticity; for example, IDA, NTA, EDTA and DTPA are tri-, tetra-, hexa- (Figure 7) and octa-dentate, respectively.

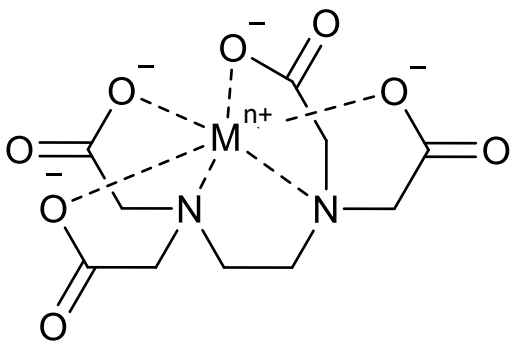

Figure 7. The hexa-dentate chemical bonding of M-EDTA complex (M = metal ion).

Generally, increasing denticity is linked to the formation of more stable metal ion complexes, as the chelate effect is stronger. Entropic and enthalpic factors contribute to the chelate effect, which refers to the enhanced thermodynamic stability of complexes of multidentate chelating ligands over that of similar non-chelating ligands. Other factors that affect metal-APCA coordination complex stability include sterics and ligand geometry (which are related to the ionic radius of the metal, which is influenced by its oxidation state), and the temperature, ionic strength and pH environment.

By definition, APCAs are amphoteric, polyprotic acids. The protonation state and relative charge of the ligand can be altered quite dramatically on going from one end of the pH scale to the other. For example, EDTA has six protonation sites which give rise to six ionic species (H_6EDTA^{2+}, H_5EDTA^{+}, H_4EDTA, H_3EDTA^{-}, H_2EDTA^{2-}, $HEDTA^{3-}$, $EDTA^{4-}$).[21] $EDTA^{4-}$ is the dominant species at high pH because deprotonation of all four carboxyl groups is favoured. At low pH, each nitrogen atom can be protonated to create an overall 2+ positive charge. The pH environment is a significant control over the solubility of the ligands, and the number of binding sites that are available for metal ion complexation.

The stability of a complex in solution is quantified by an equilibrium constant of product formation (β). β is similar to a value of K_{eq}, but can be used to encompass stepwise or cumulative constants; for example, if K_1 represents the rate of formation of the first step of a stepwise reaction (e.g. 1:2 metal-ligand complexation) and K_2 represents the second step, $K_1 \times K_2 = \beta$. The simplified equation for β is shown (Equation 1); in aqueous solution, the concentration of H_2O is effectively constant.

$$M^{n+} + xL \rightleftharpoons ML_x^{n+} \qquad \beta_x = \frac{[ML_x^{n+}]}{[M^{n+}][L]^x}$$

Equation 1. Left) generalised chemical equation for metal-ligand complexation, right) simplified equation to calculate the β stability constant of metal-ligand complexation.

Table 2 shows a selection of $\log\beta_{ML}$ stability constants for APCA-metal complexation. EDTA and DTPA only coordinate metal ions in a 1:1 ratio (ML), however, it is possible for 2:1 NTA-metal complexes to form (ML_2).[22]

Table 2. Logβ stability constants for a range of metal ion complexes of NTA, EDTA and DTPA. [23]

Metal	NTA	EDTA	DTPA
Li(I)	2.51	2.79	3.1
Na(I)	1.22	1.66	-
Mg(II)	5.41	8.79	9.3
Ca(II)	6.41	10.69	10.83
Ba(II)	4.82	7.86	8.87
Ce(III)	10.7	15.98	20.4
Eu(III)	11.33	17.35	22.49
Lu(III)	12.32	19.83	22.6
Th(IV)	13.3	23.2	28.78
U(VI)O_2	9.56	7.36	-
Mn(II)	7.44	13.87	15.6
Fe(II)	8.33	14.32	16.5
Co(II)	10.38	16.31	19.27
Ni(II)	11.5	18.52	20.32
Cu(II)	12.94	18.8	21.55
Zn(II)	10.67	16.50	18.40
Fe(III)	15.9	25.1	28
Co(III)	-	41.4	-
Ag(I)	5.16	7.32	8.61
Hg(II)	14.6	21.7	26.7
Pb(II)	11.34	18.04	18.8
Al(III)	11.4	16.3	18.6

The stability constants in Table 2 highlight some of the key factors that affect complex stability. Generally, $\log\beta_{M\text{-}NTA} < \log\beta_{M\text{-}EDTA} < \log\beta_{M\text{-}DTPA}$, which follows the trend of increasing APCA denticity and increasing contribution of the chelate effect.

Hard-soft acid-base (HSAB) theory dictates hard Lewis acids prefer to bind to hard Lewis bases and vice versa. APCA binding sites ($RCOO^-$ and NR_3) are both classed as

hard bases. The respective values of $\log\beta_{\text{Mg(II)-APCA}}$ (hard acid) and $\log\beta_{\text{Ag(I)-APCA}}$ (soft acid) are relatively similar, when HSAB theory would predict that $\log\beta_{\text{Mg(II)-APCA}} > \log\beta_{\text{Ag(I)-APCA}}$. This highlights the importance of ligand geometry and steric constraints; although more stable coordination bonds should theoretically form between the ligand and Mg(II), the small ionic radius of the metal ion increases the steric strain (six-coordinate Mg(II) ionic radius (0.72 Å) < six-coordinate Ag(I) ionic radius (1.15 Å)).[22]

The stability constants for APCA-complexes of first-row d-block transition metals are all relatively high. The ionic radii of the transition metals follows the order: Mn(II) > Fe(II) > Co(II) > Ni(II) < Cu(II) < Zn(II), which generally corresponds with the observed trend in $\log\beta_{\text{M-APCA}}$: Mn(II) < Fe(II) < Co(II) < Ni(II) < Cu(II) > Zn(II). The relationship can be partly attributed to the increasing Lewis acid hardness brought about by the increasing effective nuclear charge, but other factors contribute to the observed discontinuity between Cu(II) and Zn(II).[22]

Transition metal ions are subject to crystal field effects. Crystal field stabilisation energies (CFSE) are known to be a key influence on values of β for transition metal complexes, especially in octahedral coordination environments. The experimentally-based Irving-Williams series orders high-spin octahedral complexes of first-row d-block elements according to their 'natural order of stability'. The series overlays the effect of increasing effective nuclear charge with the contribution from crystal field stabilisation and follows the order: Mn(II) < Fe(II) < Co(II) < Ni(II) < Cu(II) > Zn(II). The Irving-Williams series corresponds with the observed trend of $\log\beta_{\text{M-APCA}}$. The stability of Zn(II) complexes are unaffected by CFSE because the metal ion has a closed shell ([Ar]$3d^{10}$) electron configuration, meaning that the energy gained from electrons in stabilised orbitals is cancelled out by electrons in destabilised orbitals. Moreover, octahedral complexes of Cu(II) are often subject to a geometrical distortion called the Jahn-Teller effect, which results in elongation of the two axial bonding modes and compression of the bonds across the equatorial plane. The distortion serves to remove the degeneracy from the electronic ground state and reduce the overall energy of complexation.

APCA-transition metal complexes are generally stabilised by increasing the oxidation number of the metal (e.g. $\log\beta_{\text{Fe(II)/Fe(III)-EDTA}} = 14.32/25.1$),[23] which is consistent with the

trend of increasing Lewis acid hardness but is also caused by the formation of an additional formal ionic coordination bond between the metal centre and a negatively charged carboxylate unit. CFSE is also potentially greater for transition metals in their third oxidation state because the greater charge density promotes a larger energy gap (Δ_o).

Particularly high stability constants are reported for APCA-transition metal complexes of Fe(III) (25.1) and Co(III) (41.4). Fe(III) has the electronic configuration [Ar]$3d^5$; unpaired electrons are distributed throughout the five d-orbitals to make a high-spin complex meaning the stabilisation gained from the three electrons in the t_{2g} energy level is negated by the two destabilised electrons in the higher-energy e_g orbitals. The overall CFSE = 0, therefore, the APCA bonding modes should theoretically have no geometrical preference as there is no way of making a more stable spatial configuration.

In reality, two different coordination modes have been suggested for the Fe(III)-EDTA solid phases and solutions; in crystalline Fe(III) salts, EDTA is usually hexa-dentate and a water molecule is coordinated as a seventh ligand, forming an approximate pentagonal-bipyramidal structure.[24-28] In the protonated form, a molecule of water and five of the EDTA binding modes make six-coordinate geometry with one protonated EDTA carboxylic acid group.[29]

Co(III) has the electronic configuration [Ar]$3d^6$; all six d-electrons are paired in the three t_{2g} energy level to make a low-spin complex. All of the 3d-electrons are in stabilised orbitals and generate a large negative value of CFSE, leading to the high thermodynamic stability of its complexes. Co(III)-complexes also tend to be kinetically inert towards ligand substitution. Both factors contribute to the exceptionally high value of $\log\beta_{Co(III)\text{-}EDTA}$ reported.[22]

1.3.3 Applications

The chelating properties of APCAs make them useful in a wide range of applications. The linking units of the nitrogen-containing backbone and the bridges between amine and carboxylate groups can be readily varied and substituted to promote selective

binding of metals and additional functionality.[30] This is useful in general separation chemistry, but also in more nuanced applications; for example, Fura-2 (2-[6-[bis(carboxymethyl)amino]-5-[2-[2-[bis(carboxymethyl)amino]-5-methylphenoxy]ethoxy]-1-benzofuran-2-yl]-1,3-oxazole-5-carboxylic acid) has a substituent that is engineered to fluoresce when the APCA selectively binds Ca(II) ions, and is used to determine calcium content in intra-cellular fluid (selectivity reduces interference of Mg(II)).[31]

APCAs are commonly employed by natural systems; both plants and bacteria are known to produce APCA molecules to selectively bind and transport metal ions in their environment. Graminaceous plants produce substances called phytosiderophores under Fe-deficient conditions, which are commonly APCA structures, such as mugeniec acid, avenic acid and nicotinamine.[32-34]

Similarly, bacteria and fungi both secrete siderophores into their extracellular environment to sequester and solubilise Fe for subsequent transport across the cell membrane. Without exception, siderophores have a greater affinity for Fe(III) than Fe(II); di-positive cations are naturally abundant (e.g. Cu(II), Zn(II), Mn(II) and Ni(II)), whereas there are fewer biologically important tri-positive cations.[33] A ligand that is selective for tri-positive metals will effectively be selective for Fe(III) in biological matrices. Siderophores are amongst the strongest known soluble Fe(III) binding agents; enterobactin is reported to have a logβ stability constant = 49 for Fe(III)-complexation.[33]

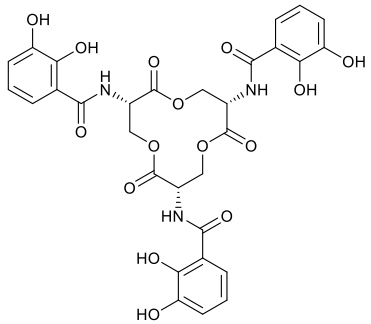

Figure 8. Structure of the siderophore enterobactin.

EDTA, DTPA and NTA are mass-produced anthropogenic chelating agents used in a range of industries. Their functionality is mostly targeted at sequestering metal ions to

either remove them from a given matrix or limit their reactivity, however, some of their uses are more specialised.

NTA is cogenerated as an impurity in the synthesis of EDTA. On an industrial scale, NTA is used chiefly as a replacement for phosphates in detergents, however, the ligand and its derivatives also have many laboratory-based applications.[30] For example, protein purification is often achieved by immobilised metal affinity chromatography, in which transition metal ions are fixed to the stationary phase matrix via a chelating ligand, often NTA or IDA. Differential bonding equilibria between the eluted proteins (usually hexahistidine tagged (imidazole sidechain)) and the transition metal (e.g. Cu(II)) result in chromatographic separation.[35] Other related biological applications of bi-functional NTA-derivatives include protein crystallisation and fluorescent labelling.[30,36]

The aqueous Gd(III)-DTPA complex is nine-coordinate, bound by the eight binding sites of DTPA and an additional coordinating water molecule.[37] The Gd(III)-DTPA complex was the first magnetic resonance imaging contrasting agent approved for clinical practice and is still used today; hydrophilic chelates of paramagnetic Gd(III) do not pass through the intact blood-brain barrier, thus, enhancing imaging of lesions or tumours where the blood-brain barrier is compromised.[38,39] The complex is removed from circulation by the renal system. DTPA-coordination of radionuclides such as ^{111}In, ^{212}Bi, ^{90}Y, ^{99m}Tc and $^{67/68}$Ga have also been considered for nuclear medicinal applications.[30]

Zn(II)- and Ca(II)-DTPA are also used for the therapeutic relief of those who have been internally contaminated by Pu, Am, or Cm. The greater charges associated with the high actinide oxidation states help them to readily displace the biologically essential Zn(II) or Ca(II) ions from the DTPA-chelate, for subsequent excretion of the actinide-complexes in urine.[40,41] Similarly, EDTA coordinated to two Na(I) ions and a Ca(II) ion, known as sodium calcium edetate, is an approved medicine for the treatment of lead poisoning.[42]

The bulk volume of the NTA, DTPA and EDTA produced is used in industrial and agricultural processes.[43-45] Figures from 1999 show that over 34,500 tonnes of EDTA were produced in Europe alone. The pattern of use is presented in Table 3. The figures are outdated (e.g. photo-chemicals mainly refer to the Fe(III)-NH_4EDTA used in the

photo-industry in the bleachfix process, which is almost certainly less common now), but give a reasonable indication of the scale of the ligand consumption.[44]

Table 3. Volumes of EDTA used in various applications in Western Europe in 1999.[44]

Use	Marketed Amount / t y^{-1}
Household detergents	2,619 (7.6%)
Industrial and institutional detergents	10,685 (31%)
Photochemicals	4,191 (12%)
Textiles	639 (1.8%)
Pulp and paper	4,002 (12%)
Metal plating	470 (1.4%)
Agriculture	5,821 (17%)
Cosmetic	756 (2.2%)
Rubber processing	469 (1.4%)
Oil production	358 (1.0%)
Exports	1,143 (3.3%)
Other	3,393 (9.8%)
Total	34,546

Chelating agents are added to cosmetic products and some foodstuffs (e.g. mayonnaise, salad dressing) to stabilise them. The ligands coordinate trace metals to prevent them from catalysing oxidative degradation through redox chemistry or forming undesirable complexes with constituent molecules in the product. For example, brown/black discolouration of potatoes is caused by the complexation of naturally present phenolic compounds with Fe, which can be prevented by addition of EDTA. Similarly, the shade of many commercially available dyes changes in the presence of trace metal ion contamination, hence the common use of EDTA in the textiles industry (1.8%, Table 3)[44] – furthermore, DTPA is widely used to stabilise hydrogen peroxide bleaching liquors against decomposition by traces of Mn, Fe and Cu. APCAs are commonly used in paper manufacturing to improve the paper brightness; again, DTPA is used to preserve the peroxide bleaching agent, and EDTA coordinates trace Mn which can later react with lignins to form dark coloured substances if not removed.[44]

Agricultural micronutrients and trace elements such as Fe, Zn, Mn and Cu are chelated by EDTA or DTPA prior to addition to fertilisers to prevent interaction and precipitation

with phosphates or other ions. Once in the soil medium, the synthetic APCAs act in a similar way to siderophores, allowing the micronutrients to translocate to the root zone for efficient uptake into the plants.[44]

Many household and industrial cleaning products contain EDTA and other APCAs. Chelating agents reduce the hardness of water for laundry applications and remove scale deposits from internal boiler surfaces. APCAs are commonly used to clean metal surfaces as they solubilise adherent oxide films to provide complete rinsing. Chemical decontamination agents used throughout the nuclear industry often contain APCAs.[15-20,46,47]

1.4 Aminopolycarboxylic Acids in Low Level Waste

1.4.1 Sources

APCAs most commonly arise in LLW through their use in chemical decontamination agents (decontaminants).[15-20]

Decontamination in the nuclear industry is carried out: i) to reduce radiation dose to staff and operators; to remove the build-up of deposits to improve plant efficiency; ii) to reduce the quantity of waste requiring geological disposal; iii) and to facilitate safe decommissioning operations. Decontamination processes include electrochemical, mechanical, by melting and chemical.[48,49]

Chemical decontamination is usually carried out by circulating the selected reagents through the system but can also be carried out on segmented parts by immersion in a solution containing the reagents. Chemical decontaminants can be mild (non-corrosive, e.g. detergents, complexants, dilute acids or alkalis) or aggressive (corrosive, e.g. strong acids or alkalis). Selecting an appropriate decontaminant depends on many factors, including: the location of the contamination; the physical integrity of the system; the type of base material; the nature of the contamination; and time, cost and safety concerns. The advantages of chemical decontamination are its simplicity and effectiveness; the disadvantages are the high-volume generation of secondary liquid waste, which itself requires appropriate processing.[48]

Commonly used chemical decontamination agents range from household cleaning products to specialised radioactive decontamination formulations, many of which contain APCAs and other polycarboxylic acids. Therefore, solid LLW can often become contaminated with quantities of APCA chemicals, the levels of which vary according to the origin of the specific wastestream and the relevant treatment processes it has undergone. Table 4 lists some APCA-containing and/or frequently used chemical decontamination agents.[17,50]

Table 4. Decontamination agents used in industry and the complexants present (composition is dependent on the form that the decontamination agent is supplied in)[17,50]

Reagent Name	Complexants Present (Composition)
SDG3 (routinely used decontamination agent; supplied as powder, cream or foam; acidic)	EDTA (13.2 - 18.5%)
	Citric acid (25.3 - 35.5%)
N10 (common alternative to SDG3; supplied as powder or cream; alkaline)	EDTA (11%)
	Sodium tri-polyphosphate (42%)
Cleaver (bacterial degreaser and drain cleaner; supplied as solution)	NTA (1 - 5%)
	Pyrophosphate (1-5%)
APAC (alkaline permanganate, ammonium citrate; present as solution)	Citric acid (unknown)
APACE (as APCA, but with EDTA)	EDTA (unknown)
	Citric acid (unknown)
DTPA (used in diluted form, as gel, or strippable coating; supplied as solution or gel)	DTPA (unknown)
Decon90 (generally diluted and used to clean or mop contaminated surfaces; alkaline)	Citric acid (unknown)
	Other sequestering agents (unknown)

Though most APCA-contamination of wastes is low level (only trace quantities of surface-adsorbed material), more heavily contaminated wasteforms can arise. For example, operation and maintenance activities of the UK's nuclear submarine fleet has led to the accumulation of vast quantities (62.1 m^3 dry volume) of EDTA- and radioactively contaminated spent ion-exchange resin. The resins are currently in storage under water within high-integrity stainless steel containers; some containers contain EDTA > 5 wt%. The resins are intended for disposal at the LLWR once the radioactivity has decayed beyond acceptable limits, though, to avoid using a disproportionate allocation of the total APCA capacity of the site, an appropriate treatment technology must be identified to destroy the ligand prior to disposal (see Chapter 3).[51]

1.4.2 Impact

The chelating properties of APCAs make them potentially environmentally hazardous because they can increase the solubility and mobility of otherwise solid-state or surface-bound radionuclides and other chemical contaminants in the repository. This can increase the likelihood of contaminant transportation in flow pathways of infiltrating water from the stabilised wasteform, through the repository near field, into the wider geo/bio-sphere.[14-20,46,47]

LLWR have undertaken multiple reviews to determine the potential impact of complexants on repository performance as part of and subsequent to the 2011 ESC. Though other complexants and chelating agents can arise in the waste, the risk associated with APCAs is distinct because of their greater environmental persistence (see section 1.5).[17-20]

EDTA has been detected in several analyses of LLWR trench pore water, generally at a concentration of around 0.1 μM.[52] An estimated quantity of EDTA in the waste consigned to Vault 8 was determined to be equal to 0.8 g per m^3 of vault disposal volume, which translates to 6 μM.[17,19]

Extensive modelling of various EDTA loadings (low, high and very high) has been undertaken to determine the impact of the ligand on the concentration of various contaminant species arising in flow pathways around the LLWR site (studies often focus on EDTA because it is the most prevalent and can act as representative of other APCAs).[19] Values for risk are calculated from the modelling data to determine EDTA concentrations that are safely and legally practicable (i.e. do not increase the risk associated with LLWR operations to > 1 μmort (μmort is a unit of risk defined as a one-in-a-million chance of death)).[53] For example, EDTA loadings equivalent to the estimated vault concentration (6 μM) increased the peak risk associated with the current disposal area drainage stream from 1.3×10^{-9} (no EDTA) to 5.7×10^{-8} morts. This is a result of the different effective solubility limits and sorption coefficients that individual contaminant species are subject to in the presence of EDTA.[17]

Thermodynamic studies have shown that EDTA can enhance the solubility of important radionuclides.[18] For example, 1 mM concentrations of EDTA were found to increase the solubility of Th(IV) by two orders of magnitude at pH 11; similarly, 10 μM EDTA concentrations were found to increase the solubility of Ni(II) by three orders of magnitude. Under reducing conditions, solubility enhancements were also found for Tc(IV) and Pu(III/IV). Migration of EDTA chelates of radioactive Co and Pu from LLW have previously been observed.[46,54,55]

The concentration of non-radiological contaminant species was also increased in the presence of EDTA. This included high levels of lead, which forms a highly stable EDTA-complex ($\log\beta_{Pb(II)\text{-}EDTA}$ = 18.04, Table 2) and resulted in additional exceedances of the water quality standard. Furthermore, based on the results of the highly cautious modelling, the calculated remaining capacity of the repository for Pb was found to be significantly less than the anticipated future disposal inventory, prompting a series of revised calculations based on less conservative figures to create a more realistic model (e.g decreased Pb corrosion rate and declining EDTA concentration over time).[17]

It has been determined that EDTA loadings of 1 μM in the LLWR trenches and 6 μM loading in the vaults does not increase the associated risk of radionuclide mobilisation beyond legal, acceptable limits (> 1 μmort).[14,19] There is greater tolerance for EDTA loadings in the vaults because of the additional radionuclide containment afforded by the containerisation and grouting of disposed waste.

1.4.3 Treatment Options

In order to limit APCA accumulation and preserve the LLWR capacity for the materials, waste can be treated to remove or destroy contaminant APCAs prior to its disposal. Methods to destroy complexants in bulk solution have been widely studied in efforts to minimise their impact on nuclear reprocessing effluent treatment technologies; many of the effluent treatment processes rely on the removal of dissolved radionuclides from solution, the effectiveness of which is impaired by the presence of ligands such as EDTA.[20] Thermal[56], chemical[57,58], photochemical[59-61] and electrochemical[62] degradation processes have all been explored.

The methods listed above have been developed for use on bulk solutions of relatively high APCA concentration. Decontaminants in solid LLW are more likely to be absorbed into clothing, cloths or paper towels, rather than in liquid form; implementation of the above methods would require leaching of the reagents prior to treatment, and the trace APCA concentrations may render them ineffective.[20]

Incineration is considered to be a more suitable process for APCA-containing LLW. Controlled incineration processes are widely used and well developed for the management of radioactive and non-radioactive wastes; they have been used to treat LLW in France, Germany and the United States of America (USA), and Pu contaminated material has been treated in the UK.[20] Incineration is facilitated by improved segregation of combustible and non-combustible waste materials on site, which can also allow for diversion of recyclable materials to appropriate facilities. Incineration of combustible wastes breaks down the reactive compounds and organics (e.g. APCAs) to create a stable wasteform (ash), and can reduce the volume of the original waste by up to 98%. The homogenous ash can often be disposed of as VLLW to appropriately permitted landfill sites.[63,64]

Disadvantages of incineration processes include the additional hazards associated with the need to segregate wastes prior to treatment, which also involves exclusion of materials that are likely to generate corrosive gases (e.g. polyvinyl chloride (PVC)). Furthermore, the large volumes of off-gas must be treated to ensure that toxic gases are not released to the atmosphere, which usually results in secondary waste. Appropriate disposal of secondary wastes (e.g. filters) and residue ash must also be considered.

The development and use of alternative treatments are part of the strategic shift in the long-term management of LLW designed to divert wastes away from LLWR in order to maximise the existing capacity and extend the site's operational lifetime. Treatment technologies open up new waste disposal routes and can make materials suitable for re-use or recycling, which ties in with the principles outlined in the Waste Hierarchy.[4,63] Other technologies for complexant treatment in solid LLW include acid digestion, wet

oxidation, wet air oxidation, microbial techniques, biological digestion, molten salt combustion and molten glass processes.[20,65]

The EDTA-contaminated spent ion-exchange resins generated by operation and maintenance of the UK's nuclear submarine fleet are an example of a specific wasteform that was considered for treatment by incineration. Analysis to confirm the complete destruction of EDTA in a trial incineration process forms the basis of Chapter 3.[51]

1.4.4 Waste Acceptance Criteria

A 2011 review of the biogeochemical aspects of the WAC at LLWR was a supporting document of the 2011 ESC. The report recommended that 'APCAs are excluded from the waste as far as is possible, unless stabilised or treated before consignment and that decontamination agents that contain APCAs should be replaced by others that contain biodegradable complexing agents, or that APCAs are chemically or thermally degraded before consignment to LLWR'.[18] The Permit granted by the Environment Agency following submission of the 2011 ESC originally prohibited the acceptance of APCA-containing wastes.[16]

The Permit was varied subsequent to LLWR application to the Environment Agency with substantiated claims regarding the safe disposal of APCAs within certain limits.[17,19,20] On the basis of the assessment calculations discussed previously (Section 1.4.2), a total APCA capacity of 1,000 kg for the current LLWR disposal area was proposed, which includes the quantities already disposed of. The LLWR WAC was updated in accordance with the varied Permit to include the newly defined site capacity and the categorisation of chemical complexants; Category 1 (require control but not a specific site allocation, e.g. carboxylic acids and tri-polyphosphates) and Category 2 (APCAs).[15]

In order to conserve the low site disposal capacity, waste producers are required to implement the best available techniques to ensure that disposed quantities of APCAs are as low as can reasonably be achieved (e.g. use of alternative reagents containing less or no Category 2 complexants).[50]

Waste producers are also required to provide waste characterisation information that is proportionately detailed to the type and quantity of complexants that are expected to be present. For example, for wastes containing Category 1 complexants 'a best estimate value should be presented, underpinned by reference to operational procedures where appropriate'; information regarding wastes containing Category 2 complexants 'should be based on the customer's [waste producer's] best available knowledge of the processes that generate the waste' and 'if additional information is required, an assessment method may be agreed with the LLWR Waste Acceptance Team, as it is important to consider whether the approach selected will determine a reasonable *de minimis* value (e.g. by applying the limit of detection (LOD) value where applicable)'.[50]

Approaches for the determining the presence of complexants vary in complexity and feasibility and should be used to reflect the degree of environmental impact that the expected complexants in the waste pose. Different approaches include experimental analysis, accountancy methods and expert judgment, which can all be used in combination and to varying extents. Experimental analysis may involve analysis of samples of similar materials (e.g. inactive representative materials) or obtained by intrusive sampling of wastestreams.

One of the main topics of this thesis is the development of a suitable method for APCA detection and quantification in complex matrices relevant to the management of LLW.

1.4.5 Other Complexants

Most complexants and chelating agents arise in the repository environment because they are a component of the waste or can form *in-situ*. This may be through their use in decontamination agents (e.g. APCAs and other polycarboxylic acids), because they are intrinsic to the waste or wasteform (e.g. isosaccharinic acid (ISA) formed in the alkaline hydrolysis of cellulosic wastes or superplasticisers added to the grout formulation)[17], or because they are naturally occurring (e.g. humic and fulvic acids[46,66], and siderophores[33]).

Complexants of interest to the 2011 ESC were identified on the basis that they could be present in the repository near field; could potentially come into contact radionuclide species; could be expected to be present in concentrations high enough to inflict a significant change in solubility or sorption characteristics of contaminant species; and could persist for long enough in the repository conditions to facilitate contaminant transport.[17]

Table 5. Complexants considered in the LLWR 2011 ESC.[15,17]

Type	Properties	Name	Origin	WAC
Inorganic complexants	Low molecular weight ions	Sulphates	In waste	Not controlled
		Nitrates	In waste	Not controlled
		Carbonates	In waste	Not controlled
		Borate	In waste	Not controlled as complexant (defined site capacity for boron)
		Orthophosphates	In waste and may form *in-situ*	Not controlled
	Di- and tri-phosphates (bi- and tri-dentate)	Pyrophosphate	In waste and may form in-situ	Not controlled
		Tripolyphosphate	In waste	Not controlled
	Ion-exchange material (multiple complexes)	Zeolites	In waste	Not controlled
Organic complexants	Mono-carboxylic acids (mono-dentate)	Formic acid	In waste and may form in-situ	Category 1
		Acetic acid	In waste and may form in-situ	Category 1
	Di-carboxylic acid (bi-dentate)	Oxalic acid	In waste	Category 1
	Polycarboxylic acid (polydenate)	Citric acid	In waste	Category 1
	Pyridine mono-carboxylic acid (mono- and bi-dentate)	Picolinic acid	In waste	Category 1
	Carboxylic acid sugar (mono-dentate)	Isosaccharinic acid (ISA)	In waste and may form in-situ	Not controlled

Organic amine (bi-dentate)	Ethylenediamine	In waste and may form in-situ	Category 1
Organophosphate (monodentate)	Tributylphosphate (TBP)	In waste	Category 1
APCAs (polydentate)	Ethylenediaminete-traacetic acid (EDTA)	In waste	Category 2
	Diethylenetriamin-epentaacetic acid (DTPA)	In waste	Category 2
	Nitrilotriacetic acid (NTA)	In waste	Category 2
Ion-exchange material (multiple complexes)	Various, predominantly polystyrene based	In waste	Not controlled as complexant (encapsulation required prior to disposal)
Superplasticisers (multiple complexes)	Sikament 10	In waste	Not controlled as complexant (used in grout formulation)

Table 5 shows the complexants considered in the LLWR 2011 ESC. Mono-dentate low molecular weight ions are expected to occur in most wastestreams in trace quantities. Sulphate and nitrate act as electron acceptors for microbial growth, meaning that their concentration can have a direct impact on the biogeochemical conditions of their environment; for example, sulphate utilisation can out-compete methanogenesis which can have the beneficial effect of reducing the release of gas-borne ^{14}C.[18] Overall, it was concluded that the expected concentrations of low molecular weight inorganic ions would not have a significant impact on repository performance.[17]

For complexants associated with ion-exchange material to become mobile and potentially harmful, the materials must first be degraded to release smaller binding units from the original polymeric structure. Alkaline hydrolysis can result in degradation reactions such as deamination, dealkylation and cleavage of the polymeric backbone, depending on the chemical composition of the ion-exchange material. Though the degradation products of certain organic ion-exchangers have been found to affect radionuclide solubility (e.g. degradation products of phenol formaldehyde based resins increased the solubility of Pu by an order of magnitude), it is anticipated

that both organic and inorganic ion-exchange materials will be reasonably stable in the real repository environment.[17,18,67]

Cellulose is a naturally occurring linear polymer of glucose found in paper and wood. Alkaline hydrolysis of cellulose can lead to the formation of significant levels of ISA (> 75% of cellulose degradation leachate) under high pH conditions. ISA is strongly complexing and can increase the mobility of most radionuclides.[17] Based on LLWR specific experiments, the concentration of ISA expected to form *in-situ* was 10 μM, however, microbial degradation, sorption and dilution reduce the concentration to below detection limits (0.9 μM). In the long-term, microbial and chemical degradation processes are expected to inhibit the accumulation of ISA formed in the repository so that the natural complexant does not exceed concentration levels that have a significant impact on radionuclide mobility.

Superplasticisers are used to improve the flow characteristics of cement in concrete, mortar and grout. LLWR add a vinyl copolymer, commercially known as Sikament 10, to their grout formulation (0.9 wt.%) to improve its rheological properties and to optimise waste encapsulation prior to disposal. Numerous experimental studies have been carried out on the effect that superplasticisers have on radionuclide sorption and solubility. The solubility of certain radionuclides in aqueous solution was found to increase with addition of superplasticiser, however, when solid cement (representative of the encapsulant grout) was added to the solutions in realistic ratios, the sorption and solubility behaviours of the radionuclides were found to be generally unaffected by the dissolved superplasticiser. This was attributed to the sorption of the high molecular weight superplasticiser to the cement (interaction with cement is part of a superplasticiser's functional specification) rendering it immobile. The overall effect was for there to be low concentrations of superplasticiser-radionuclide complexes free in the aqueous phase of the solution which, combined with the slow diffusion rates of the large organic molecules through cement, leads to a low probability of significant radionuclide mobilisation in the repository.[9,17,18]

Extensive study of the carboxylic acids and polycarboxylic acids that are often found in decontamination agents alongside the APCAs has generally concluded that their rapid

aerobic or anaerobic microbiological degradation does not allow them to form persistent radionuclide complexes, therefore, do not increase the associated risk of radionuclide mobilisation beyond acceptable limits.[17,18,20]

1.5 Degradation of the Aminopolycarboxylic Acids

Though other complexants and chelating agents are known to arise in the near field environment of the LLWR, stringent control measures, including a total site capacity, are unique to the acceptance of waste containing APCAs. This is partly because they form such highly stable complexes with a range of cationic species, but also a result of the environmental persistence of the synthetic ligands.

An environmental half-life longer than, for example, Category 1 polycarboxylic acids, means that the APCAs are more likely to accumulate to concentrations at which their impact on radionuclide solubility and mobility is potentially hazardous. Furthermore, eventual degradation of the APCAs can lead to secondary generation of ligand fragments that are themselves potent chelating agents. Some of the mechanisms that determine the ultimate environmental fate of the APCAs are discussed below.

1.5.1 Biological

Biological degradation of the APCAs, especially EDTA, have been studied extensively as it is considered to be a primary means of organic compound removal in the environment.[68] The wide usage of EDTA in a range of industries has led to concern about its ultimate release to the aquatic environment; mechanisms that affect the behaviour or destruction of the ligand and its complexes in natural waters, soils and sediments are of interest to many.[44]

Application of a range of standardised biodegradability tests (coupled units test, Zahn-Wellens test, Swiss EMPA test, Japanese MITI test, the French norm procedure AFNOR, carbon dioxide evolution test, OECD screening test, closed bottle test and the United States Environmental Protection Agency activated sludge test) have all indicated that EDTA is not biodegradable to a significant extent.[68-70] A study into the relative rates of NTA, EDTA and DTPA degradation concluded that the rate of biodegradation for NTA >

EDTA ≈ DTPA, and that degradation rates of all three chelates are not rapid enough, even under optimal conditions, to preclude concern over their release to the environment.[71]

Slow biodegradation of ^{14}C labelled EDTA and its complexes of Cu, Cd, Zn, Mn, Ca and Fe was only observed under aerobic conditions.[68] As much as 65-70% of the ^{14}C label was recovered as $^{14}CO_2$ in 315 day free EDTA biodegradation experiments.[72] Another study found that EDTA was more persistent than DTPA with respect to biodegradability; the maximum quantities of ligand mineralised by microorganisms over a 115 day period were 15% and 26%, respectively. This study also found that mineralisation of EDTA and DTPA was maximal in sediments containing different microbial populations, which is interesting given the structural similarity.[73]

A study into the susceptibility of ethylenediamine-based complexants to biodegradation concluded that the number of nitrogen atoms, and type and quantity of substituent groups all factored into the biodegradability. For example, complexants with a single nitrogen atom (e.g. NTA) succumb relatively readily to biodegradation, whereas, compounds with two or more tertiary amino groups (e.g. EDTA and DTPA) are biologically highly stable and do not undergo biodegradation (30 day experiments in activated sludge). It is also claimed that a lowering of the degree of substitution directly corresponds with an increased susceptibility to biodegradation (e.g. replacement of tertiary amino groups with secondary ones), which has implications for the biological consumption of APCA degradation products that can form as a result of any of the mechanisms listed in this section (e.g. ethylenediaminetriacetic acid (ED3A, ethylenediaminediacetic acid (EDDA), eythelenediaminemononacetic acid (EDMA) and IDA are all potential EDTA (and DTPA) degradation products, and all have lower degrees of substitution at at least one of the amino groups than the EDTA starting product; the structures of ED3A, EDDA and EDMA are shown in Figure 9).[74]

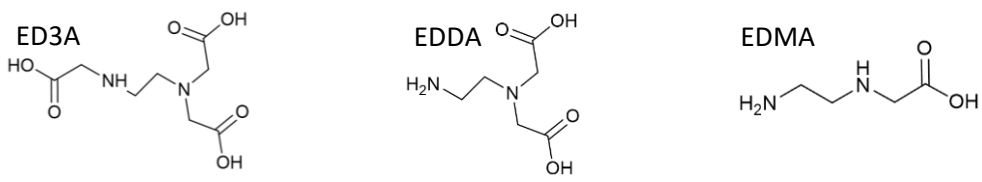

Figure 9. Chemical structure of ED3A, EDDA and EDMA.

To summarise the literature, there is widespread consensus that NTA is less resistant to biodegradation than EDTA and DTPA. NTA biodegradation has been observed under oxic and anoxic environments, with half-lives ranging from 3-7 days under aerobic conditions.[74-78] The literature is less conclusive regarding the biodegradability of EDTA and DTPA, but several groups have observed the microbial breakdown of DTPA in soils and sediments (both EDTA and NTA were formed as products) and generally find that it is less resistant to biodegradation than EDTA.[71-74,79] EDTA is largely resistant to biodegradation in the environment but slow aerobic degradation in has been reported in special cases. EDTA-degrading bacteria have been successfully isolated; some were able to grow with EDTA as the sole source of carbon, nitrogen and energy (e.g. strain BNC1/DSM 6780 of the α-branch of *Proteobacteria*).[74]

1.5.2 Chemical

In the short-term, chemical degradation is not thought to contribute significantly to the destruction of APCAs in the environment as conditions are typically too mild.[80] For example, the hydrolysis of EDTA and various metal EDTA complexes was studied at high temperatures to reveal that Cu- and Fe(III)-EDTA undergo a redox reaction and hydrolyse fast at 125 °C, with half-lives of approximately 3 h; extrapolating the high temperature kinetic data reported in this study, it was determined that it would take 128 days for 50% elimination of the complexes under the conditions of natural water (25 °C), and about 6000 days to eliminate 50% of the free EDTA.[81-83] In the context of LLWR, APCA hydrolysis may be relevant because of the long timescales that waste containment is planned for. Furthermore, the rate of hydrolytic degradation may be increased by the high pH environment afforded by the buffering effect of the grout.

Other reactivity considered in the discussion of EDTA chemical degradation in natural waters were reactions with solvated electrons, organic peroxyradicals, singlet oxygen, and hydroxyl radicals. These unstable reactive species are generated by the photolytic processes in the aqueous environment caused by sunlight. Dissolved natural organic material can absorb light to form the various photo-oxidants via reactions of excited chromophores. The species have the potential to chemically react with APCAs and their complexes, but the extent to which degradation is observed is usually limited by

the low concentrations that the radicals or otherwise excited species are present. For example, the concentration of the solvated electron is highly dependent on the time of day and its rate of reaction with free and complexed EDTA is pH-dependent; these variables result in EDTA half-lives that vary between 60 days and 732 years. The study concludes that none of the indirect photolytic pathways are relevant to the short-term degradation of EDTA in the environment.[81]

The chemical degradation of EDTA, NTA and other polycarboxylic acids in mixed nuclear wastes stored at the Hanford Site (WA, USA) has previously been studied using a nonradioactive simulant waste. The simulant consisted of an alkaline inorganic matrix plus the chelating agents EDTA, NTA, N-(2-hydroxyethyl)ethylenediaminetriacetic acid (HEDTA) and citric acid. After 171 days at ambient temperature, detailed analysis of the organics by gas chromatography/mass spectrometry (GC-MS) revealed that 61.7% of the parent organics had been degraded – HEDTA was found to be the most labile. A similar study focused on the chemo-degradation of EDTA alone and found that only 31.0% of the original EDTA remained after 175 days.[46,84]

The GC-MS detection and quantification method allowed for a detailed product study; degradation products of EDTA were found to include glyoxylic acid, IDA, ED3A and EDDA. The authors claim that the extensive changes in the organic composition of the simulant will have to be factored into the management of mixed wastes.[84] The simulant conditions used in this study are stronger than those expected in the LLWR wasteform, but suggest that the rate of chemical degradation can be elevated under the relatively harsh conditions of radioactive wastes.

1.5.3 Photolytic

Photolytic degradation pathways are thought to be a significant contributing factor to the elimination of APCAs in the environment.[68,74] The specific photochemical transformations are strongly dependent on natural conditions; for example, the photolysis rates of pollutants in pure water, seawater and inland water are dependent on conditions such as season, latitude, time of day, depth, ozone layer thickness and

light attenuation.[85] A four day half-life was determined for EDTA in river water in sunny weather, as opposed to no significant degradation in cloudy weather.[81,86]

Complexation of the APCAs to a metal centre affects their susceptibility to photolysis, which is also determined by the identity of the metal; for example, laboratory experiments found that Na(I), Mg(I), Ca(II), Ni(II), Cu(II), Zn(II), Cd(II) and Hg(II) EDTA chelates were all photostable, whereas there is wide-spread unanimity concerning the photolability of the Fe-EDTA complex.[68,74,80,87-90] It has also been reported that EDTA complexes of Mn(II), Co(III) and Cr(III) are photodegradable.[24,87] Fe-DTPA has been found to be photolabile,[68,74,89] and free DTPA has been shown to be much more photodegradable than free EDTA.[47,68,71]

In a study of environmentally relevant EDTA degradation pathways, it was concluded that direct photolysis of the Fe(III)-EDTA complex was the main control over the behaviour and fate of the ligand. Efforts have even been made to influence the speciation of EDTA by addition of Fe-salts; high fractions of Fe-EDTA in the effluents of wastewater treatment plants are favourable for the ultimate fate of EDTA in the effluent receiving rivers, since the photochemical conversion of FeEDTA is an efficient process for its elimination on a time scale of hours.[91]

A mechanistic study of the photochemistry of Fe(III)-EDTA complexes by pulse photolysis with UV-Vis detection proposed that ligand to metal charge transfer (LMCT) excitation is followed by reaction of the primary photoproduct with the parent complex to generate an intermediate dimeric species formulated as $[(H_2O)(EDTA^{\cdot+})Fe(II)(\mu\text{-}OH_x)Fe(III)\text{-}EDTA]^{x-4}$. The lifetime and pathway of decay of the intermediate species are dependent on the pH-environment and the presence of molecular oxygen, which ultimately determine the formation of degradation products. In the presence of O_2, the intermediate dimer composes fast to yield the parent complex (Fe(III)-EDTA), Fe(III)-ED3A and smaller oxidation products such as formic acid and CO_2.[24]

The recalcitrance of EDTA in the environment and the reliance on photochemical oxidation processes to prevent its accumulation has led many industries to implement advanced oxidation processes (AOP) to treat waste effluent streams prior to their

release to the environment. For example, Fenton and Fenton-like chemistry can be used to destroy the ligand in a photo-catalytic process involving H_2O_2 and UV irradiation.[92,93] With respect to LLWR, UV excitation and photolysis of APCAs will most likely be limited by the concealment of the wasteform; ligands and complexes transported in leachate or groundwater should generally only be exposed to direct sunlight once they reach the shoreline. However, the catalytic conversion of H_2O_2 to oxidative hydroxyl radical by EDTA-sequestered Fe(II) may be facilitated by radiolytic pathways.

1.5.4 Thermal

Thermal degradation of the APCAs and their metal chelates is generally not relevant to their removal from the environment as NTA, DTPA and EDTA are stable up to temperatures of 200 °C to 300 °C.[71] The exact temperature of thermal decomposition is affected by the identity of the counter-ions used to make the salt[94], metal-complexation[83,95], and the solvent environment (if any).[56,82] The thermal stability is key to the use of the complexants in systems of elevated temperature such as nuclear reactor decontamination and metal oxide solubilisation in boiler maintenance.[97]

Thermal decomposition of EDTA and NTA in pH 9.5 aqueous solution has been studied. The primary decomposition reaction of EDTA was found to be cleavage of the C-N of the ethylenediamine unit to produce IDA and *N*-(2-hydroxyethyl)iminodiacetic acid (HIDA) at 200 °C. Decomposition of NTA starts at around 290 °C and proceeds through stepwise decarboxylation reactions. Higher temperatures result in the thermal breakdown of the primary degradation products, for example, decarboxylation of IDA and HIDA result in the formation of the corresponding methylamines (Figure 10).[56,96] The aqueous thermal chemistry of DTPA is expected to be similar to that of EDTA.

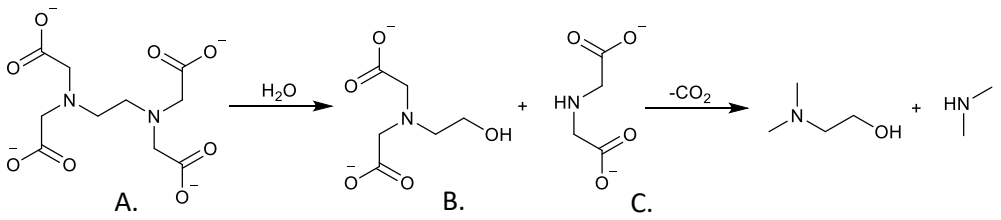

Figure 10. Thermal hydrolysis of EDTA (A) to form HIDA (B) and IDA (C), followed by decarboxylation to form the corresponding methylamines.

In a similar study, the thermal degradation of EDTA chelates of a series of metals was studied in alkaline aqueous solution. The relative order of degradation rates was found to be Mg(II) > Ca(II) > Zn(II) > Fe(II) > Ni (II). IDA and HIDA were identified as degradation products at lower temperatures (~250 °C), while methylamine and CO_2 dominated at higher temperatures.[83] Another study of the thermal behaviour of different metal-EDTA complexes under air found that the thermal stability of the complex was not related to the stability constant (β) or the heat of formation. Some of the complexes (Ca, Ba and Co) decomposed by losing two carboxyl groups first, and the remaining part of the molecule at higher temperatures, whereas in other complexes (Cu, Ni, Bi, Sb and Dy), all four carboxyl groups decomposed simultaneously.[95]

The thermal behaviour of solid-state EDTA is relevant to the work undertaken in this project because treatment of LLW to destroy contaminant APCAs by incineration relies on the thermal decomposition of the ligands at high temperatures. The efficacy of a trial incineration procedure designed to destroy the EDTA contained in spent ion-exchange resins is examined in Chapter 3.[51] The literature suggests that prolonged exposure to temperatures > 300 °C should be sufficient to completely degrade the ligand. Thermal degradation can either proceed through multiple decarboxylation reactions to produce APCA chelating agents such as ED3A, EDDA and EDMA, or cleavage of the C-N bond of the ethylene bridging unit to produce polydentate complexants such as IDA and HIDA.[56,82,83,95-98] From a LLW management perspective, it is desirable to avoid generation of secondary chelating agents, however, this outcome is preferable to waste containing EDTA as the secondary products generally do not form as stable complexes and are less environmentally persistent than the parent molecule.[74]

1.5.1 Radiolytic

APCAs contained in the LLWR may undergo radiolytic degradation because of the proximity of radioactive elements. The radionuclides in the waste produce α- and β-particles and γ-rays, which are types of ionising radiation. Ionising radiation is defined as carrying enough energy to remove an electron from an atom or molecule, meaning

that it can strongly interact with its environment to induce direct and indirect chemical changes. For example, when ionising radiation passes through an absorbing medium, such as water, radiolysis occurs. The products of water radiolysis are known as the primary yield:

$$H_2O \xrightarrow{\text{Ionising radiation}} e^-_{aq}, HO^{\cdot}, H^{\cdot}, HO_2^{\cdot}, H_3O^+, OH^-, H_2O_2, H_2$$

Direct interaction between emitted ionising radiation and low concentration solute molecules is improbable, therefore, the radiochemical behaviour of irradiated aqueous solution is largely controlled by secondary reactivity of the primary yield.

G-values are used to quantify the radiation chemical yield: *G*(X) = the number of species formed or depleted per 100 eV of energy absorbed. The number of species formed or depleted can be assessed using a range of spectroscopic or conductimetric techniques and the absorbed energy is usually quantified by Fricke dosimetry, which depends on quantification of Fe(III) produced by oxidation of Fe(II) by ionising radiation (oxidising species in the primary yield).[99]

G-values can be attributed to each component of the primary yield of water radiolysis, although, they are dependent on the pH environment, the ionic strength, and the type of absorbed radiation.[100] The different types of radiation follow different attenuation laws; α- and β-radiation behave as charged particles, while γ-rays have no charge or mass. Multiple complex mathematical models have been developed to determine the rate of water radiolysis in different environments; their success is important to many nuclear industrial applications, such as the effect of spent fuel on storage ponds.[c]

Assessing the radiological stability of specific components in the field is often difficult because systems are complex, multi-variable, and hazardous. Therefore, laboratory techniques are used to simulate the effects of radiation. These can be steady state methods, where a steady radiation dose is applied to a sample in a controlled environment (e.g. γ-radiolysis). Generally, the sample is removed from the radiation

[c] Spent fuel rods are submerged in water in storage ponds to allow time for short-lived isotopes to decay before the fuel is reprocessed. The water cools the fuel and provides radiological shielding.

field before being analysed for radiochemical transformations.[101-105] If applying steady state methods to aqueous solutions, *G*-values determined for the primary yield of water radiolysis in the given environment can be correlated with observed radiochemical transformations of the solute of interest to allow mechanistic insight.

Alternatively, degradation mechanisms can be studied by pulse radiolysis, in which pulses (2-200 ns) of high-energy electrons are delivered to an irradiation cell from a linear accelerator. The behaviour of transient species can be determined by spectroscopic or conductimetric methods.[106,107] The method can also be used to calculate fundamental parameters such as rate coefficients for transient radicals and one-electron reduction potentials of redox pairs, which can be implemented in computational modelling.

Upon irradiation, approximately equal quantities of oxidising and reducing species form in the primary yield of water radiolysis, however, in the presence of air, e^-_{aq} and $H^\cdot$ quickly combine with dissolved O_2 to form the highly reductive superoxide radical (O_2^-) and the hydroperoxyl radical (HO_2). HO_2 partially dissociates to form its conjugate base, O_2^- ($pK_a = 4.9$). The superoxide radical has been reported to have low reactivity with organic species such as phenols and aliphatic acids.[108,109] The primary oxidising species is the hydroxyl radical ($HO^\cdot$), the reactivity of which is unaffected by the presence of dissolved O_2. The hydroxyl radical commonly attacks organic compounds by H-abstraction or addition to double bonds.[107] In acidic media, it is more likely that solvated electrons combine with protons to form hydrogen atoms.

APCAs and their metal chelates have been previously studied by γ-radiolysis and pulse radiolysis. APCAs have been found to be susceptible to radiolytic breakdown; generally, oxidative H-abstraction from the α-carbon position relative to the carboxylic acid group by the hydroxyl radical or hydrogen atom initiates stepwise decarboxylation reactions. With respect to γ-radiolysis, EDTA, DTPA and NTA have been found to be similarly unstable as *G*-values tend to directly correspond with the primary yield of $HO^\cdot$. γ-irradiation of neutral aqueous solution results in $G_{HO^\cdot} = 2.7 \approx G$(-EDTA)[26] $\approx G$(-NTA)[102] $< G$(-DTPA). *G*(-DTPA) is reported to be 3.3, which has been explained by a greater susceptibility of the molecule to radical oxidation by the hydrogen atom ($G_{H^\cdot}$ =

0.6).[101] For all three APCAs, the absolute *G*-values vary with changes in the pH environment and the concentration of dissolved oxygen, both of which affect the balance of reactive oxidising and reducing radical species. A pulse radiolysis mechanistic study on the decomposition of EDTA has also been reported; solutions were saturated with N_2O prior to irradiation which is a widely used technique to convert the primary yield of e^-_{aq} to $HO^\cdot$ to allow further mechanistic insight.[107]

Complexation to a metal centre has been found to affect the radiochemical behaviour of the APCAs. Much lower *G*-values were reported for Sm-DTPA complexes than for DTPA under identical conditions; it was proposed that decarboxylation of the radical-complex formed by H-abstraction was hindered by either coordination of the carboxyl groups to the metal or an increased rigidity of the ligand.[101] Another study concluded that Fe(III)-EDTA was not degraded in aerated neutral aqueous solution, which was explained by concurrent radical reduction of the Fe(III)-centre to Fe(II) and oxidative radical attack at the ligand, with subsequent electron transfer, also resulting in Fe(II) and an intact coordinating ligand.[105] The Fe(II)-EDTA species are then oxidised back to Fe(III)-EDTA by the O_2 present in solution, hence *G*(Fe(III)-EDTA) = 0. In a similar study, Ni(II)-EDTA was found to be degraded (*G*(-Ni(II)-EDTA = 2.1).[110]

γ-irradation of chelating agents in an alkaline inorganic matrix designed to simulate the mixed nuclear wastes stored at the Hanford Site was used to evaluate APCA radiolytic degradation in a sample environment more closely representative of actual nuclear waste. A GC-MS detection and quantification method also allowed for a detailed product study. 89.1% of the EDTA was found to have degraded after 100 h of irradiation (7.5×10^6 R ≈ 65.8 kGy). The degradation products found in the highest concentrations included be *N*-hydroxymethyl-*N*-methyliminodiacetic acid, *N*-(methylamine)iminodiacetic acid and ED3A.[84,111]

Further discussion of the literature concerning APCA radiolytic degradation can be found in Chapter 4 along with the results of a γ-radiolysis study into the fundamental radiation stabilities of EDTA, Fe(III)-EDTA and Fe(III)-DTPA. Radiolysis coupled with modern detection techniques and optimised methodology were used to reassess some of the conclusions previously drawn regarding APCA behaviour in a radiation field.

Data relevant to potential APCA degradation pathways in the LLWR environment helps to underpin the position of the WAC on the acceptance of APCA containing wastes and contributes to the ongoing evaluation of its appropriateness.

1.6 Aminopolycarboxylic Acid Detection Methods

APCA detection methods are numerous and varied for their use in a range of applications and environments. From an LLWR perspective, reliable and appropriate APCA detection and quantification methods are key to ensuring that incoming wastes are compliant with the WAC, i.e. do not contain concentrations of APCAs above acceptable levels, and for the purpose of monitoring environmental APCAs concentrations in samples taken from around the site.

The following sub-sections will discuss some established APCA detection methods from the literature. The sections are broadly divided into chromatographic and non-chromatographic methods; the main analytical technique used throughout this research project is a chromatographic technique (high-performance liquid chromatography (HPLC)). Further discussion of analytical methods can be found in the introduction of Chapter 2 (Section 2.1).

1.6.1 Non-Chromatographic Methods

Multiple electrochemical methods have been developed for EDTA, DTPA and NTA determination.[112] One method presented for natural and waste water analysis reported an LOD of 0.1 μg L^{-1} for EDTA by utilising differential pulse anodic stripping voltammetry for indirect detection of the ligand.[113] A potentiometric stripping analysis was used to detect EDTA and NTA to limits of 1 μg L^{-1} and 0.2 μg L^{-1}, respectively.[114] This method used ion-exchange columns to remove unwanted ions before measuring the reduction potential of the Bi(III)-APCA for quantification. Simultaneous determination of EDTA and DTPA was achieved using voltammetry with a PbO_2 indicator electrode but with lower sensitivity (EDTA LOD = 30 mg L^{-1}).[115] Other methods include potentiometry (EDTA LOD = 15 mg L^{-1}),[116] voltammetry with a

dropping mercury indicator electrode (EDTA LOD = 15 μg L^{-1}),[117] and differential pulse polarography (EDTA LOD = 1.5 mg L^{-1}).[118]

Though most electrochemical methods are simple, inexpensive, fast and sensitive, the selectivity of the methods is generally poor meaning that determination of specific complexants in natural or waste waters is often complicated.[112] Other chelating agents (e.g. humic substances, citric acid) and the many inorganic ions present in complex environmental samples make most electrochemical APCA detection methods unsuitable for application to samples of LLW.

Spectrophotometric,[79,104,105,119] titrimetric,[79,112,120] capillary electrophoretic (CE),[121-124] mass spectrometric (MS), and infra-red spectroscopic have also been reported. Spectrophotometric methods are usually based on forming a metal-chelate complex and measuring its amount directly or indirectly. Again, most procedures lack sensitivity as they do not differentiate between the absorption of different complexants and other interfering metal ions in the sample solution. However, a method for simultaneous determination of EDTA, DTPA and NTA by UV-Vis spectrophotometry reported LOD (limits of detection) of 324, 667 and 739 μmol L^{-1}, respectively.[79] CE was used for determination of NTA and EDTA speciation of their metal complexes in aqueous solution (Fe(III)-EDTA LOD = 12 μM).[124]

Selective and sensitive inductively coupled plasma (ICP) MS and electrospray ionisation (ESI) MS techniques have been used for APCA detection. These techniques allow simultaneous determination of several elements (ICP-MS) or metal-chelate molecules (ESI-MS). ICP-MS is less selective than ESI-MS but is more sensitive and works over a larger dynamic range.[125] MS detection methods are often coupled with separation techniques such as CE or liquid/gas chromatography to increase the selectivity and sensitivity of the procedure. For instance, highly sensitive EDTA detection methods involving HPLC coupled with both ESI-MS[126] and ICP-MS[127] have been reported, EDTA LOD = 0.02 μM and 125 nM, respectively. Another highly selective method was used to simultaneously quantify various synthetic Fe(III)-chelates found in fertilisers in agricultural matrices by HPLC-ESI-MS (LOD EDTA = 2.5 μM, LOD DTPA = 3.3 μM).[125] Eight APCA were recently detected at ultra-trace concentrations using an ion

chromatography (IC) method couple with ICP-MS detection (EDTA LOD = 55 ng kg^{-1}, DTPA LOD = 171 ng kg^{-1}, NTA LOD = 31 ng kg^{-1}) by indirectly quantifying coordinated Pd(II) ions.[128]

It was concluded that an attenuated total reflectance Fourier transform infra-red spectroscopic method used to quantify aqueous solutions of Na_4EDTA to a LOD of 0.3% w/w (~8×10^{-2} M) was only applicable to samples where high concentrations of EDTA might exist.[129]

1.6.2 Chromatographic Methods

Liquid chromatography (LC) methods are more common for detection of APCAs and their metal complexes than gas chromatography (GC) because GC methods requires volatility of compounds for determination. The analytes are most commonly converted into methyl, ethyl, propyl or butyl esters to obtain volatility, which makes sample preparation time-consuming and labour intensive.[112] Nonetheless, many GC methods have been developed and reported for EDTA determination because of the high sensitivity and selectivity afforded by the technique.

Flame ionisation detectors (FID) are most frequently used in GC applications and, as discussed previously, the device can be readily coupled with MS detection. GC-FID has been used to simultaneously detect methyl-esterified EDTA and DTPA in natural and waste water (EDTA LOD = 5 μg L^{-1}, DTPA LOD = 40 μg L^{-1}),[112] and ethyl-esterified EDTA and DTPA in natural waters (EDTA LOD = 3 μg L^{-1}, DTPA LOD = 12 μg L^{-1}) has been quantified using a nitrogen phosphorus detector.[130] A GC-MS method was used to quantify EDTA and various radiolytic fragments of the ligand formed during the study of its chemo-/radiolytic stability in a complex inorganic matrix designed to simulate mixed nuclear waste.[46,103,111] Various GC methods have also been used to quantify EDTA in foodstuffs,[131] steam propulsion systems,[132] as an impurity of DTPA,[133] and in sediments and fish.[134] The main advantage of GC analysis is the high sensitivity, but this generally comes at the cost of inherently longer multi-stage sample preparation procedures. Speciation studies are not possible as complexants are quantified as derivatised esters.[112]

LC techniques for APCA quantification are numerous.[112] APCAs have been detected in sample matrices that include waste waters,[135,136] natural waters,[135,137,138] sediments,[138] fertilisers,[139] chemical cleaning solutions,[79] radioactive waste solutions,[140] boiler water,[141] foodstuffs,[142] and pharmaceuticals.[143]

Chromatographic separation of APCA species in LC methods is usually achieved by either a reversed-phase (RP) stationary phase in HPLC or by IC. RP techniques often involve addition of an ion-pair (IP) reagent to the mobile phase to convert the target compounds into neutral components and increase the retention. APCAs can be separated by IC because of their polyvalent anionic character, which means they have high affinity to anion-exchange resins.[112]

UV-Vis detection is the most commonly used in LC methods, though refractive index and MS can used for when sample absorption bands are weak, there are many interfering species in the sample matrix, or for other specialist applications. Generally, LC is not as sensitive as GC, but is highly selective and much more straightforward. Pre-concentration or sample enrichment steps can be undertaken to increase method sensitivity. Determining the speciation of APCA ligands in aqueous environmental samples is of crucial importance to their analysis; speciation is affected by factors such as pH and the type and concentration of available metal ions. LC methods can be readily used to quantify the effects of APCA speciation in environmental samples as various metal-APCA complexes can de simultaneously determined.

A method for quantification of EDTA in the surrounding liquid of canned mushrooms was outlined based on IP-RP-HPLC.[142] Cu(II) was added to the pre-analysis sample matrix to coordinate the EDTA; transition metals are often added to increase the molar absorptivity of the APCA species prior to UV detection. A water-methanol mobile doped with tetrabutylammonium IP reagent achieved a LOD for Cu(II)-EDTA at 10 mg L^{-1}. To prevent interference from Fe(III) ions ($\log\beta_{Fe(III)\text{-}EDTA} = 25.1 > \log\beta_{Cu(II)\text{-}EDTA} = 18.8$), ascorbic acid was also added to the sample matrix in order to reduce Fe(III) to Fe(II) ($\log\beta_{Fe(II)\text{-}EDTA} = 14.3$). Fe(III) ions are often to employed to coordinate APCAs for detection because of their high stability, high molar absorptivity, and the natural abundance of Fe. In this instance, the Fe(III)-EDTA chromatographic peak was found to

be partly convoluted with other matrix components, in addition to the fact that EDTA was initially added to the canned mushrooms to sequester enzymatic Cu(II) ions.

Development of the previously described method[142] to include a pre-concentration step (evaporation) and addition of Fe(III) to the sample matrix resulted in a more sensitive IP-RP-HPLC method (EDTA LOD = 0.8 μg L^{-1} (10-fold pre-concentration and 100 μL injection volume)) which was applied to various aqueous environmental samples.[137] A more recent IP-RP-HPLC method was used to quantify EDTA and DTPA in pharmaceutical formulations.[143] Again, Cu(II) and Fe(III) were each added to the sample matrices to enhance UV detection. A gradient mobile phase was used to separate the Cu(II)-EDTA from other components of the sample matrix; the gradient profile was made up of pH 6.5 buffered tetrabutylammonium phosphate (IP reagent) solution and acetonitrile (LOD = 1.5 mg L^{-1}), and a similar LOD was achieved for Fe(III)-DTPA (1.8 mg L^{-1}) using different elution parameters. The APCAs were not detected in the same chromatographic sample runs.

EDTA, DTPA and NTA have been simultaneously determined by HPLC in a method designed to determine APCA concentration in detergents solutions.[79] Fe(III) was added to the sample matrices for complexation. The mobile phase parameters were optimised from another method used to determine Fe(III)-EDTA in marine microcosms at pH 4.5;[144] the best separation of the three Fe(III)-APCA complexes was achieved at 3.25 with an aqueous mobile phase containing 0.03 M sodium acetate, 0.002 M tetrabutylammonium bromide (TBA-Br; IP reagent) and 5% methanol. The column used had a C_{18} stationary phase, which refers to the length of the carbon chain attached to the silica beads packed inside the column (all of the HPLC methods described previously use a C_{18} stationary phase). LODs for EDTA, DTPA and NTA were determined to be 0.27 μM, 0.34 μM, and 0.62 μM, respectively.

Another highly sensitive method was developed for determination of dissolved EDTA species in natural waters by HPLC.[138] TBA-Br is again used as the IP reagent in a pH 3.3 formate buffered solution containing 8% acetonitrile. With pre-concentration (IC and evaporation), the EDTA detection limit for this method is reported to be 3 nM. The method was used to quantify various metal-EDTA complexes to assess the speciation

of the ligand in natural waters. The HPLC method parameters outlined in this study form the basis for the chromatographic method developed in this project.

Finally, another method in the literature details a method for EDTA quantification in feed and premix formulations.[145] Before the analyte could be quantified by IP-RP-HPLC, it was first necessary to perform a solid-liquid phase extraction to bring the EDTA into solution. This was done using an acidified $FeCl_3$ solution, which also quantitatively converts the EDTA species to Fe(III)-EDTA for enhanced UV detection. Good recoveries were obtained from the extraction process (85.6 - 92.8%) and the overall procedural LOD was reported to be 5.5 mg kg^{-1}.

The analysis of feed and premix formulations was done using a HPLC coupled with a diode-array detector (DAD).[145] The DAD is an alternative to the standard variable wavelength detector (VWD). It can be programmed to simultaneously record chromatograms over a broad wavelength range, meaning that the absorption profiles of analyte species can be extracted from the chromatographic data post-analysis. It also allows the operator to select optimal chromatograms produced at specific absorption wavelengths after the experiment has been performed (Figure 11)

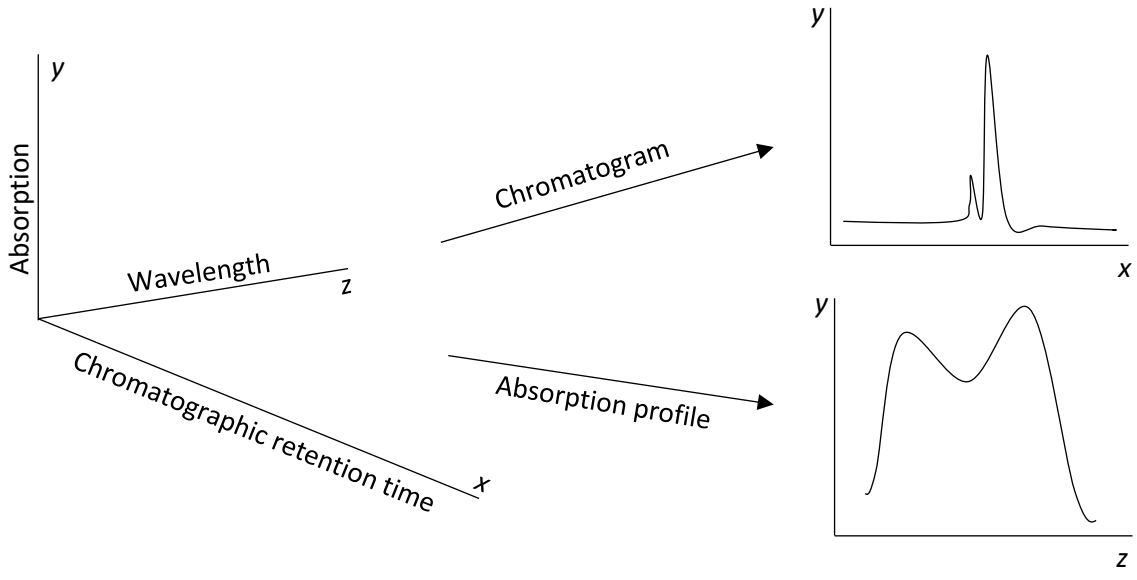

Figure 11. Schematic diagram of HPLC-DAD data.

HPLC-DAD is useful for analysis of environmental samples where ligand speciation is expected as the increased quantity of data recorded in each chromatographic analysis

affords more information to identify unknown species and optimise chromatogram profiles to minimise interference from other compounds or metal ions present in the sample matrix.

Quantification by chromatographic analysis usually relies on calculation of the peak area to give an integration result in absorbance units (AU), which is converted to concentration by comparison of the data to a calibration curve. Peak integration is usually performed on the computer software provided with the chromatographic instrument. Determination of peak area can be complicated by interfering species which can create overlapping peaks. Statistical operations of varying levels of complexity can be applied to deconvolute overlapping peaks to determine the true peak area of the analyte of interest. These include least-squares fitting (LSF) and parallel factor analysis (PARAFAC), both of which are discussed in greater detail in Chapter Two.

1.7 Project Aims

Two broad aims can be outlined for the project: i) to develop, optimise and validate an APCA quantification method that is suitable for application to samples of relevance to LLWR, and ii) to apply the method to various real samples to obtain useful data.

The targeted method must be sensitive enough to be capable of APCA determination at the trace concentrations expected to arise in wastestreams and in the environment, selective to discern between different components of the complex matrices that make up LLW and environmental samples, and robustly accurate to consistently deliver reliable results for a range of samples.

Following the process of optimisation, the method should allow detection of APCAs at concentrations on the order of 1 μM or lower. This figure relates to the finding that EDTA concentrations > 1 μM increase the risk of radionuclide mobilisation above acceptable limits.[14,19] The method should be suitably selective to allow simultaneous detection of the three key APCAs relevant to LLWR (EDTA, DTPA and NTA), whilst maintaining its sensitivity.

The selectivity of APCA detection methods in complex sample matrices can be compromised by speciation of the ligand to form a range of metal ion complexes with the various metals present in solution; development of an appropriate method for LLWR should include a strategy for addressing any complications cause by speciation, such as augmentation of the detection method with enhanced statistical data analysis tools.

Once a suitable method has been developed, optimised, and validated using standards, it should be ready for application to a range of real samples of relevance to LLWR; i) trench leachate from the site, ii) the residue generated by incineration of spent ion-exchange resins intended for disposal, and iii) samples from γ-radiolysis experiments designed to determine the radiological fate of the key APCAs and their complexes.

Trials on different samples should necessitate further development steps to modify and optimise certain aspects to ensure maximal compatibility of method and sample (e.g. sample pre-treatment steps). Analysis of trench leachate aims to provide confidence that APCAs are not present in leachate in concentrations that have been deemed to be unsafe (> 1 μM). Further sampling for EDTA in trench leachate to enhance confidence in previous findings[52] was specifically requested by the Environment Agency.[14]

Samples of incinerated ion-exchange resin have been generated by a trial incineration procedure intended to make the waste suitable for disposal. LLWR require demonstration of the destruction of the EDTA content to below acceptable concentrations because the waste currently contains levels of EDTA that would consume a disproportionate amount of the remaining APCA capacity. Application of the quantification method aims to demonstrate that the ligand has been destroyed to concentrations that are below an acceptably low LOD (1 mg kg^{-1}).

Radiolysis experiments will be performed on the APCAs and their metal complexes to determine their behaviour in a γ-radiation field. Following irradiation, application of the method will aim to quantify the degraded parent species and detect potential

radiolytic degradation products. Greater understanding of the potential degradation mechanisms of the APCAs in the repository environment helps to underpin the position of the WAC on the acceptance of APCA containing wastes and contributes to the ongoing evaluation of its appropriateness.

1.8 References

1. Nuclear Decommissioning Authority (NDA), *Radioactive Wastes in the UK: A Summary of the 2016 Inventory*, ISBN: 978-1-905985-33-3, NDA, Cumbria, UK, 2017.
2. NDA, *Understanding Activities that Produce Radioactive Wastes in the UK*, Ref: 23527545, NDA, Cumbria, UK, 2015.
3. NDA, *Radioactive Wastes in the UK: UK Radioactive Waste Inventory Report*, ISBN: 978-1-90585-33-3, NDA, Cumbria, UK, 2017.
4. Department of Energy and Climate Change (DECC), *UK Strategy for the Management of Solid Low Level Waste from the Nuclear Industry*, URN 15D/472, DECC, London, UK, 2016.
5. LLWR, *The 2011 Environmental Safety Case: Environmental Safety Case – Main Report*, LLWR/ESC/R(11)10016, LLWR, Cumbria, UK, 2011.
6. LLWR, *Environmental Safety Case: Site History and Description*, LLWR/ESC/R(11)10018, LLWR, Cumbria, UK, 2011.
7. LLWR, *Environmental Safety Case: Inventory*, LLWR/ESC/R(11)10019, LLWR, Cumbria, UK, 2011.
8. LLWR, *Environmental Safety Case: Engineering Design*, LLWR/ESC/R(11)10020, LLWR, Cumbria, UK, 2011.
9. LLWR, *Environmental Safety Case: Near Field*, LLWR/ESC/R(11)10021, LLWR, Cumbria, UK, 2011.
10. LLWR, *Environmental Safety Case: Optimisation and Development Plan*, LLWR/ESC/R(11)10025, LLWR, Cumbria, UK, 2011.
11. Imagery: TerraMetrics. Map data: Google. Accessed through: maps.google.com, 2019.
12. Imagery: CNES/Airbus, Infoterra Ltd & Bluesky, Landsat/Copernicus, Maxar Technologies. Map data: Google. Accessed through: maps.google.com, 2019.
13. Environment Agency (EA), *Guidance on Requirements for Authorisation: Geological Disposal Facilities on Land for Solid Radioactive Wastes*, GEHO0209BPJM-E-E, EA, Bristol, UK, 2009.
14. Environment Agency (EA), *Review of LLW Repository Ltd's 2011 Environmental Safety Case: Inventory and Near Field*, Issue 1, EA, Bristol, UK, 2015.
15. LLWR, *Waste Acceptance Criteria – Low Level Waste Disposal*, WSC-WAC-LOW – Version 5.0, LLWR, Cumbria, UK, 2016.
16. LLWR, *Waste Acceptance Criteria – Supercompactable Waste*, WSC-WAC-SUP – Version 3.0, LLWR, Cumbria, UK, 2012.
17. LLWR, *Review of the Potential Effects of Complexants on Contaminant Transport at the* LLWR, LLWR,ESC/R(13)10054, LLWR, Cumbria, UK, 2013.
18. M. Randall, C. Lennon and B. Rigby, *Biogeochemical Aspects of the Waste Acceptance Criteria at LLWR*, NNL(10) 11348 Issue 3.0, LLWR, Cumbria, UK, 2011.
19. M. Kelly, *Preliminary Calculations to Assess the Impact of EDTA on Health Hazards Arising from the LLWR*, LLWR/ESC/SPE(12)098, LLWR, Cumbria, UK, 2013.
20. J. S. Small, L. Abrahamsen and M. Angus, *Information to Underpin the Waste Acceptance Criteria for the LLWR*, NNL(11) 11889, LLWR, Cumbria, UK, 2013.

21. D. C. Harris, *Quantitative Chemical Analysis*, W. H. Freeman and Company, New York, 7th edn., 2007.
22. G. A. Lawrence, *Introduction to Coordination Chemistry*, Wiley, New York, 1st edn., 2010.
23. R. M. Smith, A. E. Martell, *Critical Stability Constants*, Plenum Press, New York, 6th edn., 1989.
24. P. Kocot, A. Karocki and Z. Stasicka, *J. Photochem. Photobiol.*, 2006, **179**, 176-183.
25. J. L. Hoard, M. D. Lind, J. V. Silverton, *J. Am. Chem. Soc.*, 1961, **83**, 2770-2771.
26. M. D. Lind, M. J. Hamor, T. A. Hamor, J. L. Hoard, *Inorg. Chem.*, 1964, **3**, 34-43.
27. M. Dellert-Ritter, R. van Eldik, *J. Chem. Soc., Dalton Trans.*, 1992, 1037-1044.
28. A. Brausen, R. van Eldik, *Inorg. Chem.*, 2004, **43**, 5351-5359.
29. J. L. Lambert, C. E. Godsey, L. M. Setz, *Inorg. Chem.*, 1963, **2**, 127-129.
30. L. Lattuada, A. Barge, G. Cravotto, G. B. Giovenzana and L. Tei, *Chem. Soc. Rev.*, 2011, **40**, 3019-3049.
31. G. Grynkiewicz, M. Poenie and R. Y. Tsien, *J. Biol. Chem.*, 1985, **260**, 3440-3450.
32. D. K. Tripathi, S. Singh, S. Gaur, S. Singh, V. Yada, S. Liu, V. Singh, S. Sharma, P. Srivastava, S. M. Prasad, N. Dubey, D. K Chauhan and S. Sahi, *Front. Environ. Sci.*, **5**, 2017.
33. R. C. Hider and X. Kong, *Nat. Prod. Rep.*, 2010, **27**, 637-657.
34. M. Takahashi, Y. Terada, I. Nakai, H. Nakanishi, E. Yoshimura, S. Mori and N. K. Nishizawa, *The Plant Cell*, 2003, **15**, 1263-1280.
35. H. Block, B. Maertens, A. Spriesterbach, N. Brinker, J. Kubicek, R. Fabis, J. Labahn and F. Schäfer, in M*ethods in Enzymology*, ed. R. R. Burgess and M. P. Deutscher, Elsevier, Amsterdam, 2nd edn., 2009, vol. 463, ch. 27, pp. 439-473.
36. I. T. Dorn , K. R. Neumaier and R. Tampé , *J. Am. Chem. Soc.*, 1998, **120** , 2753-2763.
37. A. Dean Sherry, P. Caravan and R. E. Lenkinski, *J. Magn. Reson. Imaging*, 2009, **30**, 1240-1248.
38. H. J. Weinmann, R. C. Brash, W. R. Press and G. E. Wesbey, *Am. J. Roentgenol.*, 1984, **142**, 619-624.
39. P. Caravan, J. J. Ellison, T. J. McMurry, R. B. Lauffer, *Chem. Rev.*, 1999, 99, 2293-2342.
40. R. J. Abergel, in *Metal Chelation in Medicine*, ed. R. R. Crichton, R. J. Ward and R. C. Hider, Royal Society of Chemistry, Cambridge, 2016, ch. 6, pp. 183-212.
41. G. J.-P. Deblonde, M. P. Kelley, J. Su, E. R. Batista, P. Yang, C. H. Booth and R. J. Abergel, *Angew. Chem. Int. Edit.*, 2018, **57**, 4521-4526.
42. World Health Organisation (WHO), *WHO Model List of Essential Medicines (21st List)*, WHO/MVP/EMP/IAU/2019.06, Geneva, 2019.
43. J. R. Hart, in *Ullmann's Encyclopedia of Industrial Chemistry*, ed. Wiley-VCH, Weinheim, Germany, 2011, vol. 13, pp. 573-578.
44. European Chemical Bureau (ECB), *European Union Risk Assessment Report – Tetrasodium Ethylenediaminetetraacetate Summary*, ECB, Ispra, Italy, 2004.
45. C. Oviedo and J. Rodriguez, *Quim. Nova*, 2003, **26**, 901-905.
46. A. P. Toste and T J. Lechner-Fish, *Waste Manag.*, 1993, **13**, 237-244.
47. J. L. Means and C. A. Alexander, *Nucl. Chem. Waste Mgt.*, 1981, **2**, 183-196.
48. Nuclear Energy Agency Task Group on Decontamination, *Decontamination Techniques Used in Decommissioning Activities*, Nuclear Energy Agency, 1998.
49. Radioactive Waste Management (RWM), *Geological Disposal: Guidance on the disposability of waste packages containing chemical decontamination agents*, WPS/928/01, RWM, Oxford, UK, 2017.
50. LLWR, *Guidance on WAC Requirements for Complexants*, LLWR/ESC/Mem(16)292, LLWR, Cumbria, UK, 2016.

51. Ministry of Defence, *Ion-Exchange Resin Information Pack*, RESIN IP101, Draft Final, 2015.
52. D. J. Wilkinson, *Results of the Measurement of the Concentration of Dissolved EDTA in Trench Waters from LLWR by HPLC*, NVR1068b/Babcock, 2013.
53. R. Howard, in *Societal risk assessment: how safe is safe enough?*, eds. J. Richard, C. Schwing and W. A. Albers, Springer, New York, 1980, pp. 89-113.
54. T. F. Rees and J. M. Cleveland, *Characterization of plutonium in waters at Maxey Flats, Kentucky, and near the Idaho Chemical Processing Plant, Idaho*, IAEA-SM-257/66, International Atomic Energy Agency (IAEA), Vienna, Austria, 1982.
55. D. J. Silviera, *The potential influence of organic compounds on the transport of radionuclides from a geologic repository*, PNL-3414, Pacific Northwest Laboratory, Richland, WA, 1981.
56. A. E. Martell, R. J. Motekaitis, A. R. Fried, J. S. Wilson and D. T. MacMillan, *Can. J. Chem.*, 1975, **53**, 3471-3476.
57. Department of the Environment (DOE), *Wet Oxidation of Organic Wastes*, DoE/HMIP/RR/91/016, DOE, London, UK, 1991.
58. J. Rämö and M. Sillanpää, *J. Clean. Prod.*, 2001, **9**, 191-195.
59. K. R. Butter and A. L. Goldsmith, *Photodecomposition of Decontamination Reagents: Active Process Development*, Report R 2334, Atomic Energy Establishment of Winfrith (AEEW), Dorset, UK, 1988.
60. J. Brunning, K. R. Butter, H. Chapman C. R. and Mitchel, *Photodecomposition of Decontamination Reagents: Fate of Active Species and Temperature Dependence of the Reaction,* Report R 2525, AEEW, Dorset, UK, 1989.
61. Butter, K. R. and Goldsmith, A. L., *Photodecomposition of Decontamination Reagents: Inactive Process Development*, Report R 2281, AEEW, Dorset, UK, 1987.
62. S. N. R. Pakalapatti, B. N. Popov, R. E. White and D. T. Hobbs, *J. Electrochem. Soc.*, 1996, **143**, 1636-1643.
63. LLWR, *National Waste Program Strategic Review*, NWP/REP/147, LLWR, Cumbria UK, 2016.
64. R. H. Flowers and D. H. Day, *Organic Materials in Waste for Land Burial*, WMSC(85)7, Atomic Energy Research Establishment, Harwell, UK, 1985.
65. International Atomic Energy Agency (IAEA), *Predisposal Management of Organic Radioactive Waste*, Technical Reports Series No. 427, IAEA, Vienna, Austria, 2004.
66. R. W. D. Killey, J. O. McHugh, D. R. Champ, E. L. Cooper and J. L. Young, *Environ. Sci. Technol.*, 1984, **18**, 157-163.
67. P. Biddle, B. F. Greenfield, B. J. Myatt, G. P. Robertson and M. W. Spindler, *The Effects of the Degradation of Some Organic Polymers and Ion-exchange Resins on Plutonium Solubility in the Near Field*, AEAT/ERRA-0355, AEA Technology, Harwell, UK, 2002.
68. M. Sillanpää, *Rev. Environ. Contam. Toxicol.*, 1997, **152**, 85-111.
69. P. Gerike and W. K. Fischer, *Ecotoxicol. Environ. Saf.*, 1979, **3**, 159-173.
70. P. Gerike and W. K. Fischer, *Ecotoxicol. Environ. Saf.*, 1981, **5**, 45-55.
71. J. L. Means, T. Kucak and D. A. Crerar, *Environ. Pollut. B*, 1980, **1**, 1, 45-60.
72. J. M. Tiedje, *Appl. Microbiol.*, 1975, **30**, 327-329.
73. H. Bolton, S. W. Li, D. J. Workman and D. C Girvin, *J. Environ. Qual.*, 1993, **22**, 125-132.
74. V. Sykora, P. Pitter, I. Bittnerova and T. Lederer, *Water Res.*, 2001, **34**, 2010-2016.
75. J. M. Tiedje and B. B. Mason, *Soil Sci. Am. Proc.*, 1974, **38**, 278-283.
76. T. E. Ward, *Ecotoxicol. Environ. Saf.*, 1985, **11**, 112-125.
77. R. J. Shimp, E. V. Lapsins and R. M. Ventullo, *Environ. Toxicol. Chem.*, 1994, **13**, 205-212.
78. M. A. Tabatabai and J. M. Bremner, *Soil Biol. Biochem.*, 1975, **7**, 103-106.
79. P. Laine and R. Matilainen, *Anal. Bioanal. Chem.*, 2005, **382**, 1601-1609.

80. R. Frank and H. Rau, *Ecotoxicol. Environ. Saf.*, 1990, **19**, 55-63.
81. F. G. Kari and W. Giger, *Environ. Sci. Technol.*, 1995, **29**, 2814-2827.
82. R. J. Motekaitis, D. Hayes and A. E. Martell, *Can. J. Chem.*, 1979, **57**, 1018-1024.
83. R. J. Motekaitis, B. X. Cox, P. Taylor, A. E. Martell, B. Miles and T. J. Tvedt, *Can. J. Chem.*, 1982, **60**, 1207-1213.
84. A. P. Toste, K. J. Polach and T. Ohnuki, *J. Radioanal. Nucl. Chem.*, 2005, **263**, 559-565.
85. R. G. Zepp and D. M. Cline, *Environ. Sci. Technol.*, 1977, **11**, 359-366.
86. S. Trapp, R. Briiggemann and B. Miinzer, in *Water Pollution: Modelling, Measuring and Prediction*, ed. L. C. Wrobel and C. A. Brebbia, Computational Mechanics, Southampton, 1991, vol. 1, pp 195.
87. H. B. Lockhart and R. V. Blakely, *Environ. Lett.*, 1975, **9**, 19-31.
88. H. B. Lockhart and R. V. Blakely, *Environ. Sci. Technol.*, 1975, **9**, 1035-1038.
89. A. Svenson, L. Kaj and H. Björndal, *Chemosphere*, 1989, **18**, 1805-1808.
90. J. M. Tiedje, *J. Environ. Qual.*, 1977, **6**, 21-26.
91. F. G. Kari and W. Giger, *Water Res.*, 1996, **30**, 122-134.
92. J. B. Rodriguez, A. Mutis, M. C. Yeber, J. Freer, J. Baeza and H. D. Mansilla, *Water Sci. Tech.*, 1999, **40**, 267-272.
93. K. Pirkanniemi, S. Metsärinne and M. Sillanpää, *J. Hazard. Mater.*, 2007, **147**, 556-561.
94. W. W. Wendlandt, *Anal. Chem.*, 1960, **32**, 848-849.
95. T. R. Bhat and R. K. Iyer, *J. Inorg. Nucl. Chem.*, 1967, **29**, 179-185.
96. J. Chen, J. Gao and X. Wang, *J. Braz. Chem. Soc.*, 2006, **17**, 880-885.
97. D. L. Venezky and W. E. Rudzinski, *Anal. Chem.*, 1984, **56**, 315-317.
98. *Eur. Pat.*, WO9603643, 1995.
99. C. E. de Almeida, R. Ochoa, M. C. de Lima, M. G. David, E. J. Pires, J. G. Peixoto, C. Salata and M. A. Bernal, *PLoS One*, 2014, **9**.
100. M. E. Dzaugis, A. J. Spivack and S. D'Hondt, *Rad. Phys. Chem.*, 2015, **115**, 127-134.
101. N. E. Bibler, *J. Inorg. Nucl. Chem.*, 1972, **34**, 1417-1425.
102. K. Sahul and B. K. Sharma, *J. Radioanal. Nucl. Chem.*, 1987, **109**, 321-327.
103. A. P. Toste, K. J. Polach and T. Ohnuki, *J. Radioanal. Nucl. Chem.*, 2005, **263**, 559-565.
104. S. N. Bhattacharyya and K. P. Kundu, *Int. J. Radiat. Phys. Chem.*, 1972, **4**, 31-41.
105. K. P. Kundu and N. Matsuura, *Int. J. Radiat. Phys. Chem.*, 1975, **7**, 565-571.
106. C. Houée-levin, in *Redox Cell Biology and Genetics Part B, Methods in Enzymology*, eds. C. K. Sen and L. Packer, Elsevier, Amsterdam, 2002, Chantal Houée-levin, in Methods in Enzymology, 2002, vol. 353, ch. 4, pp. 35-44.
107. B. Höbel and C. von Sonntag, J. Chem. Soc., Perkin Trans. 2, 1998, 509-513.
108. M. Sánchez-Polo, J. López-Peñalver, G. Prados-Joya, M. A. Ferro-García and J. Rivera-Utrilla, *Water Res.*, 2009, **43**, 4028-4036.
109. A. A. Basfar, H. M. Khan, A. A. Al-Shahrani and W. J. Cooper, *Water Res.*, 2005, **39**, 2085-2095.
110. S. N. Bhattacharyya and K. P. Kundu, *Rad. Res.*, 1972, **51**, 45-55.
111. A. P. Toste, *J. Radioanal. Nucl. Chem.*, 1998, **235**, 213-219.
112. M. Sillianpää, M.-L. Sihvonen, *Talanta*, 1997, **44**, 1487-1497.
113. A. Voulgaropoulos and N. Tzivanakis, *Electroanalysis*, 1992, **4**, 647-651.
114. M. Fayyad, M. Tutunji and Z. Taha, *Analyt. Lett.*, 1988, **21**, 1425-1432.
115. T. Yoshimura, *Fresen. J. Anal. Chem.*, 1981, **307**, 197-201.
116. J. Horacek and R. Pribil, *Talanta*, 1969, **16**, 1495-1499.
117. T. Kitagawa and Y. Kanei, *Bunseki Kagaku*, 1979, **19**, 482-487.
118. R. J. Stolzberg, *Anal. Chim. Acta*, 1977, **92**, 139-148.

119. T. Hamano, Y. Mitsuhashi, N. Kojima, N. Aoki, M. Shibata, Y. Ito and Y. Oji, *Analyst*, 1993, **118**, 909-912.
120. G. G. Clinckemaille, *Anal. Chim. Acta*, 1968, **43**, 518-520.
121. S. Motomizu, M. Oshima, S. Matsuda, Y. Obata, H. Tanaka, *Anal. Sci.*, 1992, **8**, 619-624.
122. T. Wang and S. F. Y. Li, *J. Chromatogr. A*, 1995, **707**, 343-353.
123. B. Baraj, M. Martinez, A. Sastre and M. Aguilar, *J. Chromatogr. A*, 1995, **695**, 103-111.
124. G. Owens, V. K. Ferguson, M. J. Mclaughlin, I. Singleton, R. J. Reid and F. A. Smith, *Envrion. Sci. Technol.*, 2000, **34**, 885-891.
125. A. Álvarez-Fernández, I. Orera, J. Abadía and A. Abadía, *J. Am. Soc. Mass Spectrom.*, 2007, **18**, 37-47.
126. A. Dodi and V. Monnier, *J. Chromatogr. A*, 2004, **1032**, 87-92.
127. A. A. Ammann, *Anal. Bioanal. Chem.*, 2002, **372**, 448-452.
128. D. Nette and A. Seubert, *Anal. Chim. Acta*, 2015, **884**, 124-132.
129. L. Suárez, R. Garciá, F. A. Riera, and M. A. Diez, *Talanta*, 2013, **115**, 652-656.
130. M. Sillianpää, J. Sorvari and M.-L. Sihvonen, *Chromatographia*, 1996, **42**, 578-582.
131. D. T. Williams, *J. Assoc. Off. Anal. Chem.*, 1974, **57**, 1383-1385.
132. P. J. Sniegoski and D. L. Venezky, *J. Chromatogr. Sci.*, 1974, **12**, 359-361.
133. M. L. Blank and F. Snyder, *J. Chromatogr.*, 1979, **170**, 379-383.
134. Y. Nishikawa and T. Okumura*, J. Chromatogr. A*, 1995, **690**, 109-118.
135. J. Dai, G. R. Helz, *Anal. Chem.*, 1988, **60**, 301-305.
136. C. Randt, R. Wittlinger and W. Merz, *Fresen. J. Anal. Chem.*, 1993, **346**, 6, 728-731.
137. P. J. M. Bergers and A.C. De Groot, *Wat. Res.*, 1994, **28**, 639-642.
138. B. Nowack, F. G. Kari, S. U. Hilger and L. Sigg, *Anal. Chem.,* 1996, **68**, 561-566.
139. I. V. Gucht, *J. Chromatogr. A*, 1994, **671**, 359-365.
140. M. Unger, E. Mainka and W. König, *Fresen. J. Anal. Chem.*, 1987, **329**, 50-54.
141. D. L. Venezky and W.E. Rudzinski, *Anal. Chem.*, 1984, **55**, 315-317.
142. J. De Jong, A. Van Polanen and J. J. M. Driessen, *J. Chromatogr.*, 1991, **553**, 243-248.
143. G. Wang and F. P. Tomasella, *J. Pharm. Anal.*, 2016, **6**, 3, 150-156.
144. J. Virtapohja and R. Alén, *Chemosphere*, 1999, **38**, 143-154.
145. F. Chiumiento, A. D'Aloise, F. Marchegiani and V. Melai, *Food Chem.*, 2015, **175**, 452-456.

Blank page

Chapter Two: Quantification of Common Aminopolycarboxylic Acids in Trench Leachate from the Low Level Waste Repository

James A. O'Hanlon[a†], Robert D. Chapman[b], Frank Taylor[c] and Melissa A. Denecke[d]

[a,b,d] The Chemistry Building, The University of Manchester, Oxford Road, Manchester, UK, M13 9PL.

[c]Pelham House, Pelham Drive, Calderbridge, Seascale, Cumbria, UK, CA20 1DB.

[†]Corresponding Author e-mail: james.ohanlon@manchester.ac.uk.

Scope

The first results of this thesis are presented in Chapter Two in the form an author accepted manuscript.[1] The scope of the research was to develop, validate and implement a method for APCA quantification in complex environmental matrices. HPLC was selected as literature review and preliminary experimentation determined the technique to be suitably selective (chromatographic separation) and sensitive (UV-detection of Fe(III)-APCA complexes).

HPLC method parameters were initially based on those outlined by Nowack *et al.* but optimised for the purposes of this study.[2] Stationary phase, mobile phase and injection parameters have all been adjusted. Once optimised, the method was validated using standards of Fe(III)-EDTA, Fe(III)-DTPA and Fe(III)-NTA, and calibrated accordingly. Highlighted results can be found in this chapter and a more comprehensive dataset is presented in the Supplementary Information (Appendix 1).

The chromatographic peaks of Fe(III)-EDTA and Co(III)-EDTA were found to be unresolvable. This was judged to be potentially problematic for the quantification procedure, which relies on determination of the Fe(III)-EDTA peak area. Therefore, assessment of the comparative performance of two peak deconvolution strategies was

included in the method development phase of this project; the results of which can be found in Section 2.5 of this chapter and in Appendix 1.

Finally, the optimised, validated and calibrated HPLC procedure was applied to samples of trench leachate from the LLWR site to determine the APCA concentration in real environmental samples, the findings of which are presented in this chapter.

The aim of this work was to prove that a sensitive and selective method had been successfully developed and provide justification for the final parameters. Application of the method to samples from LLWR aimed to build confidence in the understanding of APCA levels in the repository near field; in order for the results to be useful, a substantial body of empirical evidence was required to underpin the validity of the detection method.

CRediT Author Statement:

J. A. O'Hanlon: Conceptualisation, Methodology, Validation, Formal analysis, Investigation, Data curation, Writing – original draft preparation, Visualisation. R. D. Chapman: Software, Formal analysis. F. Taylor: Resources, Writing – reviewing and editing, Project administration, Funding acquisition. M. A. Denecke: Conceptualisation, Methodology, Writing – review and editing, Supervision, Project administration, Funding acquisition.

1. J. A. O'Hanlon, R. D. Chapman, F. Taylor and M. A. Denecke, *J. Radioanal. Nucl. Chem.*, 2019, **322**, 1915-1929.
2. B. Nowack, F. G. Kari, S. U. Hilger and L. Sigg, *Anal. Chem.,* 1996, **68**, 561-566.

Abstract

The aminopolycarboxylic acids (APCAs), ethylenediaminetetraacetic acid (EDTA), diethylenetriaminepentaacetic acid (DTPA) and nitrilotriacetic acid (NTA), are used as decontamination agents throughout the nuclear industry; therefore, APCAs are often found in radioactive waste. Limits of acceptance on APCAs are imposed on wastes consigned to the Low Level Waste Repository (LLWR) because, when present in the waste, the ligands have the potential to mobilise otherwise surface-bound or solid radionuclides, making them available for transport to groundwater and ultimately to

the bio-sphere. A selective and sensitive methodology to detect and quantify these ligands in a range of complex matrices is advantageous in supporting waste acceptance processes. A reversed-phase high-performance liquid chromatography (HPLC) procedure has been applied for quantification of EDTA, DTPA and NTA in their Fe(III)-complex form. Method validation results show linearity (r^2 > 0.999), precision (intra/inter-day %RSD ≤ 10%), accuracy (recovery = 100 ± 3%), sensitivity (minimum limits of detection = 0.31, 0.38 and 4.3 μM for EDTA, DTPA and NTA, respectively) and selectivity (simultaneous determination of the three APCA complexes achieved with baseline resolution) for Fe(III)-APCAs in aqueous solution. Chromatographic peak overlap is observed for samples containing Fe(III)- and Co(III)-EDTA; two deconvolution methods (2D least-squares fitting vs. parallel factor analysis (PARAFAC)) were applied to resolve the peaks and the performances compared. The optimised HPLC method was applied to trench leachate samples from the LLWR site. EDTA was detected with 0.4 μM < concentrations < 1 μM in samples from four of the six sampling locations tested. The levels are not considered sufficient to increase the risk of radionuclide mobilisation. The technique is considered to be robust and will be considered further in informing limits of acceptance on APCAs.

Keywords

High-performance liquid-chromatography, aminopolycarboxylic acids, ethylenediaminetetraacetic acid, PARAFAC, low level radioactive waste.

2.1 Introduction

The Low Level Waste Repository (LLWR, near Drigg, Cumbria) is the United Kingdom's national facility for the disposal of low level radioactive waste (LLW). LLW consigned to the repository is encapsulated in a cementitious grout within mild steel ISO containers and stacked in engineered vaults. Operations at the site are planned to extend into the early part of the next century.[1]

The aminopolycarboxylic acids (APCAs), ethylenediaminetetraacetic acid (EDTA), diethylenetriaminepentaacetic acid (DTPA) and nitrilotriacetic acid (NTA), are used

throughout the nuclear industry in decontamination agents used, for example, in decommissioning processes.[2-5] Left untreated, APCAs can be present in repository consigned wastes. These ligands are chelators and can potentially coordinate, solubilise and mobilise otherwise surface adsorbed or solid radionuclides in the waste. This can lead to a negative impact on the environment; upon contact with infiltrating water, radioactive or heavy metal ions complexed and sequestered by APCAs can be transported out of the repository, through the near field, and into the geo/bio-sphere.[4-7] Another related effect of such chelating and mobilisation is potential destabilisation of cementitious wasteforms through coordination and solubilisation of Ca^{2+} in the cement.[8] For these reasons, the APCAs were part of LLWR's focus in the 2011 Environmental Safety Case (2011 ESC), which is a pre-requisite for the granting of an Environmental Permit to dispose of LLW in the repository.[1]

The environmental permit for the LLWR originally prohibited acceptance of wastes containing organic complexants.[9] An application to the Environment Agency was made in 2015 to vary the permit to allow the disposal of organic complexants, alongside other improvements, provided evidence from geochemical modelling that APCAs could be safely disposed in waste under stringent controls.[10-12] Modelling of radionuclide behaviour in the presence of EDTA indicated that a concentration of 1 μM in the LLWR trenches and 6 μM loading in its vaults does not increase the associated risk of radionuclide mobilisation beyond legal, acceptable limits.[11,13]

To fulfil the constraints outlined by the revised permit and detailed in the current Waste Acceptance Criteria (WAC)[12], a robust methodology to quantify APCAs at trace concentrations to an acceptable degree of certainty is of considerable benefit to demonstrate waste compliance. The method must be capable of quantifying the analytes in a range of matrices; potential matrices include water derived from trench leachate and incoming waste-streams from a range of sources (e.g. ion-exchange resins generated from the operation and maintenance of submarine nuclear reactors[14]).

An additional aspect important for APCA quantification and related to waste acceptance is the fact that the APCAs, distinct from other organic complexants, exhibit

varying degrees of environmental persistence. EDTA is known to be highly resistant to biodegradation, especially under anaerobic or reducing conditions, whilst microbial degradation of NTA has been observed. [4,8,11,13,15-18] Reports in the literature are less conclusive about the environmental fate of DTPA, but suggest that it will degrade faster than EDTA, but at a slower rate than NTA.[4,16,19] Abiotic factors that also impact the rate of APCA degradation include photolytic[20], radiolytic[21] and chemical degradation pathways.[22] The latter are facilitated by a high ionic strength of disposed waste[23] and a high pH environment caused by the grouting cement.[24]

Historically, different methods have been used for APCA determination, e.g. titrimetric, liquid/gas-chromatographic[16,18,25], potentiometric[16,26], capillary electrophoretic[27] and spectrophotometric methods.[28] High-performance liquid-chromatography (HPLC) has been proven to be a reliable method for APCA analysis in complex sample matrices, owing to its high selectivity and sensitivity.[16,18,25,29-31] Most HPLC methods involve a reversed-phase (RP) system with UV-detection of APCA as its Fe(III) or Cu(II) complex[16,30,31] (use of other metal ions has been reported, e.g. Ni, Cr(III), Zn, Co, Pb[18], Gd(III), Lu(III)[28]). A range of mobile phases have been successfully applied to elute the complex species (e.g. acidified Fe(III) chloride solution[29], water-methanol and acetonitrile-phosphate buffer[30]). In 1996 Nowack *et al.* report a RP-HPLC metal-EDTA quantification method, implementing a formate-formic acid buffer.[18] Upon inclusion of a pre-concentration step, they reported the limit of detection (LOD) to be 3 nM for Fe(III)-EDTA. Nowack's method was designed for EDTA analysis in natural aqueous samples with heterogeneous phases, making it ideal for application to LLWR samples.

We have developed and tested a modification of the Nowack method for simultaneous detection of EDTA, DTPA and NTA in the form of their Fe(III)-complexes. Our results using this method following optimisation are compared with those from the literature.[16,25,32] Developments in modern stationary phase technology have seen the rise of monolithic silica columns as a viable alternative to conventional particle-based columns.[33] We have performed comparative test of the method using both types of

stationary phase: commercially available monolithic silica (Chromolith) and a conventional C_{18} column.

The RP-HPLC EDTA quantification method relies on the conversion of unbound-EDTA or complexed-EDTA to Fe(III)-EDTA for detection at a pre-determined wavelength of maximum absorption (258 nm) and retention time. The ferric ion was used because of its relatively high $\log\beta_{\text{M-EDTA}}$ stability constant (25)[34] and environmental ubiquity. However, real sample matrices may contain a range of metal ions with the potential to interfere with the analysis. One example of this is the Co(III) ion, which has an EDTA stability constant many orders of magnitude higher than that of Fe(III) ($\log\beta_{\text{Co(III)-EDTA}}$ = 40)[34]. Therefore, if the Co(III) ion or Co(III)-EDTA exist in the sample matrix, formation of or conversion to the Fe(III)-EDTA complex species may be thermodynamically unfavourable. In this case, the interfering species must also be quantified to accurately quantify the EDTA present.

The quantification of both Fe(III)-EDTA and Co(III)-EDTA is challenging, due to their chemical similarity. Their HPLC retention times using our method are roughly 0.15 min apart, meaning that the chromatographic peaks are convoluted. The difference in the electronic configuration between the two transition metal centres contribute to distinctive UV-absorption maxima (Fe(III)-EDTA λ_{max} = 258 nm (ε_{258} = 9.255 mAU μmol^{-1} L), Co(III)-EDTA λ_{max} = 228 nm (ε_{228} = 17.02 mAU μmol^{-1} L)) (AU = absorption units). The HPLC-UV detector used is a diode-array detector (DAD), which allows simultaneous data acquisition over a broad spectral range, for the entire chromatographic range, resulting in three-dimensional datasets, such as that plotted in Figure 1 (x = retention time, y = intensity and z = wavelength of absorption). From Figure 1 it is evident that, although the two M(III)-EDTA have different absorption maxima, both species absorb over the majority of the UV-wavelength range.

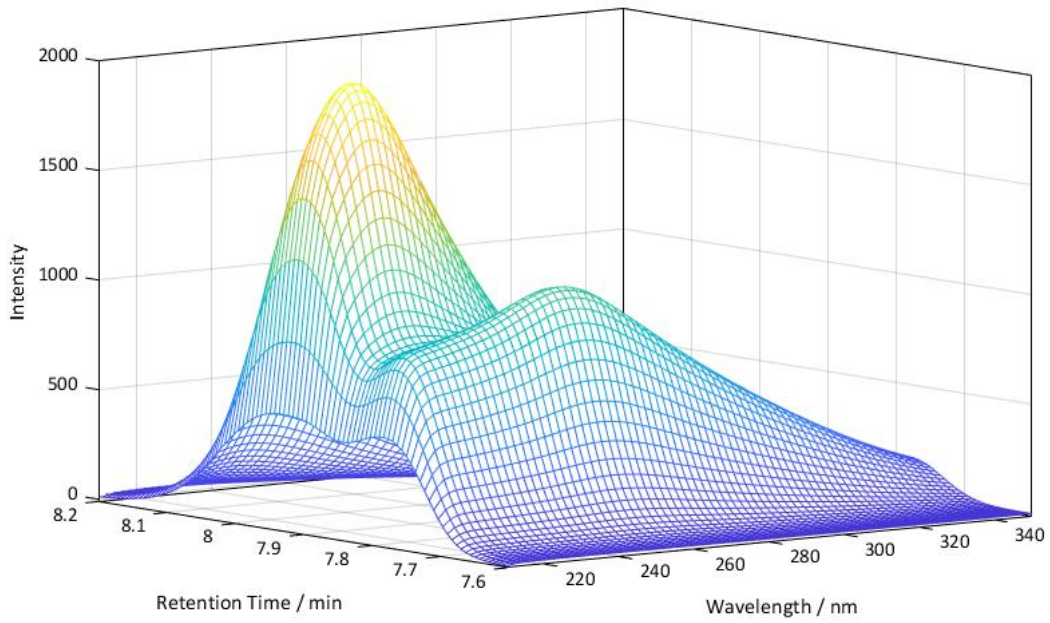

Figure 1. 3D plot showing the experimental chromatographic peaks of a 1:1 mixture of Fe(III)-EDTA and Co(III)-EDTA with respect to both retention time and absorption wavelength.

To accurately quantify EDTA in Fe(III)-EDTA and Co(III)-EDTA mixtures, HPLC chromatographic peaks must first be deconvoluted, both in terms of retention times and detected absorption. The generous quantity of data afforded by the DAD enables peak deconvolution. Two distinct methods have been explored: a conventional least-squares fitting approach and a newer chemometric technique (Parallel Factor Analysis (PARAFAC)).[35] PARAFAC is a multi-way decomposition method for high-order datasets. The method originated in psychometric data analysis[36,37], but is constantly growing in popularity as a chemometric tool.[35] Application of PARAFAC to HPLC-DAD has been reported previously.[38,39] We have compared the accuracy and efficiency of each deconvolution method applied to HPLC-DAD data collected for a series of mixtures containing varying concentrations of Fe(III)-EDTA and Co(III)-EDTA.

Ultimately, the optimised and validated HPLC and deconvolution methods, were applied to a series of trench leachate samples collected from various sampling locations around the LLWR site.

2.2 Materials and Method

2.2.1 Chemicals and Reagents

EDTA disodium salt ($Na_2EDTA{\cdot}2H_2O$), iron trichloride hexahydrate ($FeCl_3{\cdot}6H_2O$), iron-EDTA monosodium trihydrate ($NaEDTA\text{-}Fe(III){\cdot}3H_2O$), DTPA (protonated form), NTA (protonated form), ethanol, tetrabutylammonium bromide (TBA-Br), sodium formate, acetonitrile (HPLC Grade, > 99.9%) (Sigma-Aldrich, Merck KGaA, Darmstadt, Germany), formic acid, hydrogen peroxide (> 30% m/v) (Fisher Scientific, Loughborough, UK) and cobalt dichloride hexahydrate ($CoCl_2{\cdot}6H_2O$) (MP Biomedicals, Irvine, CA, USA) were obtained at ACS reagent grade or above. Deionised (DI) water (>18 MΩ cm^{-1}) used for all applications was obtained from a Millipore® system, fitted with a SimPak® 1 cartridge (Merck Chemicals Ltd, Nottingham, UK).

2.2.2 Chromatography

2.2.2.1 Chromatographic Equipment

HPLC analysis was performed on an Agilent 1260A system (Agilent Technologies, Santa Clara, CA, USA) coupled to a diode-array detector (DAD). The DAD was programmed to record UV-absorption (190 – 400 nm) over the entire chromatographic retention time range (absorption quantified in absorption units (AU)). The system was fitted with a quaternary pump, online degasser, autosampler with 100 μL sample loop and thermostatic column oven. The monolithic silica column was a Chromolith® HighResolution RP-18 end-capped (4.6 × 150 mm) analytical column fitted with a Chromolith® HighResolution monolithic silica RP-18 end-capped (4.6 × 5 mm) guard cartridge (Merck Millipore, Merck Chemicals Ltd, Nottingham, UK). The particle-based column was a Phenomenex® HyperClone 5 μM BDS C_{18} (4.6 x 250 mm) fitted with SecurityGuard© C_{18} guard cartridge (4.6 x 5 mm) (Phenomenex Ltd, Macclesfield, UK).

2.2.2.2 Chromatographic Conditions

All chromatography was carried out isocratically at 25 °C with a 0.6 mL min^{-1} flow-rate of buffered mobile phase (20 mM formate buffer, pH 3.3, prepared by dissolving 10 mM TBA-Br ion-pair agent, 5 mM sodium formate, 15 mM formic acid, and 8%

acetonitrile in DI water), with two exceptions: 1) elution of Fe(III)-DTPA was performed using a 90:10 ratio of formate buffer:acetonitrile, to raise the total composition of acetonitrile to 17.2%, and 2) separation of solutions containing three Fe(III)-APCA complexes was achieved using a gradient elution (0-10 min, a gradient flow of formate buffer:acetonitrile ran from 100:0 to 90:10; 10-20 min, the system pumped isocratically at the final ratio (90:10)). The injection volume was 10 μL and always performed in duplicate. Elution was monitored at the respective λ_{max} of either M(III)-APCA complex (258 nm and 228 nm).

2.2.3 Preparation of Samples for Method Validation

2.2.3.1 Synthesis of Co(III)-EDTA

Equimolar quantities of $CoCl_2 \cdot 6H_2O$ and $Na_2EDTA \cdot 2H_2O$ were dissolved in a minimal amount of mildly basic (three NaOH pellets; roughly pH 10) aqueous solution. The solution was heated under reflux for 24 h, over which period three 2 mL aliquots of H_2O_2 solution were added at evenly spaced intervals. Crystallisation was allowed to occur during evaporation. The resulting precipitate was collected by vacuum filtration and washed with cold ethanol. Recrystallization from a mixture of water and ethanol yielded deep-purple, needle-like crystals, which were collected by vacuum filtration, washed with cold ethanol and dried in a vacuum desiccator. The Co(III)-EDTA complex was characterised by MS, UV-Vis, P-XRD, TGA, ICP-MS and HPLC (characterisation data in Appendix 1). The structure was found to be NaEDTA-Co(III)$\cdot 2H_2O$. Single crystal XRD analysis of the Co(III)-EDTA product was prohibited by the fine needle crystal morphology. The synthesis was based on the method reported by Nowack *et al*.[18]

2.2.3.2 Calibration Samples

Fe(III)-EDTA/DTPA/NTA stock solutions were each prepared by dissolving $Na_2EDTA \cdot 2H_2O$ (0.3722 g, 1 mmol), DTPA (0.3935 g, 1 mmol) or NTA (0.1911 g, 1 mmol) in DI water (70 mL). Solutions of Fe(III) were prepared by dissolving 0.2750 g (0.02 molar excess over APCAs) of $FeCl3 \cdot 6H_2O$ in DI water (10 mL) and added to the APCA solutions. Solutions were heated to 100 °C under stirring (1 h), thermally equilibrated (3 h), added to a volumetric flask (100 mL), and then made up to 100 mL (10 mM).

Another stock solution of Fe(III)-EDTA was prepared by dissolving NaEDTA-Fe(III) $\cdot 3H_2O$ (0.8484 g, 2 mmol) in DI water (95 mL) in a 100 mL volumetric flask, swirled until dissolved, thermally equilibrated (3 h) and then made up to 100 mL (20 mM). A stock solution of Co(III)-EDTA was prepared from the synthesised product by the same method (0.8120 g, 100 mL, 20 mM). Stock solutions were diluted in triplicate to yield 1000, 100, 10, 1 and 0.1 μM solutions and transferred to 2 mL autosampler vials for analysis. When not in use, all samples and stock solutions were refrigerated at 4 °C and kept under darkness to limit thermal/photo-degradation.

2.2.3.3 Co/Fe(III)-EDTA Mixtures

The 20 mM stock solutions of Fe(III)-EDTA and Co(III)-EDTA (prepared from crystalline samples) were diluted in triplicate to 2000, 200, 160, 120, 80, 40, 20, 2 and 0.2 μM. Samples of Fe(III)/Co(III)-EDTA mixtures were made by combining 0.5 mL aliquots of stock solution in 2 mL autosampler vials, yielding 25 distinct sample mixtures, each with nine replicates.

2.2.4 Preparation of Trench Leachate Samples

All heterogeneous leachate samples taken from various sampling locations around the LLWR site (designated GD6, GD7, GD8, GD10, GD12 and GD13) were filtered by vacuum filtration (Whatman® Grade 1 90 mm filter paper) prior to analysis. Three of the leachate samples were spiked with known amounts of EDTA at three concentration levels. All filtered solutions were also analysed with the HPLC method in their original, un-spiked form. All analyte solutions were prepared in triplicate.

To prepare the EDTA-spiked samples, an EDTA stock solution (7.82 mM) was prepared by dissolving $Na_2EDTA \cdot 2H_2O$ in DI water (0.2911 g, 0.782 mmol, 100 mL) and diluted to 782 and 78.2 μM. Nine 9 mL aliquots of liquid-phase from GD10, GD11 and GD12 were transferred to 14 mL screwcap glass vials. 1 mL of the EDTA stock solutions (7820, 782 and 78.2 μM) was added to the 9 mL aliquots of trench leachate, to make three concentrations of EDTA-spiked samples (782 μM, 78.2 μM and 7.82 μM spikes). Aliquots of the spiked samples were transferred to 2 mL autosampler vials and analysed by HPLC. Both the spiked and un-spiked samples were heated (65 °C, 12 h) in

the capped glass vials in a sand bath and, after cooling, analysed by the same HPLC method.

2.2.5 Peak Deconvolution and Data Processing

HPLC data of single species chromatograms was initially processed using Agilent's ChemStation OpenLAB software (V. A.01.02). Chromatograms recorded for Fe(III)/Co(III)-EDTA mixtures and trench leach samples underwent further processing to deconvolute the overlapping peaks.

2.2.5.1 Least-Squares Fitting (LSF)

An average two-dimensional array was calculated from the HPLC-DAD data recorded for each calibration solution and Fe(III)/Co(III)-EDTA mixtures replicates prior to their input into the least-squares fitting (LSF) procedure. A value for %RSD (percent relative standard deviation) was calculated from the mean and standard deviation of the absorption intensity at the wavelength and retention time of maximum absorption of each raw chromatogram. Chromatograms were accepted into the final dataset if they met the acceptance criteria (%RSD ≤ 10%). Two single-wavelength chromatograms were extracted from the averaged, multi-wavelength data for each sample at 258 nm and 228 nm. Chromatograms of the calibration samples were fit first to determine the peak shape and fitting parameters (detailed in next paragraph). The fitting parameters obtained during analysis of the calibration data were used to guide the initial parameter input during the analysis of the convoluted data obtained from the sample mixtures.

The baseline of each chromatographic peak was determined as a straight line connecting the respective absorption minima ($d^2y/dx^2 = 0$) at retention times before and after the peak elution. The line connecting these points was then rescaled to y = 0. A Gram-Charlier A Series (GCAS), which is a modified Gaussian curve and used widely for gas chromatographic data[40,41], was found to best fit the calibration data. The peak position and shape are determined by five fitting parameters: centre, amplitude, half-width and two expansion factors defining the asymmetry of the peak and used to capture the effect of chromatographic peak tailing. Characteristic values of the

expansion factors were determined from all calibration chromatograms; these values were inputted and held constant during the analysis of the sample mixture chromatograms, not doing so usually resulted in unrealistic peak shapes. All peak fitting operations and peak area calculations were carried out using OriginPro 2017.

2.2.5.2 PARAFAC

The PARAFAC method is one of the main deconvolution methods for multi-way data. PARAFAC is an extension to principal component analysis (PCA) and can automatically determine factors and components from high-order datasets.

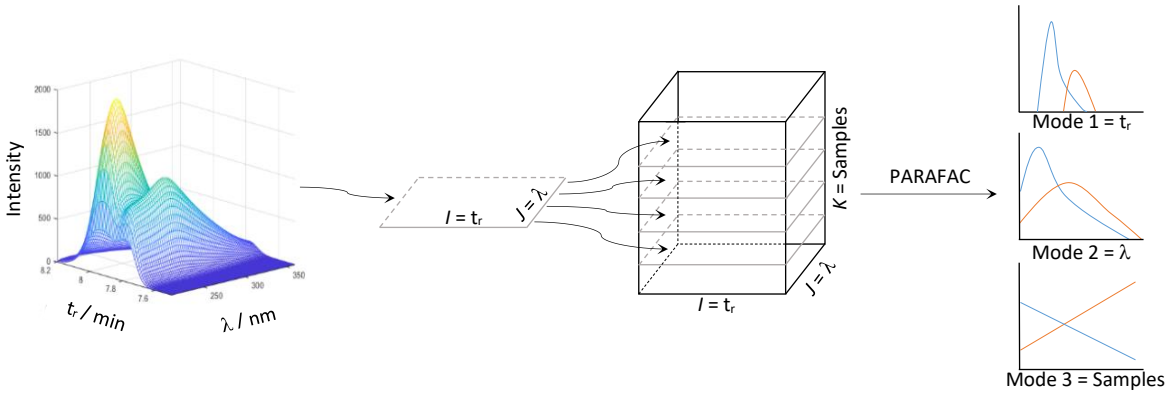

Figure 2. Schematic of PARAFAC methodology applied to HPLC-DAD data containing two principal components.

The two-dimensional data arrays obtained from the HPLC-DAD were collated into a three-dimensional data array (Figure 2) and PARAFAC was then used to decompose this array. The 3D matrix ($I \times J \times K$) is separated into three loadings matrices in Modes 1, 2 and 3, which can then be recombined to produce new 3D matrices unique to each component and containing information regarding each component's contribution in each dimension. The PARAFAC software in MATLAB requires at least two 2D arrays of the same dimensions and each individual dataset must show a change in contribution to the model; the variable *K* must involve a change that affects the magnitude of *I* and *J*. In this case, *I* and *J* describe the UV-absorption intensities over the chromatographic range, and *K* varies according to the concentration of each component.

PARAFAC deconvolution operations and peak integration were carried out on MATLAB R2018a.[35] The PARAFAC code can be found in the N-way Toolbox. CORCONDIA

diagnostic evaluates the core consistency of a given PARAFAC model. It was found that the best values for CORCONDIA were obtained by creating two separate datasets; the first containing the results of the samples containing 1000, 100 and 10 μM concentrations of each complex and another containing the data from the 80, 60, 40, 20 μM samples. This is likely due to the fact that the samples were run on different dates, without identical operating conditions, resulting in small differences in peak shape and retention time. The results of the CORCONDIA diagnostic were 99.98 (12 iterations) and 99.99 (18 iterations) for the first and second dataset, respectively.

After the contribution of each component in each dimension was determined, single-wavelength chromatograms of each complex at their respective λ_{max} were extracted and peak areas calculated using the *trapz()* integration function.

2.2.5.3 Trench Leachate Samples

All chromatograms recorded for trench leachate samples were exported into OriginPro 2017 to undergo the LSF procedure outlined in Section 3.5.1 to determine the Fe(III)-EDTA peak area at 258 nm.

2.2.6 Method Validation

2.2.6.1 Calibration

The linearity was assessed by calculating the linear regression (r^2) of each calibration curve (mean integrated peak vs. [M(III)-APCA]) (acceptance criteria: $r^2 \geq 0.98$). LODs and values for the limit of quantification (LOQs) were calculated as $3.3(\sigma/S)$ and $10(\sigma/S)$, respectively, where S is the slope of the calibration curve and σ is the standard deviation of the peak intensities for samples of lowest, measurable concentration. The calculated LOD/LOQ for Fe(III)-EDTA was verified using the Miller and Miller method, where σ is the mean intensity plus the standard deviation of the blank.[42]

The intra-day precision has been expressed as %RSD (relative standard deviation), calculated from the standard deviation of the mean peak area for each data point (acceptance criteria: %RSD ≤ 10%). The inter-day precision was assessed using Fe(III)-

EDTA as a model system; a value for %RSD was calculated from data recorded for equivalent samples but on different days (when the column was new and after it had been in frequent use for nine months) (acceptance criteria: %RSD ≤ 10%). Fe(III)-EDTA made by forming the complex in solution was also used to assess the accuracy of the method by expressing mean peak areas recorded for these solutions as percent recovery of the equivalent data for the stock solution made by dissolving the crystalline complex (acceptance criteria: recovery = 100 ± 10%).

Additionally, calibration data was assessed for r^2, LOD/LOD, *S* and %RSD (intra-day) when analysed using the two peak deconvolution methods, LSF and PARAFAC, discussed in the next section.

2.2.6.2 Peak Deconvolution

The accuracy of each peak deconvolution method was assessed by plotting the deconvoluted peak area obtained for mixtures of Fe(III)- and Co(III)-EDTA using either the LSF or PARAFAC method, expressed as a percentage of the expected value (known concentrations). A linear regression of such a plot should ideally give the equation y = 100%. The extent to which the linear regression of each real dataset diverges from this ideal value gives a measure of the accuracy and suggests potential trends in the systematic error.

The error associated with the peak areas recorded for Fe(III)/Co(III)-EDTA mixtures represent the statistical error from the LSF procedure, which is the vector sum of the statistical error associated with the three variable fitting parameters used to define each GCAS curve (position of centre, half-width and amplitude). The error associated with the results of the PARAFAC method represent one standard deviation calculated from the integrated peak areas recorded for each chromatogram at each concentration.

2.2.6.3 Trench Leachate Samples

Three samples of trench leachate were spiked with EDTA disodium salt at three concentration levels to assess the recovery and behaviour of the ligand in a real sample matrix. No Fe(III)-salt was added; it was expected that sufficient concentrations

of Fe(III) would naturally be present in the environmental matrix to 1:1 complex trace concentrations of EDTA. Indeed, as we demonstrate in Section 2.2.3, this was the case. This was also designed to allow insight into the speciation behaviour of the ligand under the real sample conditions.

The percent recovery of EDTA as Fe(III)-EDTA was defined as the peak areas recorded for the EDTA-spiked samples normalised to the expected areas calculated from calibration data obtained for Fe(III)-EDTA in purely aqueous conditions, multiplied by 100. The percent recovery was used to estimate the amounts of free EDTA and Fe(III)-EDTA complex, when the ligand is present at varying concentrations in a real sample matrix. Extrapolation of the linear trend of a logarithmic plot of [Fe(III)-EDTA (detected)] vs. percent recovery of EDTA as Fe(III)-EDTA from the spiked samples was used to estimate the total concentration of EDTA present in un-spiked trench leachate samples by an inverse operation of the concentration detectable as Fe(III)-EDTA.

2.3 Results and Discussion

2.3.1 Calibration

The determined metrics describing sensitivity and linearity of the HPLC method, applied to three types of M(III)-APCA complexes and using the monolithic silica column, are displayed in Table 1. Equivalent results obtained using a different column (conventional particle-based C_{18}) and a greater injection volume (100 μL) can be found in the SI. The monolithic stationary phase was found to afford greater chromatographic precision and sensitivity than the C_{18} column. Unless stated otherwise, the results presented in this paper were obtained from the monolithic silica column.

Table 1. LOD, LOQ, slope, linearity and %RSD values for the M(III)-APCA complexes under the chromatographic conditions. M(III)-APCA* = crystalline complex used to make stock solution. %RSD reported for 10 μM calibration standards.

M(III)-APCA	LOD / μM	LOQ / μM	ε / mAU μmol^{-1} L	r^2	%RSD
Co(III)-EDTA*	0.13	0.38	17.02	0.9999	3.8
Fe(III)-EDTA*	0.37	1.1	9.255	0.9999	3.4
Fe(III)-EDTA	0.31	0.94	9.298	0.9999	3.0
Fe(III)-DTPA	0.38	1.1	9.084	0.9999	1.8
Fe(III)-NTA	4.3	13	5.563	0.9999	4.1

All reported values of r^2 for the linear regression of the calibration curves fulfil the acceptance criteria ($r^2 \geq 0.98$). The method is highly sensitive for the EDTA and DTPA complexes tested (LOD range = 0.13 - 0.38 μM) but less sensitive for Fe(III)-NTA (LOD = 4.3 μM). This is due to the lower molar extinction coefficient (ε_i) for the Fe(III)-NTA complex compared to those for M(III)-EDTA/DTPA, for example, $\varepsilon_{Fe(III)\text{-}NTA}$ = 5.6 mAU μmol^{-1} L and $\varepsilon_{Fe(III)\text{-}EDTA}$ = 9.3 mAU μmol^{-1} L; values for ε_i derived from the slope of the linear calibration curves. Additionally, the Fe(III)-NTA chromatographic peak exhibited poorer resolution versus that of M(III)-EDTA/DTPA. Both the effect of peak asymmetry and low $\varepsilon_{Fe(III)\text{-}NTA}$ are best visualised in Figure 3, where the chromatogram of a mixture of Fe(III)-complexes of EDTA, DTPA and NTA at equal concentrations is displayed. Despite being present in equal quantities, the Fe(III)-NTA peak (t_r = 5.13 min, Peak 1) is of smaller area and exhibits much greater peak tailing, with a significant shoulder on the high t_r flank.

Table 2. Accuracy and intra/inter-day precision of the HPLC method applied to Fe(III)-EDTA over a range of concentrations. See text for details

[Fe(III)-EDTA] / μM	Accuracy / %	Intra-day Precision / %RSD	Inter-day Precision / %RSD
1000	100	0.2	0.5
100	99	1.0	0.8
10	99	3.0	2.8
1	96	9.9	7.8

Table 2 shows the accuracy and intra/inter-day precision of the method applied to Fe(III)-EDTA. At all concentrations tested, the accuracy (percent recovery) and precision fall within the acceptance criteria (recovery = 100 ± 10%, %RSD ≤ 10%).

A solution containing all three APCA-complexes can be separated to baseline resolution (Figure 3) by implementing a gradient elution (Section 2.2.2).

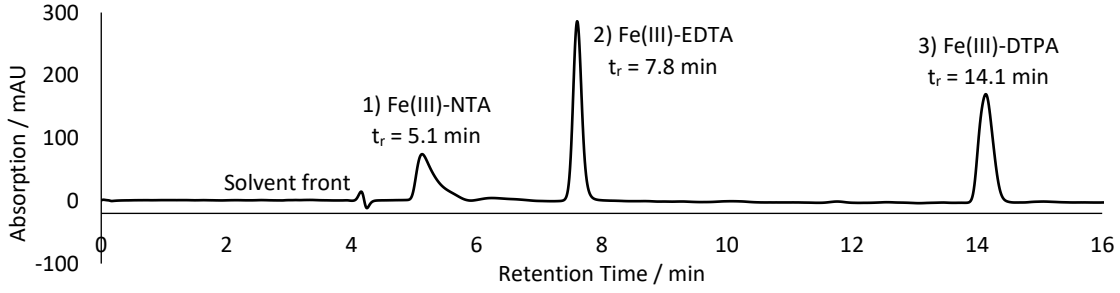

Figure 3. Chromatogram recorded for an aqueous solution containing three 300 μM Fe(III)-APCA complexes (EDTA, DTPA and NTA), absorption at 258 nm.

The identity of the complex responsible for each peak was confirmed by comparison of the retention times and UV-absorption profiles obtained from the analysis of the mixture to equivalent data recorded for single-species calibration samples. Fe(III)-DTPA (Figure 3, Peak 3) has the longest of the three retention times (t_r = 14.14 min), and requires a mobile phase with a greater acetonitrile composition than Fe(III)-NTA/EDTA to maintain the sharpness of the peak. No improvement to the symmetry of the Fe(III)-NTA peak was observed throughout the graduated mobile phase screening process; shifting the peak to a lower t_r with an increased mobile phase acetonitrile concentration led to overlap with the solvent front.

Although it was possible to separate mixtures containing various Fe(III)-APCA complexes, chromatographic peaks recorded for samples containing mixtures of Fe(III)- and Co(III)-EDTA were convoluted with respect to both retention time and UV-absorption.

2.3.2 Peak Deconvolution

Two distinct peak deconvolution methods have been explored, LSF and PARAFAC. The results of the analysis of the single-species calibration data by each method are presented in Table 3.

Table 3. LOD, LOQ, slope, linearity and %RSD Fe(III)-EDTA and Co(III)-EDTA, recorded at their respective wavelengths of maximum absorption, obtained by application of comparative data analysis techniques.

	Least-Squares Fitting					**PARAFAC**				
	LOD / µM	**LOQ / µM**	**Slope**	r^2	**%RSD**	**LOD / µM**	**LOQ / µM**	**Slope**	r^2	**%RSD**
Fe(III)-EDTA	0.35	1.1	0.15	0.9999	5.08	2.3	7.1	0.10	0.9999	14.2
Co(III)-EDTA	0.13	0.39	0.29	0.9999	0.81	4.4	13	0.15	0.9999	14.0

Both methods of peak analysis produce r^2 values above the acceptance criteria ($r^2 \geq 0.98$). The values of %RSD at most concentrations indicate good precision (%RSD ≥ 10%); however, high %RSD values were recorded for low concentration samples analysed by PARAFAC (1 µM Fe/Co(III)-EDTA = 69/86 %). The respective chromatographic peaks at these low concentrations are still clearly separable from background noise. Analysis using LSF of the identical dataset delivers reasonably precise results (1 µM Fe/Co(III)-EDTA = 10.8/3.97 %). The difference may lie in the

misalignment of the peak maxima (i.e. slight shifts in retention times with slight variations in chromatographic conditions), which can impact the quality of the PARAFAC model, whereas this can easily be accounted for when fitting the peaks in two-dimensions.

The LOD for Fe(III)- and Co(III)-EDTA obtained by LSF (0.35 and 0.13 μM, respectively) is comparable to the values obtained by integration using Agilent's ChemStation software. The LOD for Co(III)-EDTA is lower, which likely reflects the nearly two-fold larger molar extinction coefficient of the Co(III)-complex at its wavelength of maximum absorption (also reflected in the calibration curve slopes: Fe/Co(III)-EDTA slope = 0.15/0.29). The LOD values obtained by PARAFAC are an order of magnitude higher, which results from the greater variance associated with the lowest measurable peak.

LSF and PARAFAC were each used to analyse a sample series of varying Fe(III)- and Co(III)-EDTA concentrations, made by combining aliquots of single-species stock solutions. The accuracy of each method has been assessed by comparison of the deconvoluted peak area with that of expected values, expressed as percent. The results are shown in Figure 4; each data point represents 18 chromatograms.

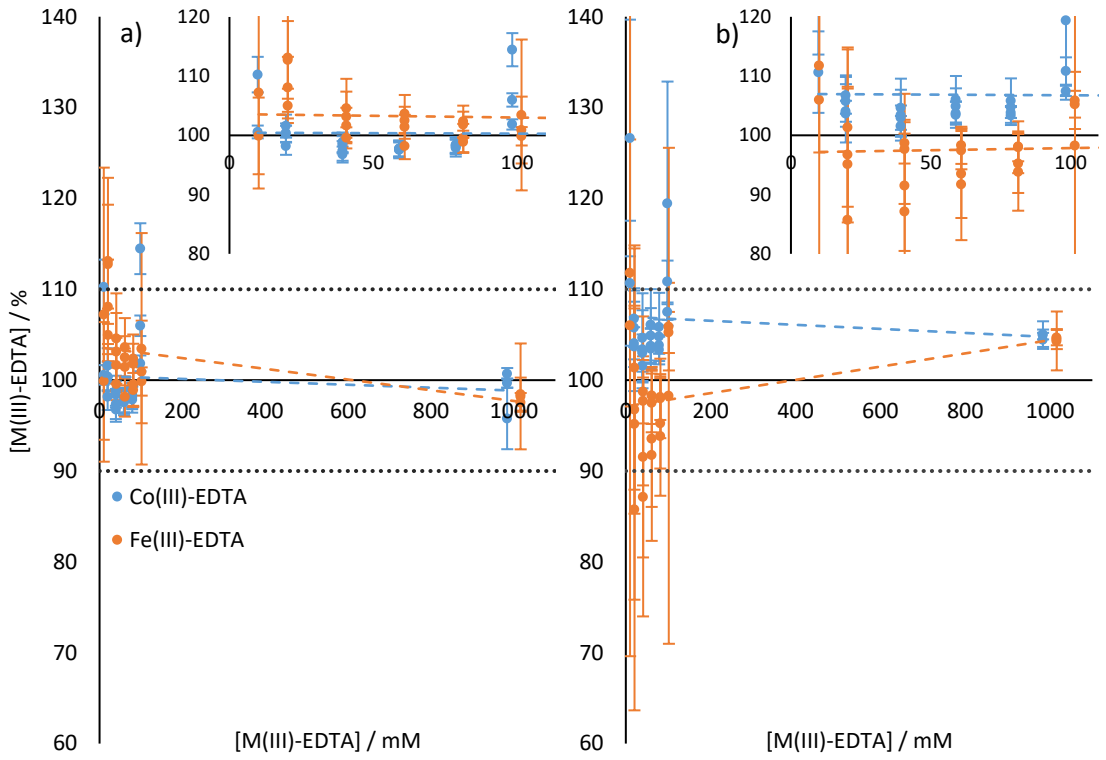

Figure 4. a) The percent concentration determined from least-squares fitting, relative to expected concentrations, plotted against the Fe(III)-EDTA and Co(III)-EDTA concentrations in each sample mixture (error bars = standard error). b) The percent concentration determined from PARAFAC, relative to expected concentrations, plotted against the Fe(III)-EDTA and Co(III)-EDTA concentrations in each sample mixture (error bars = %RSD). Horizontal dotted lines (y = 100 ± 10) denote confidence interval (100 ± 10%). Inserts: Expansion of the low concentration region of the graphs.

The %M(III)-EDTA in Figure 4a,b mostly fall within a range of 100 ± 10%, showing reasonably good accuracy for both methods. All peaks were quantifiable, except the low intensity peak recorded for samples containing a concentration difference of two orders of magnitude (1000 μM/10 μM). Despite the 10 μM concentration generally being above the LOQ, accurate quantification is precluded by interference from the high intensity peak.

Systematic error can be identified by linear regression analysis of the data in Figure 4; the extent to which each trend deviates from $y = 100$ provides two terms (m and c) that can be used to measure the error and the trend that it follows (Table 4). For example, Figure 4a shows the results of the LSF analysis; both slopes (m) are negative, suggesting that there is a systematic overestimation of each species when they are present in low concentrations. This effect is more pronounced for Fe(III)-EDTA than for Co(III)-EDTA (i.e. steeper negative gradient and larger y-intercept). This observation is

in agreement with the calculated average value of determined/expected concentrations in percent (Fe(III)/Co(III)-EDTA = 102.6 ± 4.2/100.2 ± 4.3%).

Table 4. Parameters of linear equations derived from the linear regression of plots of deconvolution results from the least-squares fitting or PARAFAC method. *m* = gradient and *c* = *y*-intercept.

	Least-Squares Fitting			**PARAFAC**		
	m	***c***	r^2	***m***	***c***	r^2
Fe(III)-EDTA	-0.0059	103.6	0.2073	0.0073	97.12	0.1432
Co(III)-EDTA	-0.0016	100.45	0.0136	-0.0022	106.98	0.0159

Figure 4b shows the PARAFAC results; a positive slope and *x*-intercept < 100 was determined for Fe(III)-EDTA and a negative slope and *x*-intercept > 100 for Co(III)-EDTA (Table 4). This result suggests the analysis yields an overestimation of Fe(III)-EDTA at high concentrations, but tends towards a systematic underestimation with decreasing concentration. The concentration of Co(III)-EDTA appears to be consistently overestimated. These observations are also in line with the average measurement accuracies (Fe(III)/Co(III)-EDTA = 98.4 ± 6.3/106.6 ± 5.6%).

The values of random error associated with each measurement are generally greater for Fe(III)-EDTA than Co(III)-EDTA and exhibit more variation in the results of both deconvolution methods (LSF mean standard error of Fe(III)/Co(III)-EDTA = 4.5 ± 3.7/1.5 ± 0.7%, PARAFAC mean %RSD of Fe(III)/Co(III)-EDTA = 9.8 ± 8.9/3.6 ± 3.4%). Furthermore, in both cases the error associated with Fe(III)-EDTA measurements tends to increase with decreasing concentration of the complex in the sample mixture, whereas the magnitude of the error associated with Co(III)-EDTA generally remains consistent over the studied range.

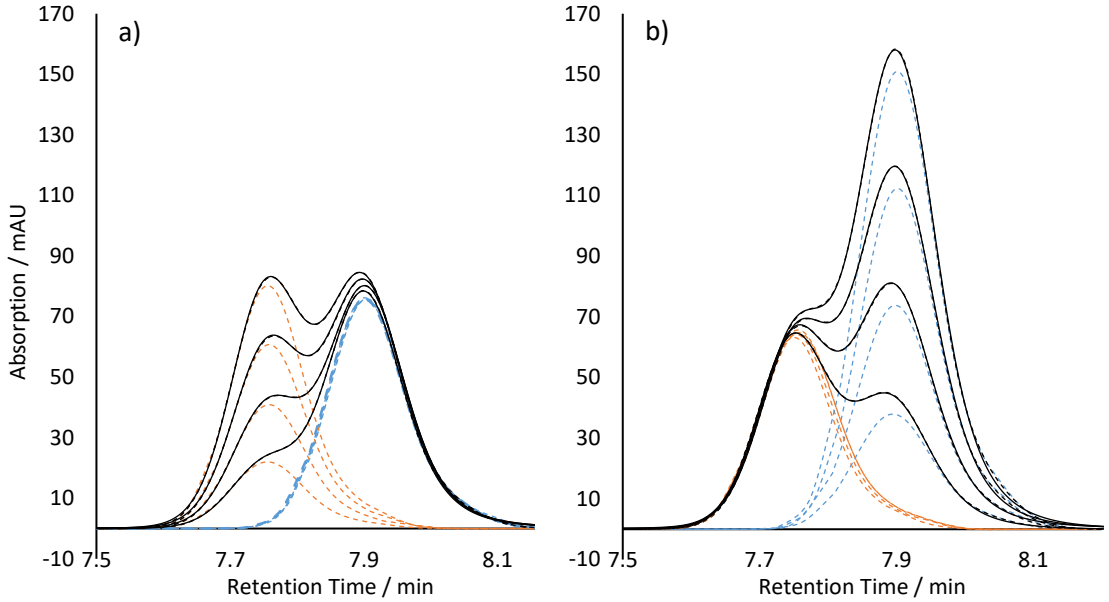

Figure 5. Graphical view of fitted chromatographic data of sample mixtures in the 80 – 20 μM range. Orange dashes = Fe(III)-EDTA fit results, blue = Co(III)-EDTA fit results, black dashes = overall fit, and black lines = experimental data. a) [Co(III)-EDTA] = 80 μM, varying [Fe(III)-EDTA] = 20, 40, 60, 80 μM (recorded at 258 nm = Fe(III)-EDTA λ_{max}), b) [Fe(III)-EDTA] = 80 μM, varying [Co(III)-EDTA] =20, 40, 60, 80 μM (recorded at 228 nm = Co(III)-EDTA λ_{max}).

The graphs in Figure 5 visualise the effect that the UV-absorption characteristics of the two complexes have on peak resolution. Because of the greater molar extinction coefficient for Co(III)-EDTA at its maximum absorption, the relative peak interference observed for each complex is not equal (Co(III)-EDTA ε_{228} = 17.02 mAU μmol^{-1} L > Fe(III)-EDTA ε_{258} = 9.255 mAU μmol^{-1} L). Figure 5a and 5b illustrate the two extremities: high [Co(III)-EDTA] and variable [Fe(III)-EDTA], and high [Fe(III)-EDTA] and variable [Co(III)-EDTA], recorded at 258 and 228 nm, respectively. Proportionally, the peak overlap is greater for the Fe(III)-EDTA peak at 258 nm than for Co(III)-EDTA at 228 nm. This effect is expressed by the greater standard error associated with the LSF of the Fe(III)-EDTA peaks.

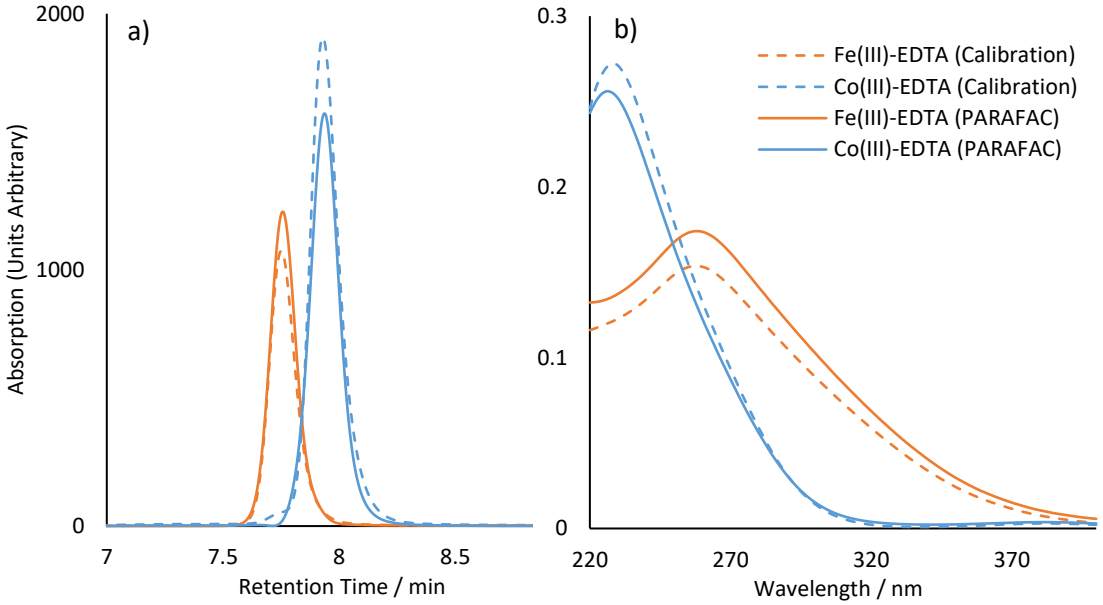

Figure 6. Overlay of loadings determined by PARAFAC in Modes 1 (chromatographic) (a) and 2 (spectral) (b) and raw chromatographic and spectral data obtained from calibration samples.

In PARAFAC, the three-way data array from the HPLC-DAD is decomposed into three loading matrices. Mode 1 (Figure 6a) shows the loadings with respect to chromatographic retention time. The two component peaks are clearly identifiable as Fe(III)-EDTA and Co(III)-EDTA by comparison to the calibration data. The loadings of Mode 2 (Figure 6b) show the deconvoluted UV-spectra of the two components. The peak shapes and relative peak maxima align with the UV-absorption profiles determined for reference spectra of each complex.

2.3.3 Trench Leachate

Three trench leachate samples (GD10, GD12 and GD13) were spiked with EDTA at three concentrations. The HPLC chromatograms recorded for these samples (258 nm detection wavelength) are depicted in Figure 7. All chromatograms are the average of the six chromatograms recorded for each sample. Though peaks other than the Fe(III)-EDTA peak were observable, none were identifiable as Fe(III)-NTA or Fe(III)-DTPA. No peaks were observed to suggest that interfering metal complexes are formed from competing ions that would have a deleterious effect on the quantification of results.

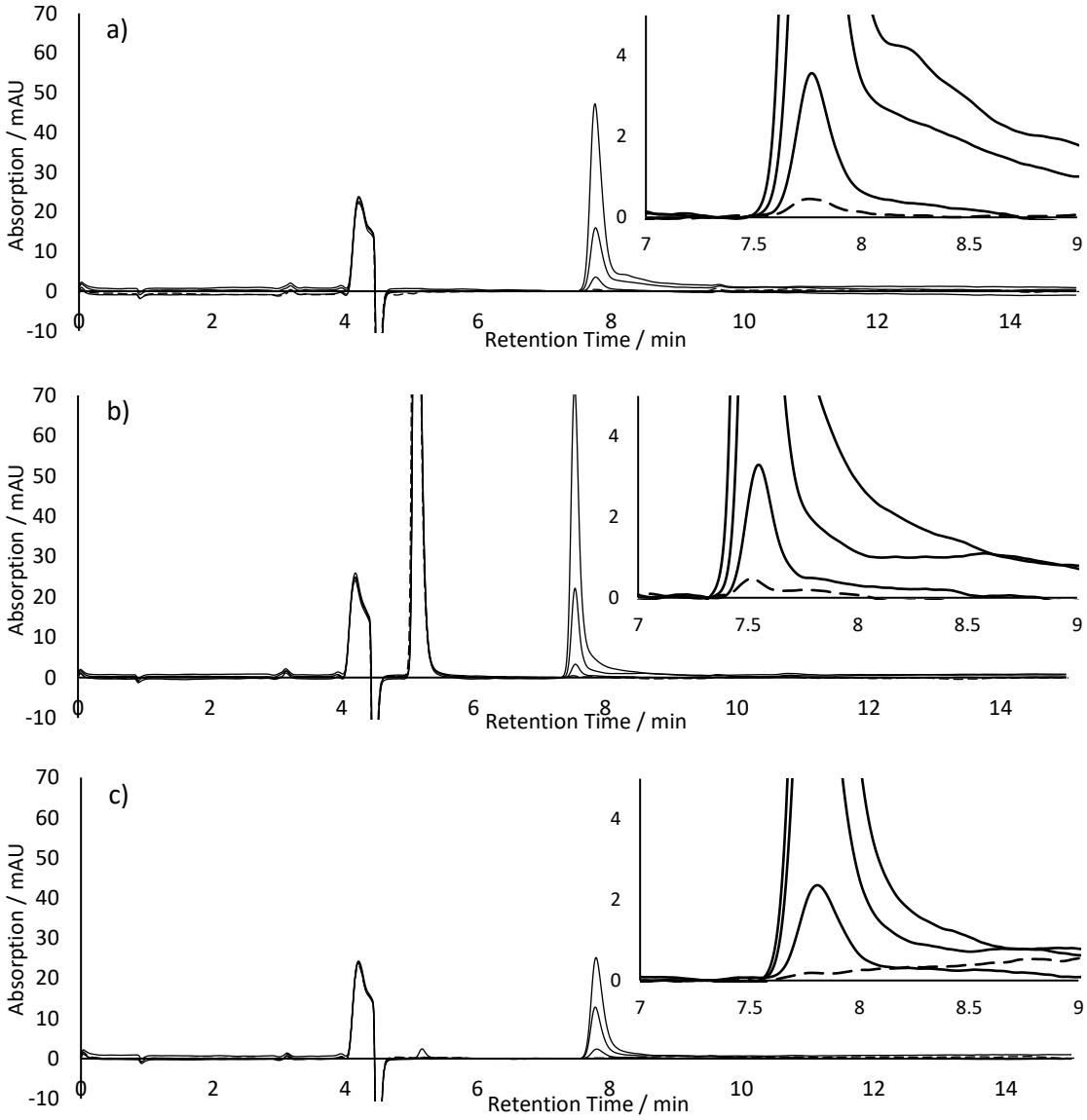

Figure 7. Chromatograms recorded for trench leachate samples from GD10 (a), GD12 (b) and GD13 (c). Dashed lines represent the chromatograms for un-spiked samples, full lines represent the chromatograms for samples spiked with EDTA at various concentrations.

The chromatograms of GD13 trench leachate samples (Figure 7c) exhibit a small peak at $t_r \approx 5.2$ min, which is only visible in chromatograms of samples that have been spiked with the ligand. A large and well-resolved peak is observed in all the chromatograms recorded for the GD12 trench leachate samples (Figure 7b, $t_r \approx 5.1$ min). The UV λ_{max} of the associated species is 264 nm; hence, the feature is prominent in the data recorded at 258 nm. The peak is not caused by Fe(III)-NTA, Fe(III)-DTPA or Fe(III)-EDTA but could represent another of the organic complexants known to occur in the repository such as citric acid or ISA.[24]

The Fe(III)-EDTA chromatographic peak shape and position (Figure 7, $t_r \approx 7.8$ min) deviates from those observed in the chromatograms recorded for purely aqueous solutions (calibration and Fe(III)/Co(III)-EDTA mixtures). This is most likely attributable to the variable chemistries of the environmental matrix of the trench leachate samples. A chromatographic shift is observed in one of the EDTA-spiked trench leachate samples (GD12, Figure 7b) to a shorter retention time ($\Delta t_r \approx 0.2$ min). Extraction of The UV-absorption profiles at the chromatographic peak maxima ($t_r \approx$ 7.54 min (GD12) and $t_r \approx 7.76$ min (GD10/13)) shows that both of the detected species exhibit similar shapes and identical local absorption maxima, confirming that both are Fe(III)-EDTA.

To varying extents, all three EDTA-spiked leachate samples produce Fe(III)-EDTA peaks with greater asymmetry (peak tailing, Figure 7). This effect may be associated with co-elution of the Fe(III)-EDTA with chemically similar species; the matrix may affect the protonation state of the ligand before it was injected into the buffered mobile phase, its mode of complexation, or associated counter-ions. A portion of the area associated with the peak tail was removed during the LSF procedure by holding the expansion factors that determine the extent of the asymmetry of the GCAS peak constant to the factors determined in the analysis of the calibration data. Therefore, some of the EDTA that is not accounted for in the percent recovery as Fe(III)-EDTA is identifiable in the peak area that makes up the peak tails.

The spiked samples were analysed by HPLC before and after heating. The resulting chromatographic data was processed using the LSF procedure; LSF was found to be more reliable at low concentrations than PARAFAC (LSF/PARAFAC Fe(III)-EDTA LOD = 0.35/2.3 μM) and better suited for analysis of chromatograms with small variations in t_r. Table 5 shows the results as percent recovery.

Table 5. Concentration of Fe(III)-EDTA detected in each trench leachate sample spiked with EDTA at three concentrations and the values of percent recovery of the spike (chromatographic peak area detected to expected peak area for spike concentration, expressed as percent). Data recorded before and after the spiked solutions were heated for 12 h at 65 °C.

	GD10		GD12		GD13		Average		σ	
[EDTA-spike] / μM	**No heat**	**Heat**	**No heat**	**Heat**	**No heat**	**Heat**	**No heat**	**Heat**	**No heat**	**Heat**
	[Fe(III)-EDTA (detected)] / μM									
782	47	70	48	74	33	39	43	61	8.2	19
78.2	18	26	20	23	18	19	19	22	1.2	3.4
7.82	3.6	5.1	4.2	3.9	3.9	3.9	3.9	4.3	0.3	0.7
	Percent Recovery of EDTA-spike as Fe(III)-EDTA / %									
782	5.9	8.9	6.2	9.5	4.3	4.9	5.5	7.8	1.0	2.5
78.2	23	33	26	29	23	24	24	29	1.6	4.3
7.82	46	65	54	50	50	50	50	55	4.1	9.0

The lowest values of percent recovery were observed for samples spiked with the highest concentration of EDTA (782 μM). Here, the recovery of EDTA as Fe(III)-EDTA may have been limited by the quantity of Fe(III) available for complexation in the solution. Note that unbound EDTA does absorb in the UV-region of the spectrum (λ_{max} = 270 nm (disodium EDTA))[43], but the absorption is weak and renders the uncomplexed ligand undetectable in the chromatograms. The mean concentration of Fe(III)-EDTA found in these samples was 61 μM; if Fe(III)-complexation is assumed to be 100% in a roughly 1:10 excess of metal:ligand; this value gives an indication of the Fe(III) naturally present in the samples. We assume that the majority of the EDTA not recovered as Fe(III)-EDTA remains uncomplexed in solution, noting that metal-EDTA complexes that do not absorb in the UV-region (190 - 400 nm) would not have been detected and could feasibly account for a portion of the EDTA not recovered as Fe(III)-EDTA. The lowest mean recovery for the samples spiked with 78.2 μM of EDTA was 24%. The recovery is still relatively low despite there being a roughly 1:1 molar equivalence of metal:ligand present in solution, assuming 61 μM is a reasonable approximation of the Fe(III) available for complexation. Other matrix effects may contribute to the low recovery, for example, the pH/E_h environment or competing ions.

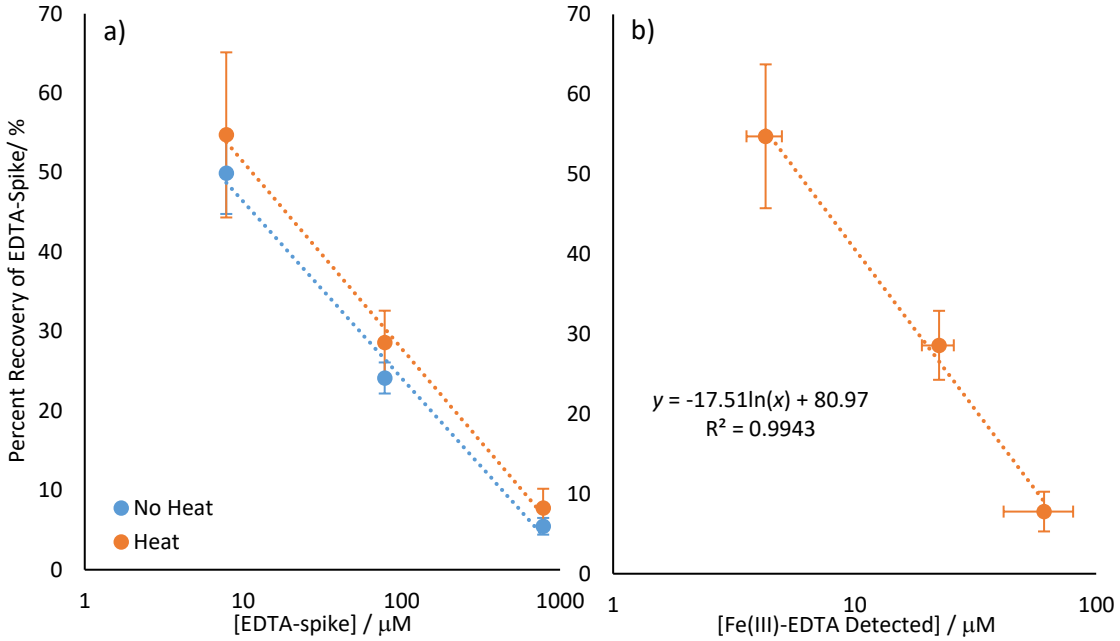

Figure 8. a) Plot of the $\log_{10}$ of spiked concentration of EDTA against the mean percent recovery as Fe(III)-EDTA from the trench leachate samples before (blue) and after (orange) heating, b) plot of the $\log_{10}$ of Fe(III)-EDTA concentration detected as a function of the mean percent recovery of spiked EDTA after heating. The result of linear regression the plot is indicated and used for calculating total amounts of EDTA in un-spiked trench leachate samples. See text for details.

Figure 8a shows that the recovery increases logarithmically with decreasing concentration of EDTA and that heating the samples at 65 °C for 12 h only marginally increases the recovery. The percent recovery of the EDTA-spike as Fe(III)-EDTA (Figure 8b) can be used to calculate the total EDTA in un-spiked trench leachate solutions, given the respective concentrations of Fe(III)-EDTA detected in each sample (i.e. substituting *x* for the detected Fe(III)-EDTA concentration into the linear equation for Figure 8b, $y = -17.51\ln(x) + 80.97$ and solving for *y*, then dividing the Fe(III)-EDTA detected by *y* to obtain the total concentration of EDTA). The results are presented in Table 6.

Table 6. Concentrations of Fe(III)-EDTA detected in un-spiked samples of trench leachate from various sampling locations, the fraction of the total EDTA (as a percentage) determined by extrapolation of the trend in Fig. 8b, and the calculated total concentration of EDTA in each sample.

Trench Leachate Sample	[Fe(III)-EDTA] / µM	Fraction of Total EDTA / %	[EDTA] / µM
GD6	0.7	87	0.8
GD7	0.4	99	0.4
GD8	ND	ND	ND
GD10	0.5	92	0.6
GD12	0.4	98	0.4
GD13	ND	ND	ND

ND = not detected

Fe(III)-EDTA was detected in four out of the six samples of trench leachate tested. All of the concentrations determined from the peak area obtained by LSF of the chromatographic data fall between the LOD and the LOQ. The concentrations reported here are similar to those obtained in a previously reported analysis.[44] This and that study both suggest that the EDTA loading in trench leachate from the sampling locations tested does not exceed 1 μM.

2.4 Conclusion

Optimising the method originally outlined by Nowack *et al.*, a robust and sensitive RP-HPLC procedure has been developed to detect three common APCAs at trace concentrations in complex aqueous matrices. The respective LODs for Fe(III)-EDTA, DTPA and NTA were found to be 0.31, 0.38 and 4.3 μM. The results for Fe(III)-EDTA and DTPA are similar to others reported in the literature; in 2005, Laine *et al.* reported LODs of 0.27, 0.34 and 0.62 in the simultaneous chromatographic detection of EDTA, DTPA and NTA, respectively.[16] The sensitivity of our method for EDTA and DTPA was found to be suitably high for application to LLWR leachate samples.

The monolithic stationary phase used in this analysis was found to afford greater peak resolution than a conventional particle-based C_{18} column (SI). The monolithic silica was also proven to be robust (inter-day %RSD < 10%), which has economical value as it helps to offset the greater investment associated with the polymeric stationary phase.

Method validation has demonstrated the HPLC method to be linear ($r^2 > 0.98$), precise (intra/inter-day %RSD ≤ 10%) and selective. Full conversion of EDTA to Fe(III)-EDTA was observed in a sample matrix containing only H_2O (recovery = 100 ± 5%); however, the experimental results of the EDTA-spiked samples of trench leachate suggest that the recovery is, of course, limited by the amount of Fe(III) in solution available for binding but also decreases significantly when subject to matrix effects (recovery of 7.82 μM EDTA-spike = 55 ± 9%). Addition of Fe(III) to amounts well above the unknown EDTA concentration of an analyte solution can adversely impact the UV-Vis detection in the procedure. To account for the decreased recovery due to matrix effects, the recovery of EDTA spiked to a series of leachate samples was used to determine a logarithmic

trend between concentration and recovery, which in turn was used to introduce a correction factor in the analysis of un-spiked samples. Without this correction factor for low EDTA concentrations in the samples studied, the result underestimates the amount of EDTA by around 15%.

To guard against the potential complications introduced to the procedure by competing ions or other interfering species, two peak deconvolution methods have been successfully applied to HPLC-DAD data recorded for various mixtures of Fe(III)- and Co(III)-EDTA. The accuracy of each method was comparable; most data points fell within the range 100 ± 10% (deconvoluted peak area as a percentage of calibration sample peak area). Neither deconvolution method was able to accurately quantify the low intensity peak in mixtures where the concentration disparity was two orders of magnitude (1000/10 μM). The LSF procedure was found to be more reliable at low concentrations (LSF/PARAFAC Fe(III)-EDTA LOD = 0.35/2.3 μM), hence, it was used in the analysis of trench leachate samples from LLWR.

Each deconvolution method has pros and cons. For example, there is a significant time penalty associated with the LSF procedure, though this could be reduced by introducing a coded routine to perform the task automatically. The PARAFAC model could process the data much faster, but the software is not a black-box; some amount of time and understanding is required to get a reasonable output. In the future, the PARAFAC model could be improved by introducing PARAFAC2 code, which is more flexible than PARAFAC, allowing for certain shifts in one of the modes (e.g. could account for chromatographic retention time drift).[45]

Of the six trench leachate samples that were tested, four were found to contain trace concentrations of EDTA, all of which fall below the LOQ (1 μM). The total concentration of Fe(III)-EDTA found in the trench leachate samples ranges from 0.4 - 0.7 μM, which translates to an EDTA concentration range of 0.4 - 0.8 μM, should the correction calculation by extrapolation of recoveries of spiked samples be taken into account. The levels are not considered sufficient to increase the risk of radionuclide mobilisation. The technique is considered to be robust and will be considered further in informing limits of acceptance on APCAs.

2.5 References

1. LLWR, *The 2011 Environmental Safety Case: Environmental Safety Case – Main Report,* LLWR/ESC/R(11)10016, LLWR, Cumbria, UK, 2011.
2. A. L. Rufus, S. Velmurugan, V. S. Sathyaseelan and S. V. Narasimhan, *Prog. Nucl. Energ.*, 2004, **44**, 1, 13-31.
3. M. Butcheli-Witschel and T. Elgi, *FEMS Microbiol. Rev.*, 2001, **25**, 1, 69-106.
4. J. L. Means and C. A. Alexander, *Nucl. Chem. Waste Man.*, 1981, **2**, 186-193.
5. Radioactive Waste Management (RWM), *Geological Disposal Behaviour of Radionuclides and Non-radiological Species in Groundwater Status Report*, NDA Report no. DSSC/456/01, RWM, Oxford, UK, 2016.
6. Norwegian Radiation Protection Authority (NRPA), *Study of Issues Affecting the Assessment of Impacts of Disposal of Radioactive and Hazardous Waste*, NRPA Report 2018:6, Østerås, Statens strålevern, 2018.
7. R. J. Serne, K. J. Cantrell, C. W. Lindenmeier, A. T. Owen, I. V. Kutnyakov, R. D. Orr and A. R. Felmy, *Radionuclide-Chelating Agent Complexes in Low-Level Radioactive Decontamination Waste; Stability, Adsorbtion and Transport Potential*, NUREG/CR-6758 PNNL- 13774, U.S. Nuclear Regulatory Commission (NRC), Washington D.C., 2002.
8. S. Smillie and F. P. Glasser, *Adv. Cem. Res.*, 1999, **11**, 2, 97-101.
9. LLWR, *Waste Acceptance Criteria – Supercompactable Waste*, WSC-WAC-SUP – Version 3.0, LLWR, Cumbria, UK, 2012.
10. LLWR, *Developments Since the 2011 ESC*, LLWR/ESC/R(13)1005 Issue 1, LLWR, Cumbria, UK, 2013.
11. Environment Agency (EA), *Review of LLW Repository Ltd's 2011 Environmental Safety Case: Inventory and Near Field*, Issue 1, EA, Bristol, 2015.
12. LLWR, *Waste Acceptance Criteria – Low Level Waste Disposal*, WSC-WAC-LOW – Version 5.0, LLWR, Cumbria, UK, 2016.
13. M. Kelly, *Preliminary Calculations to Assess the Impact of EDTA on Health Hazards Arising from the LLWR*, Report AMEC/006357/002, AMEC, Cumbria, UK.
14. Health and Safety Executive (HSE), *Rosyth Royal Dockyard Ltd's Stategy for Decommissioning the Rosyth Nuclear Licenced Site*, HSE, Merseyside, UK, 2004.
15. M. Sillanpää, in *Rev. Environ. Contam. Toxicol.*, ed. G. W. Ware, 1997, **152**, 85-111, Springer, New York, NY.
16. P. Laine and R. Matilainen, *Anal. Bioanal. Chem.*, 2005, **382**, 1601-1609.
17. V. Sýkora, P. Pitter, I. Bittnerová and T. Lederer, Water Res., 2001, **35**, 8, 2010-2016.
18. B. Nowack, F. G. Kari, S. U. Hilger and L. Sigg, *Anal. Chem.,* 1996, **68**, 561-566.
19. J. L. Means, T. Kucak and D. A. Crerar, *Environ. Pollut. B*, 1980, **1**, 1, 45-60.
20. A. Svenson, L. Kaj and H. Björndal, *Chemosphere*, 1989, **18**, 9, 1805-1808.
21. A. P. Toste, *J. Radioanal. Nucl. Chem.*, 1992, **161**, 549-559.
22. A. P. Toste, B. C. Osborn, K. J. Polach and T. J. Lechner-Fish, *J. Radioanal. Nucl. Chem.*, 1995, **194**, 1, 25-34.
23. K. Tian, C. H. Benson and J. M. Tinjum, *J. Hazard. Toxic Radioact. Waste*, 2017, **21**, 4, 04017010.
24. LLWR, *Review of the Potential Effects of Complexants on Contaminant Transport at the LLWR*, LLWR/ESC/R(13)10054, LLWR, Cumbria, UK, 2013.
25. C. Randt, R. Wittlinger and W. Merz, *Fresen. J. Anal. Chem.*, 1993, **346**, 6, 728-731.
26. M. Taddia, M. T. Lippolis and L. Pastorelli, *Microchem. J.*, 1979, **24**, 1, 102-106.
27. C. S. Bürgisser and A. T. Stone, *Environ. Sci. Technol.*, 1997, **31**, 9, 2656-2664.
28. M. Sillanpää and M-L. Sihvonen, *Talanta*, 1997, **44**, 8, 1487-1497.

29. Kemmeia, S. Kodamaa, A. Yamamotob, Y. Inouec and K. Hayakawad, *Food Chem.*, 2013, **138**, 2, 866-869.
30. J. De Jong, A. Van Polanen J. J. M. Driessen, *J. Chromatogr. A*, 1991, **553**, 243-248.
31. G. Wang and F. P. Tomasella, *J. Pharm. Anal.*, 2016, **6**, 3, 150-156.
32. R. Geschke and M. Zehringer, *Fresen. J. Anal. Chem.*, 1997, **357**, 6, 773-776.
33. I. Ali, V. D. Gaitonde, H. Y. Aboul-Enein, *J. Chromatogr. Sci.*, 2009, **47**, 432-442.
34. R. M. Smith, A.E. Martell, Critical Stability Constants, 6, Plenum Press, New York, 1989.
35. R. Bro, Chemom. Intell. Lab. Syst., 1997, **38**, 149-171.
36. R. A. Harshman, UCLA Working Papers in Phonetics, 1970, **16**, 1-84.
37. J. D. Carroll and J. Chang, Psychometrika, 1970, **35**, 3, 283-319.
38. F. C. Guizellini, G. G. Marcheafave, M. Rakocevic, R. E. Bruns, I. S. Scarminio and P. K. Soares, Food. Res. Int., 2018, **113**, 9-17.
39. P. K. Soares, G. G. Marcheafave, A. A. Gomes, I. S. Scarminio and R. E. Bruns, Chromatographia, 2018, **81**, 8, 1189-1200.
40. F. Dondi, A. Betti, G. Bio and C. Bighi, Anal. Chem., 1981, **53**, 496-504.
41. E. Grushka, *J. Phys. Chem.*, 1972, **76**, 18, 2586-2593.
42. J. N. Miller and J. C. Miller, *Statistics and Chemometrics for Analytical Chemistry*, Pearson, Harlow, UK, 6th edn., 2010.
43. S. Kamboj, D. Sharma, A. B. Nair, S. Kamboj, R. K. Sharma, J. Ali, K. Pramod and S. H. Ansari, *Pharm. Methods*, 2011, **2**, 2, 148-151.
44. D. J. Wilkinson, *Results of the Measurement of the Concentration of Dissolved EDTA in Trench Waters from LLWR by HPLC*, NVR1068b/Babcock, 2013.
45. P. J. H. Jørgensen, S. F. V. Nielsen, J. L. Hinrich, M. N. Schmidt, K. H. Madsen and M. Mørup, *Probabilistic PARAFAC2*, arXiv:1806.08195 [stat.ML].

Chapter Three: Extraction and Quantification of EDTA from an Incinerated Ion-Exchange Resin Matrix

James A. O'Hanlon[a†], Frank Taylor[b] and Melissa A. Denecke[c]

[a,c] The Chemistry Building, The University of Manchester, Oxford Road, Manchester, UK, M13 9PL.

[b]LLW Repository Ltd, Pelham House, Pelham Drive, Calderbridge, Seascale, Cumbria, UK, CA20 1DB.

[†]Corresponding Author e-mail: james.ohanlon@manchester.ac.uk.

Scope

The research presented in Chapter Three was targeted at further developing the APCA quantification procedure for application to solid-state samples. A trial incineration procedure was carried out on batches of EDTA-contaminated ion-exchange resins to assess its ability to destroy the ligand in order to create a suitable wasteform for acceptance at the LLWR. The resulting residue was sent to The University of Manchester for EDTA determination using the optimised HPLC method.

To maximise the potential of the sensitivity of the liquid chromatographic detection method, it was necessary to develop and optimise a solid-liquid phase extraction to bring the analyte into solution. Parameters such as extraction time, extractant solution, particle size and preconcentration were all investigated to deliver a simple and effective method. The target sensitivity of the overall extraction and quantification procedure was 1 mg kg^{-1}; it was deemed that the wasteform could be accepted at LLWR if it could be confirmed that EDTA was not present in concentrations > 1 mg kg^{-1}.

The Results and Discussion section of Chapter Three is divided into two sections: i) Method Optimisation and ii) Method Validation. The rationale behind moving from the preliminary extraction method to the final method is discussed in Method Optimisation, with justification provided for each of the modifications. Once finalised,

the method was tested on various samples of ion-exchange resin residue to ensure reliability and accuracy in different experimental matrices. Differences in the extraction recovery between samples were found which prompted further study into the physical and chemical composition of the residue itself. The results of these tests are presented in Method Validation.

CRediT Author Statement:

J. A. O'Hanlon: Conceptualisation, Methodology, Validation, Formal analysis, Investigation, Data curation, Writing – original draft preparation, Visualisation. F. Taylor: Resources, Writing – reviewing and editing, Project administration, Funding acquisition. M. A. Denecke: Conceptualisation, Methodology, Writing – review and editing, Supervision, Project administration, Funding acquisition.

Abstract

Ion-exchange (IX) resins are integral to the control of radionuclide contaminants produced during the operation and maintenance of the United Kingdom's nuclear submarine fleet. Large quantities (> 60 m^3) of spent IX resin material are currently being held in temporary storage, where they await final disposal at facilities such as the Low Level Waste Repository (LLWR). For the waste to be compliant with LLWR's Waste Acceptance Criteria (WAC), the chemically contaminated IX resin must first be treated to destroy its ethylenediaminetetraacetic acid (EDTA) content (up to 6% by mass). The amount of EDTA complexant in waste destined for disposal is controlled by LLWR because of its potential to mobilise radionuclides in the final wasteform. Incineration is one of the proposed treatment strategies for radioactively contaminated IX resins. To demonstrate compliance against the WAC, residues arising from incineration must be tested to determine if the EDTA has been fully destroyed. A method has been developed for the quantification of trace amounts of EDTA in an incinerated IX resin matrix using solid-liquid phase extraction and reversed-phase ion-pair high-performance liquid-chromatography (HPLC) with UV detection. EDTA was extracted directly into an aqueous Fe(III) solution to undergo complexation and eluted on a high-resolution monolithic silica column using a pre-optimised and validated

method (detection at 258 nm, Fe(III)-EDTA λ_{max}). The overall procedure was validated for its accuracy (mean EDTA percent recovery = 78 ± 3.3%), precision (intra-/inter-day %RSD ≤ 10%), sensitivity (limit of detection/quantification = 0.32/1.0 mg kg^{-1}, respectively), selectivity and robustness by analysis of various EDTA-spiked IX residue samples. EDTA-thermal degradation products present in the incinerated resin matrix form Fe(III)-complexes during the solid-liquid extraction, which create chromatographic peaks that overlap with the Fe(III)-EDTA peak; this was successfully resolved by implementing a least-squares fitting procedure.

Keywords

High-performance liquid-chromatography, reverse-phase, ion-pair, aminopolycarboxylic acids, ethylenediaminetetraacetic acid, low level radioactive waste, spent ion-exchange resins.

3.1 Introduction

The Royal Navy currently operates three classes of nuclear submarine, all of which are powered by generational designs of the pressurised water reactor (PWR); thermal energy generated in nuclear fission is transferred to a circulatory water system that produces steam to run the turbines. Over time, the coolant water circulating in the primary circuit of the PWRs becomes contaminated with radionuclides. Ion-exchange (IX) resins are insoluble, functionalised, polymeric microbeads that are tailored to bind harmful species in exchange for the release of more innocuous ones. The resins are used on the submarine fleet to control the levels of radioactivity both on-shore and off-shore. During normal operation, resins inside the primary circuit are contained within highly shielded vaults, which localises and limits the external radiation hazard to crewmembers at sea. Land-based maintenance procedures also involve ion-exchange decontamination steps to ensure safe access to the reactor core during refuel and refit.

As a result of such operations, the Ministry of Defence (MOD) has accumulated stocks of radiologically contaminated spent IX resins (62.1 m^3 dry volume), the majority of

which are in temporary storage at Rosyth and Devonport Dockyards.[1] Much of the material currently constitutes intermediate level waste (ILW)[2], therefore, final disposal at the Low Level Waste Repository (LLWR) near the village of Drigg, Cumbria, the UK's national facility for the disposal of solid low level waste (LLW), has been delayed to allow the waste to decay to LLW (specific activity not exceeding 4 GBq t^{-1} alpha-emitting radionuclides; 12 GBq t^{-1} all other radionuclides).[3]

In addition to the radiological specifications, waste consignments to LLWR must meet other acceptance criteria before they can be disposed of at the site. Requirements regarding the physical and chemical characteristics of the waste are also controlled; for example, limitations on the levels of chemical complexing or chelating agents. LLWR's Waste Acceptance Criteria (WAC) divides chemical complexants into two categories: Category 1 complexants include carboxylates (e.g. citrate, picolinate, oxalate and formate) and inorganic compounds (e.g. tripolyphosphates); Category 2 ligands are the aminopolycarboxylic acids (APCAs, e.g. ethylenediaminetetraacetic acid (EDTA), diethylenetriaminepentaacetic acid (DTPA) and nitrilotriacetic acid (NTA)). Control measures are implemented on complexants from both categories. Category 1 materials are controlled at the level of recording their content in waste, not exceeding 1 kg bulk mass. Category 2 materials are controlled against a site-wide capacity of 1000 kg for all APCAs.[3]

Complexants often arise in the waste because of their use throughout the nuclear industry in the decontamination agents used in the decommissioning process.[4-7] Left untreated, they are problematic because they have the potential to coordinate, solubilise and mobilise otherwise surface adsorbed or solid radionuclides in the waste. Upon contact with infiltrating water, complexed and sequestered ions can be transported out of the repository near field and into the geo/bio-sphere, which can lead to range of a negative environmental impacts.[6-9] The risk associated with Category 2 complexants (APCAs) is greater than that of Category 1 complexants mainly because of the greater environmental persistence of the APCAs.[5,10-13] For these reasons, the APCAs were part of LLWR's focus in the 2011 Environmental Safety Case (2011 ESC), which is a pre-requisite for the Environment Agency to grant an Environmental Permit

to dispose of LLW in the repository. The ESC is a primary source of information to underpin the WAC.[14]

MODIX (multi-stage oxidative decontamination with ion-exchange clean-up) was developed specifically for the decontamination of nuclear submarine reactor circuits. The process uses low concentration chemicals to remove the contaminated magnetite film from the stainless-steel surfaces of the primary circuit boundary.[15,16] Three stages of chemical injection into the coolant flow, including injection of complexants, condition and remove the oxide layer whilst the circulating coolant is treated by ion-exchange to restore it to a specified purity. MODIX resins, commercially known as Purolite® NRW-37, comprise the bulk volume majority of the spent IX resins in storage. Based on analytical results, chemical contamination of the resins in storage vary according to the levels displayed in Table 1.

Table 1. Chemical contamination of MODIX resins in storage.[1]

Chemical Contaminant	**LLWR WAC Category**	**Min. - Max. Contaminant Quantity per Single Containment Vessel (mass by %)**
EDTA	Category 2	0 - 5.97
Picolinic acid	Category 1	0 - 10.7
Formic acid	Category 1	0 - 0.17
Citric acid	Category 1	0 - 4.21
Total ligands		0 - 10.87

Table 1 shows that ligands from both Categories 1 and 2 are present in the IX resin waste; because of their greater availability for biological remediation and other destructive processes, Category 1 complexants are not subject to as stringent control as the waste EDTA content.[17] Before the IX resin waste can be accepted for disposal at LLWR, a treatment method to completely destroy the contaminant EDTA (beyond an acceptable limit of detection (LOD)) must be identified.

Treatment methods under consideration include pyrolysis, vitrification, wet oxidation and incineration, all of which have undergone trials using inactive simulant IX resin waste. In this paper, we assess the efficacy of an incineration method in the thermal-destruction of EDTA in an IX resin matrix.[18-20]

There are numerous examples of incineration processes being used to treat spent IX resins throughout the international community. One major point of difference between incineration strategies is that some rely on a mixed waste feed, where spent resins are combined with other combustible wastes prior to burning, whilst other designs are solely dedicated to the purpose of IX resin destruction. The calorific value of the resins usually varies between 2 and 6 MJ/kg depending on the water content (dependent on the concentration of styrene cross-links), and is insufficient to allow the resins to self-burn.[20] Therefore, purpose-built incinerators must also incorporate a liquid fuel injection system to maintain the temperature in the combustion chamber and are, hence, usually a more complex design than conventional waste incinerators. It has also been noted that resins have a tendency to form large clusters by melting before burning resulting in incomplete combustion and problems for the incinerator refractory.[21-27]

Advantages of incineration for the management of LLW include its significant volume reduction factor (suggested to range from 30 - 100)[20], which allows for immobilisation with smaller quantities of solidifying material, making a more stable wasteform and optimising repository capacity. The oxidative process also serves to release ^{14}C from the IX resin matrix as CO_2 gas, which is beneficial from an LLWR perspective, which has a defined total site capacity of 130 TBq for ^{14}C, and this can be restrictive for wastes with a high content of this radionuclide.[28] Carbon-14 accounts for the third largest portion of the total activity in the spent IX resins (9%), behind ^{55}Fe (39%) and ^{60}Co (43%).[1] However, the half-life of ^{14}C ($t_{1/2}$ = 5730 y) makes its potential environmental impact persist for a much greater period than ^{55}Fe ($t_{1/2}$ = 2.74 y) and ^{60}Co ($t_{1/2}$ = 5.27 y). Ideally, > 99% of the ^{14}C should be removed from the resin during the selected treatment process.[1]

EDTA is generally only stable up to around 200 °C, though the absolute thermal degradation temperature of the molecule is dependent on a range of factors (e.g. water content, oxygen level, pH, degree of sodiation, metal complexation).[29] A thermal-destructive process potent enough to oxidise > 99% of the ^{14}C content is expected to be capable of completely destroying the contaminant EDTA.

Demonstration of the complete destruction of the ligand by application of a bespoke analytical procedure is beneficial as it allows the finite capacity of the repository for EDTA to be reserved and optimised.

Historically, different methods have been used for EDTA determination, e.g. gas/liqiud-chromatography[12,13,30], potentiometry[12,31], capillary electrophoresis[32] and a number of spectrophotometric methods.[33] High-performance liquid-chromatography (HPLC) has been demonstrated to be a reliable method for EDTA analysis in complex sample matrices, owing to its high selectivity and sensitivity. EDTA is usually eluted and detected in the form a metal-complex, using a reversed-phase (RP) system coupled with UV-detection. Use of a range of metal-ions and mobile phases has been reported.[12,13,30,33-36] Previous work in this group sought to optimise a method originally outlined by Nowack *et al*. in 1996[13] for RP-HPLC quantification of Fe(III)-APCA species in complex environmental matrices, with chromatographic separation achieved on a monolithic silica stationary phase. An LOD of 0.35 μM for Fe(III)-EDTA using the optimised method was achieved.[37] In order to perform liquid-chromatographic analysis on the EDTA content of the solid IX resin residue, an extraction procedure is required; solid-liquid phase extraction of EDTA with subsequent RP-HPLC analysis has been reported previously, including direct addition of transition metal solution (Cu(II)) (LOD = 10 mg/L).[34,35] Here, we report on an optimised method for EDTA determination in an incinerated IX resin matrix.

3.2 Materials and Method

3.2.1 Chemicals and Reagents

EDTA disodium salt ($Na_2EDTA{\cdot}2H_2O$), iron trichloride hexahydrate ($FeCl_3{\cdot}6H_2O$), iron-EDTA monosodium trihydrate (NaEDTA-Fe(III)$\cdot 3H_2O$), tetrabutylammonium bromide (TBA-Br), sodium formate, sodium hydroxide, acetonitrile (HPLC Grade, >99.9%), acetone, hydrochloric acid (Sigma-Aldrich, Merck KGaA, Darmstadt, Germany), formic acid (Fisher Scientific, Loughborough, UK) were obtained at ACS reagent grade or above. Deionised (DI) water (>18 MΩ/cm) used for all applications was obtained from

a Millipore® system, fitted with a SimPak® 1 cartridge (Merck Chemicals Ltd, Nottingham, UK).

3.2.2 Incinerated Ion-Exchange Resin

Incinerated IX resin material was obtained from Babcock International Group (Devonport Royal Dockyard, Plymouth, UK). Representative MODIX resin (Purolite® NRW-37) was doped with EDTA in the quantity 60 g EDTA / 1 kg resin (dry weight), representative of a worst-case scenario chemical complexant content (Table 1). Incineration was carried out in a laboratory furnace at 400 °C for 8 h and the resulting residue was left to cool overnight. The quantity of residue was higher than anticipated (10 % by mass), possibly owing to incomplete combustion.[27] A blank residue was produced by the same method but without inclusion of EDTA. The residues constituted hard, black spheres (roughly 0.5 mm diameter). Batches of these incineration products were received at The University of Manchester in March 2017.

3.2.3 Preparation of Samples

An EDTA stock solution (2.69 mM) was prepared by dissolving $Na_2EDTA{\cdot}2H_2O$ (0.1001 g) in DI water (100 mL). Sequential dilution of the stock solution yielded five further standard solutions (269, 26.9, 2.69, 0.269 and 0.0269 μM).

Incinerated IX resin residue was ball-milled to a fine talc-like powder. 500 mg aliquots of the powder were weighed out into 2 mL centrifuge tubes (Safe-Lock, Eppendorf, Stevenage, UK) and 500 μL of EDTA standard solution was added to each aliquot of ash. The centrifuge tubes were capped and shaken to ensure complete homogenisation of the two phases, then left in a vacuum desiccator for one week to evaporate to complete dryness (uncapped), to produce EDTA-spiked residue samples at 1000, 100, 10, 1, 0.1 and 0.01 mg kg^{-1}. Un-spiked samples of residue were produced by an identical method but substituting the aliquots EDTA standard solutions with DI water. All samples were produced in quadruplicate.

3.2.4 Solid-Liquid Extraction

3.2.4.1 Preparation of Extractant

An Fe(III) solution (10 mM) was prepared by dissolving $FeCl_3 \cdot 6H_2O$ (0.2730 g) in DI water (100 mL) (pH 2.45). The Fe(III) extractant solution was always freshly prepared on the day of its use to minimise the effect that Fe(III) hydrolysis and precipitation could have on the chemical and physical environment of the extraction matrix.

3.2.4.2 Extraction Procedure

1 mL of the Fe(III) extractant solution was added to each of the centrifuge tubes containing samples of IX resin residue. The samples were shaken to ensure complete homogenisation of the two phases and then left capped and undisturbed for 2 hours for the extraction to proceed. The samples were then centrifuged at 14000 rpm for 30 min; the resulting supernatants were transferred to 0.5 mL tubes and centrifuged again at 14000 rpm for a further 30 min. The final supernatants were collected, transferred to 2 mL autosampler vials, and analysed by HPLC.

3.2.5 Chromatography

3.2.5.1 Chromatographic Equipment

HPLC analysis was performed on an Agilent 1260A system (Agilent Technologies, Santa Clara, CA, USA) coupled to a diode-array detector (DAD). The DAD was programmed to record UV-absorption (190 - 400 nm) over the entire chromatographic retention time range. The system was fitted with a quaternary pump, online degasser, autosampler with 100 μL sample loop and thermostatted column oven. The column was a monolithic silica Chromolith® HighResolution RP-18 end-capped (4.6 × 150 mm) analytical column fitted with a Chromolith® HighResolution monolithic silica RP-18 end-capped (4.6 × 5 mm) guard cartridge (Merck Millipore, Merck Chemicals Ltd, Nottingham, UK).

3.2.5.2 Chromatographic Conditions

All chromatography was carried out isocratically at 25 °C with a 0.6 mL/min flow-rate of buffered mobile phase (20 mM formate buffer, pH 3.3, prepared by dissolving 10

mM TBA-Br ion-pair agent, 5 mM sodium formate, 15 mM formic acid, and 8% acetonitrile in DI water). The injection volume was 10 μL and always performed in duplicate. Elution was monitored at 258 nm (λ_{max} Fe(III)-EDTA).

3.2.5.3 Calibration

An Fe(III)-EDTA stock solution (10 mM) was produced by dissolving NaEDTA-Fe(III)·3H_2O (0.4242 g, 1 mmol) in DI water (100 mL) and diluted in triplicate to yield solutions of the concentration 5000, 1000, 500, 100, 50, 10, 5, 1 and 0.5 μM. The HPLC system was calibrated by plotting the chromatographic response (integrated peak area (mAU)) of the aqueous Fe(III)-EDTA samples against the concentration to produce a calibration curve.

3.2.6 Data Processing

All chromatograms were initially processed using Agilent's ChemStation OpenLAB software (V. A.01.02). Peak integration was performed using ChemStation when the Fe(III)-EDTA peak was not convoluted with other chromatographic peaks. When peak overlap was observed, the data was exported to OriginPro 2017 (8.5.1) to be treated with a least-squares fitting (LSF) procedure. The Fe(III)-EDTA standard calibration data was analysed by both data processing methods. The concentration of EDTA recovered from real samples by solid-liquid extraction was determined by comparison of the calculated Fe(III)-EDTA peak area to the appropriate calibration data.

3.2.6.1 Least-Squares Fitting

Chromatograms of the HPLC calibration samples (aqueous solutions of Fe(III)-EDTA) were fit first to determine the peak shape and fitting parameters. The fitting parameters obtained during analysis of the single-species calibration data were used to guide the initial parameter input during the analysis of the convoluted data obtained from the real samples.

The baseline of each peak was determined as a straight line connecting the respective absorption minima ($d^2y/dx^2 = 0$) at retention times before and after the Fe(III)-EDTA peak elution. The line connecting these points was then rescaled to $y = 0$. A Gram-

Charlier A Series (GCAS), which is a modified Gaussian curve and used widely for gas chromatographic data[38,39], was found to best fit the calibration data. The peak position and shape are determined by five fitting parameters: centre, amplitude, half-width and two expansion factors defining the asymmetry of the peak and used to capture the effect of chromatographic peak tailing. Characteristic values of the expansion factors were determined from all calibration chromatograms; these values were inputted and held constant during the analysis of the Fe(III)-EDTA peak in chromatographic data derived from IX resin residue samples.

3.2.7 Method Optimisation

The method described above gives details of the final, optimised quantification procedure. Here, we provide an overview of the steps taken to arrive at this method and the justification for each of them.

At the outset of the project, HPLC was selected as the analytical method of choice because of the sensitivity and selectivity of the pre-optimised Fe(III)-EDTA detection system.[37] For the EDTA associated with the solid IX residue to undergo the liquid-chromatographic analysis, and to maximise the potential sensitivity of the HPLC system, it was apparent that it would be necessary to develop and optimise an efficient solid-liquid phase extraction procedure. The primary objective of the extraction procedure was to ensure the liquid-phase contained a maximal concentration of Fe(III)-EDTA per unit mass of solid IX resin residue. Other factors such as speed, simplicity, reliability, precision and universality were also considered.

The following experimental outline was initially proposed: the solid residue was to undergo extraction in an aqueous medium with a tailored pH, before an aliquot of extractant was removed, filtered and evaporated to dryness to leave an EDTA precipitate, which was then re-dissolved in a smaller volume of $FeCl_3$ solution to complex the ligand for HPLC analysis and concentrate the analyte (pre-concentration). A systematic trial phase was conducted to optimise the variables in this experimental outline: residue particle size, extractant pH, extraction time, solid:liquid ratio and pre-concentration volumes.

Unless stated otherwise, EDTA-spiked samples of blank residue (blank residue = no EDTA added prior to incineration) were used in the optimisation process. These samples were prepared as described in Section 3.2.3 (evaporation of an aqueous EDTA solution to leave an EDTA precipitate of specified mass).

The residue particle size was altered by differing the technique (or time/work) used to grind the starting material (e.g. unground, pestle and mortar or motorised ball-mill), the particle size distribution was measured by sieve analysis (500, 180, 75 μm mesh apertures) and the arithmetic mean was calculated using GRADISTAT.[40] Extractant media of varying pH were produced by pH balancing DI water with NaOH or HNO_3 (pH 1 - 12 tested). The progression of the extraction as a function of time was monitored by removing aliquots of the extractant from the extraction matrix over a series of increasing time intervals (0, 30, 60, 120, 180 min extraction periods). The effect of the solid:liquid ratio was assessed by varying the volume of extractant medium in contact with different quantities of residue.

From this work, a formative method was developed and tested on samples of residue that were generated from IX resin doped with EDTA prior to incineration. The parameters of the method were as follows: 10 mL of DI water was added to 0.5 g of samples of EDTA-spiked residue in a glass vial; the extraction was left to proceed for 2 h before 5 mL of extractant was removed, filtered and evaporated to dryness in a new glass vial; the resulting EDTA precipitate was then re-dissolved in 1 mL of Fe(III)-EDTA solution and analysed by HPLC. From here on in, this extraction method will be referred to as Method 1. The final, optimised extraction method reported in Section 3.2.4 will be referred to as Method 2.

The impact that specific steps of Method 1 had on the EDTA percent recovery was tested by preparing solutions of known EDTA concentration to simulate extractant solutions of 100% recovery. Using these solutions to bypass certain stages of the method (e.g. solid-liquid extraction, pre-concentration) it was possible to elucidate the contribution of each step to the observed loss of EDTA over the course of a given trial method.

The major points of difference between Method 1 and Method 2 are the elimination of the pre-concentration and the introduction of Fe(III) solution as the extractant medium. The reasons for these adaptations are discussed in the sections that follow.

3.2.8 Method Validation

The HPLC Fe(III)-EDTA calibration data were assessed for linearity (linear regression (r^2) (acceptance criteria: $r^2 \geq 0.98$)), sensitivity (limit of detection (LOD) and limit of quantification (LOQ) = 3.3(σ/S) and 10(σ/S), respectively, where S is the slope and σ is the standard deviation of the peak intensities for samples of lowest, measurable concentration) and precision (relative standard deviation (%RSD) (intra-day) of the mean chromatographic response at each concentration (acceptance criteria: %RSD ≤ 10%)).

At all stages of development, the overall quantification procedure was also validated for its accuracy, precision, selectivity and sensitivity. The accuracy was evaluated by calculating the mean percent recovery of EDTA from the EDTA-spiked residues (accuracy calculated for extraction from both samples of residue (blank and EDTA-doped)). The precision has been expressed as %RSD and was calculated from the standard deviation of the mean concentration of EDTA recovered from each EDTA-spiked sample; the comparative results of intra- and inter-day precision were obtained by performing analyses in duplicate on two separate days (acceptance criteria: %RSD ≤ 10%).

The selectivity of the method was confirmed by comparison of the chromatographic Fe(III)-EDTA peak obtained in the analysis of samples of IX resin residue to the single-species Fe(III)-EDTA HPLC calibration data; equivalent retention times and UV-profiles, obtained from the DAD, help to verify the identity of the analyte. The goodness-of-fit of the LSF procedure was monitored by regression analysis (r^2) and maintained above acceptable criteria ($r^2 \geq 0.98$).

The LOD of the overall procedure was determined by extrapolation of the trend in EDTA recovery, with respect to molarity, to the LOD of the HPLC detection method.

This was compared with the theoretical procedural LOD obtainable if 100% recovery was assumed.

The robustness of the final method was tested by applying it to different variations of EDTA-spiked incinerated IX resin; resin doped with EDTA prior to incineration and ball-milled, doped with EDTA prior to incineration and left unground, and samples of the blank incineration product both ball-milled and unground. Following observations that the recovery of the EDTA-spike was affected by the presence of EDTA in the pre-incineration matrix, Brunauer-Emmett-Teller (BET) theory was applied to assess the surface area of each sample on the assumption that the micro/macro-porous area was affected by the thermal degradation products of the EDTA starting material, and that this may be correlated with the differences in observed percent recovery. The samples were purged of adsorbed water by heating under helium using a FlowPrep 060 and BET analysis was performed under nitrogen using a Gemini 2360 Surface Area Analyser (Micromeritics Instruments Corp., Norcross, GA, USA).

To further corroborate these findings, an acetone wash was performed on the powdered IX resin doped with EDTA prior to incineration by leaving 1 g of the material submerged in 10 mL of acetone for 24 h to extract a portion of the EDTA thermal degradation products associated with the residue. Filtration was used to separate the washed residue from the acetone extractant which, after evaporation of the solvent, was found to leave a grease-like solid presumed to contain a mixture of EDTA thermal degradation products; treating the blank residue by the same acetone extraction procedure left behind no visible product. Following the treatment with acetone, the IX residue was spiked with EDTA to undergo extraction and quantification using the final method described previously.

3.3 Results and Discussion

3.3.1 Method Optimisation

The variable parameters of the extraction procedure were optimised in a systematic trial phase using the experimental procedure outlined in Section 3.2.7. Initial refinement of the variables led to the generation of Method 1.

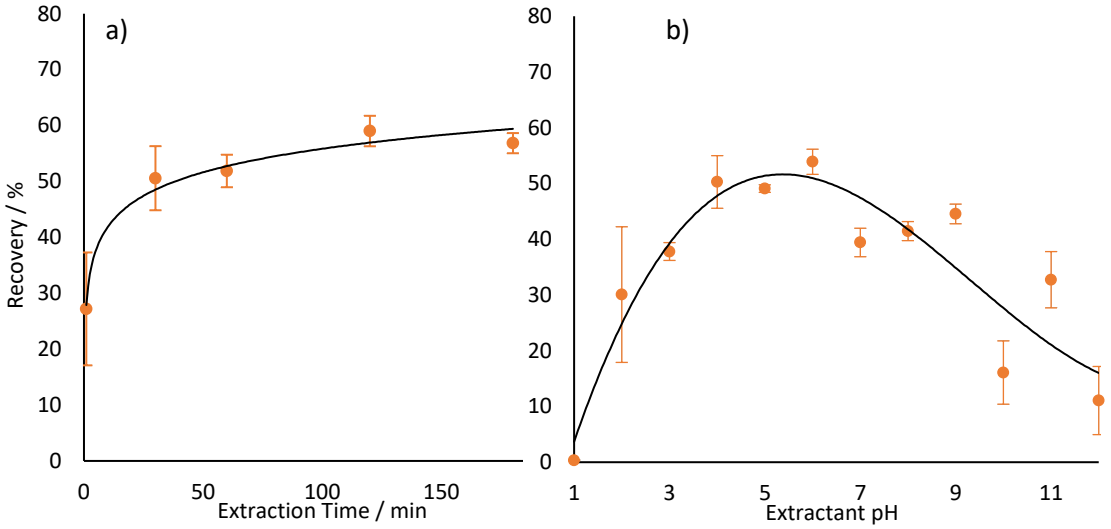

Figure 1. a) EDTA percent recovery as a function of extraction time (other parameters: EDTA-spike extracted from blank residue in DI water), b) EDTA percent recovery as a function of extractant pH (other parameters: EDTA-spike extracted from blank residue for 2 h). Error = σ.

The percent recovery of EDTA as a function of extraction time is displayed in Figure 1a. The data has been fitted with a logarithmic curve. An extraction time of two hours has been recommended in the final method, which represents a compromise between experimental expedience and maximisation of the recovery. Analysis of the trend in standard deviation suggests that the magnitude of σ decreases with increasing time, before plateauing at around the 2 h mark (σ < 3%). This suggests that sufficient time had been allowed for equilibration of the EDTA between the liquid and solid phases.

The extraction medium was pH balanced with solutions of HNO_3 and NaOH before addition to the incineration residue. The residue itself had no measurable effect on the pH of the solution, nor did the EDTA in the quantities used to spike the samples. The data has been fitted with a third order polynomial curve to highlight the optimal pH (Figure 1b), though the actual trend may be more complex as it follows a relationship between the recovery and the seven states of EDTA ionic speciation afforded by the six protonation sites (H_6EDTA^{2+}, H_5EDTA^{+}, H_4EDTA, H_3EDTA^{-}, H_2EDTA^{2-}, $HEDTA^{3-}$, $EDTA^{4-}$). Of the results presented in Figure 1b, DI water was found to give rise to the greatest EDTA percent recovery. $HEDTA^{3-}$ is the dominant species at this pK_a.[41]

Ultimately, a 10 mM aqueous solution of $FeCl_3$ (pH 2.45) replaced DI water as the extractant of choice in Method 2. Three reasons underpinned this: the thermodynamic favourability of direct Fe(III)-complexation in solution induced a sufficiently favourable

distribution coefficient between the solid and liquid phases; complexation of the EDTA with Fe(III) in the first step of the procedure removed the need to dilute the extract by addition of Fe(III) solution at a later stage; and the procedural simplification led to greater efficiency and improved accuracy by elimination of the potential error associated with additional measurements. Therefore, the results presented in Figure 1b have no bearing on Method 2 as the pH of the extractant is determined by the concentration of the Fe(III) in the solution. Method 2 recommends a 2 h extraction period, which is an artefact from the parameters of Method 1 (determined by the results in Figure 1a), as the kinetics of the updated extraction procedure were not reassessed.

The particle size of the residue to undergo extraction was found to have an insignificant effect on the EDTA recovery; for example, mean particle size (diameter) = 110 μm, percent recovery = 66 ± 5% vs. mean particle size = 60 μm, percent recovery = 71 ± 4%. However, a ball-milled residue powder has been included in the final experimental procedure as it is assumed that any EDTA to have resisted thermal degradation will have done so with the shielding afforded by encapsulation within the hard spheres that form as the resin melts during incineration.[27]

A pre-concentration step was included in Method 1. It was anticipated that its effect would be to lower the overall procedural LOD by promoting the primary objective of maximising the concentration of Fe(III)-EDTA of the extractant liquid per unit mass of solid IX resin residue.

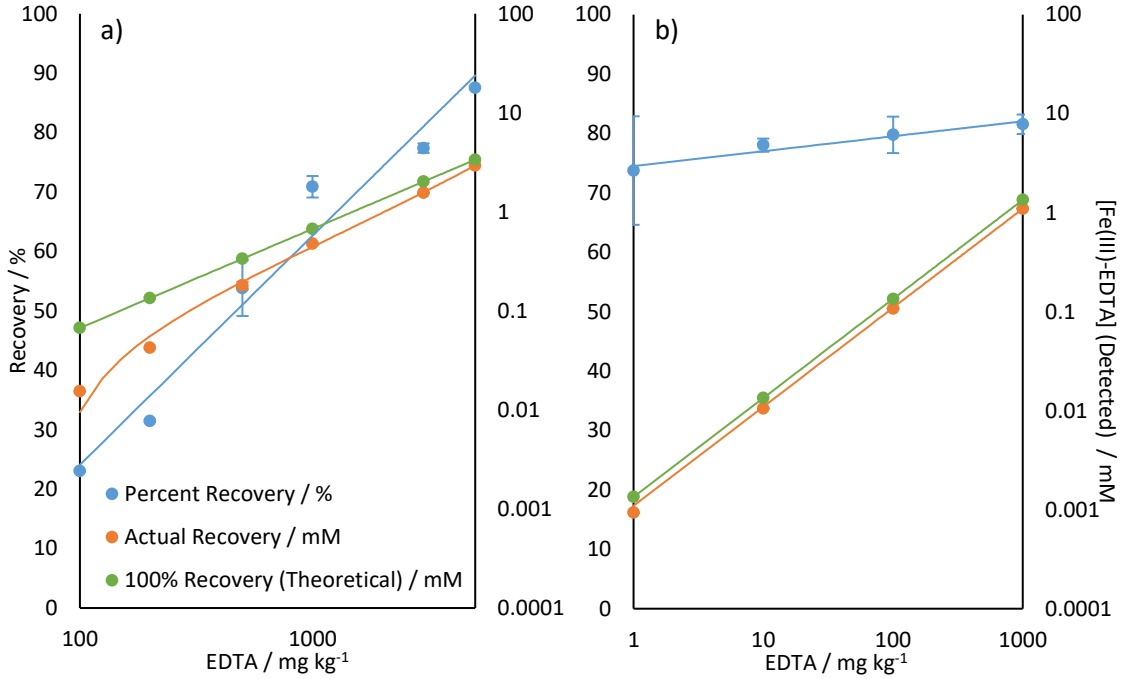

Figure 2. a) Method 1 b) Method 2 (see text for details). Trends: percent recovery (blue, left *y*-axis, %), actual recovery (orange, right *y*-axis, mM), theoretical result assuming 100% recovery (green, right *y*-axis, mM). Left *y*-axis = $\log_{10}$ [Fe(III)-EDTA] available in solution for detection by HPLC in mM. Error = σ.

Figure 2a shows the results of a trial experiment that involved pre-concentration of the extractant before HPLC analysis (Method 1). Tests of the method revealed an exponential decrease in the percent recovery of the EDTA-spike as the concentration of the spike was decreased. Extrapolation of the theoretical linear trend traced by the extractant concentration when 100% recovery was assumed predicted a procedural LOD of 0.52 mg kg^{-1}; extrapolation of the observed polynomial trend of the actual results obtained by application of Method 1 predicted an LOD of 71 mg kg^{-1} (Table 2). Comparative results for the final optimised method are displayed in Figure 2b; extrapolation of the linear trend in actual recovery gives a procedural LOD of 0.32 mg kg^{-1} (Table 2).

Table 2. Parameters of equations derived from regression analysis of the plots of actual and theoretical EDTA recovery as a function concentration of the EDTA-spike. Calculated LOD determined by extrapolation of trends to LOD of the HPLC detection system. Details of Methods 1 and 2 available in text.

	Method 1			**Method 2**		
	Equation of Trendline	r^2	**Calculated LOD / mg kg^{-1}**	**Equation of Trendline**	r^2	**Calculated LOD / mg kg^{-1}**
100% Recovery	$y = 0.0007x$	1	0.52	$y = 0.0013x$	1	0.26
Actual Recovery	$y = 3\times10^{-8}x^2 + 5\times10^{-4}x - 0.0358$	0.9997	71	$y = 0.0011x$	0.9999	0.32

The theoretically obtainable LOD of Method 2 is half that of Method 1 despite the removal of the pre-concentration step (also expressed in the factor of 2 difference between the gradients of the linear trends for each method's theoretical 100% recovery) (Table 2). This was mainly achieved by increasing the solid:liquid ratio (Method 1 = 0.5 g: 10 mL, Method 2 = 0.5 g: 1 mL) and changing the extractant to an Fe(III)-solution (promoting a favourable distribution coefficient and removing the need for dilution after extraction).

Analysis of simulant extraction solutions was used to probe the effect of each stage of the procedure on the overall observed percent recovery. EDTA solutions of known concentration were made to simulate a 100% effective solid-liquid extraction and analysed using the remainder of the procedure to determine where the EDTA was lost (e.g. pre-concentration or HPLC analysis).

Only 23% of the 100 mg kg^{-1} EDTA-spike (67.2 μM, Figure 3) was recovered using Method 1. 52% of the simulant extractant solution was recovered after pre-concentration and HPLC analysis. Without extraction or pre-concentration (addition of an Fe(III)-solution to an EDTA solution followed by HPLC analysis), roughly 100% recovery was observed at all concentrations tested. Therefore, for the 100 mg kg^{-1} spiked sample, only roughly 29% of the EDTA not recovered as Fe(III)-EDTA can be attributed to the solid-liquid extraction. 48% was calculated to have been lost during pre-concentration, hence its removal from the procedure. This effect may be attributable to strong adsorption interactions that form between the ligand and the surface of the glass vial after evaporation to dryness.

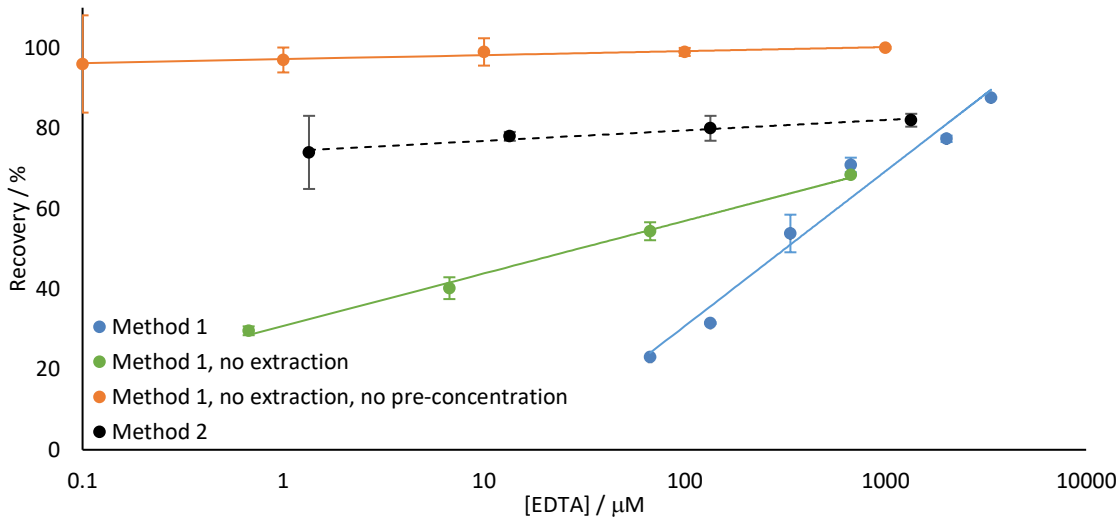

Figure 3. EDTA percent recovery as a function of EDTA concentration (μM). Method 1 (blue) = solid-liquid extraction, pre-concentration, HPLC analysis. Method 1, no extraction (green) = simulant extraction solutions, pre-concentration, HPLC analysis. Method 1, no extraction, no pre-concentration (orange) = simulant extraction solutions, Fe(III) solution added, HPLC analysis. Method 2 = optimised method. Error = σ.

Figure 3 shows the percent recovery results for the Method 1 simulant extractions compared with the results of the optimised Method 2. To varying extents, all of the logarithmic trends decrease with decreasing concentration of EDTA; the recoveries of Method 1 fall off very sharply, explaining the high LOD predicted for the procedure. The trend in green (Method 1, no extraction) shows that the effect of pre-concentration on reducing the recovery is greater for samples of low concentration. Though the results of Method 2 decrease logarithmically, the recoveries are much more consistent across the range (1000 mg kg^{-1} (1344 μM) = 82%, 1 mg kg^{-1} (1.344 μM) = 74%) allowing for greater sensitivity (see later; Table 4).

3.3.2 Method Validation

The HPLC detection system was calibrated using aqueous samples of Fe(III)-EDTA reference material. The LOD, LOQ, slope, linearity (r^2) and precision (%RSD at 1 μM) are reported in Table 3. The method has previously been optimised and applied for the detection of Fe(III)-EDTA in complex matrices. The results in Table 3 have been determined by calculating the peak area of the chromatographic response using the LSF procedure, which was also validated in previous work.[37]

Table 3. LOD, LOQ, slope, linearity and %RSD values for Fe(III)-EDTA under the pre-optimised chromatographic conditions, determined using aqueous samples of crystalline Fe(III)-EDTA reference material. %RSD reported for 1 μM standard solutions.

	LOD / μM	LOQ / μM	Slope	r^2	%RSD (1 μM)
Fe(III)-EDTA	0.35	1.1	0.15	0.9999	10.8

The optimised extraction and quantification procedure (Method 2) has been validated for its accuracy, precision, selectivity and sensitivity on a range of IX resin incineration residue matrices. The results are presented in Table 4.

Table 4. Method validation results for optimised extraction procedure (Method 2). BET surface area, percent recovery and intra/inter-day recovery determined for EDTA-spikes (post-incineration) at various concentrations. Results also determined for various IX resin matrices; EDTA-doped pre-incineration or blank residue, ground or unground.

IX Resin Matrix	BET Surface Area / $m^2\ g^{-1}$	EDTA Added to Residue / mg kg^{-1}	Total EDTA Recovered / %	Intra-day Precision / %RSD	Inter-day Precision / %RSD
EDTA doped prior to incineration, residue ball-milled	1.4 ± 0.1	1000	82 ± 1.6	1.6	2.0
		100	80 ± 3.1	2.6	3.9
		10	78 ± 1.1	1.5	1.4
		1	74 ± 9.1	9.5	12.4
		0	ND	ND	ND
EDTA doped prior to incineration	0.1 ± 0.06	1000	89 ± 1.4	1.4	1.6
		100	87 ± 1.3	0.7	1.5
		10	81 ± 0.9	1.4	NT
		0	ND	ND	ND
No EDTA prior to incineration, residue ball-milled	87 ± 2.7	1000	47 ± 2.6	1.2	5.5
		100	38 ± 1.0	1.8	2.8
		10	28 ± 2.2	2.8	7.9
		0	ND	ND	ND
No EDTA prior to incineration	34 ± 0.8	1000	46 ± 2.3	4.2	5.1
		100	39 ± 1.7	1.8	4.3
		10	33 ± 3.0	2.0	9.0
		0	ND	ND	ND

ND = not detected, NT = not tested.

Application of Method 2 to ball-milled samples of residue formed from IX resin doped with EDTA prior to incineration resulted in a mean recovery 78 ± 3.3% over the concentration range tested. This result is considered acceptably high as evidence from the method optimisation process points to a limitation on the percent recovery (< 100%) brought about by the partitioning of the EDTA during solid-liquid extraction (29% of the 100 mg kg^{-1} spike not recovered as Fe(III)-EDTA attributed to sorption to the IX residue (extraction in DI water)).

Values of intra/inter-day precision, presented as %RSD, are generally low (%RSD < 5%) and fall well within the acceptance criteria (%RSD ≤ 10%). The only exception is the 1 mg kg^{-1} standard (inter-day %RSD = 12.4%). 100% recovery of the 1 mg kg^{-1} spike would have resulted in 1.3 μM solution; the actual recovery (74 ± 9.1%) produced a 0.93 μM solution; the LOQ of the HPLC detection system is 1.1 μM. Therefore, the concentration of the Fe(III)-EDTA extractant solution produced for HPLC analysis was slightly below the LOQ of the system and subject to more variance.

Taking into account the LOQ of the HPLC detection system, the LOQ of the overall procedure was calculated to be 1.0 mg kg^{-1}. Figure 4 shows the chromatographic response obtained from extraction of the various EDTA-spiked standards; the Fe(III)-EDTA peak produced by extraction and analysis of the 1 mg kg^{-1} standard is clearly visible (t_r ≈ 7.7 min, Figure 4, inlay). The LOD of the overall procedure has been calculated to be 0.32 mg kg^{-1} by extrapolation of the trend in actual recovery to the LOD of the HPLC system.

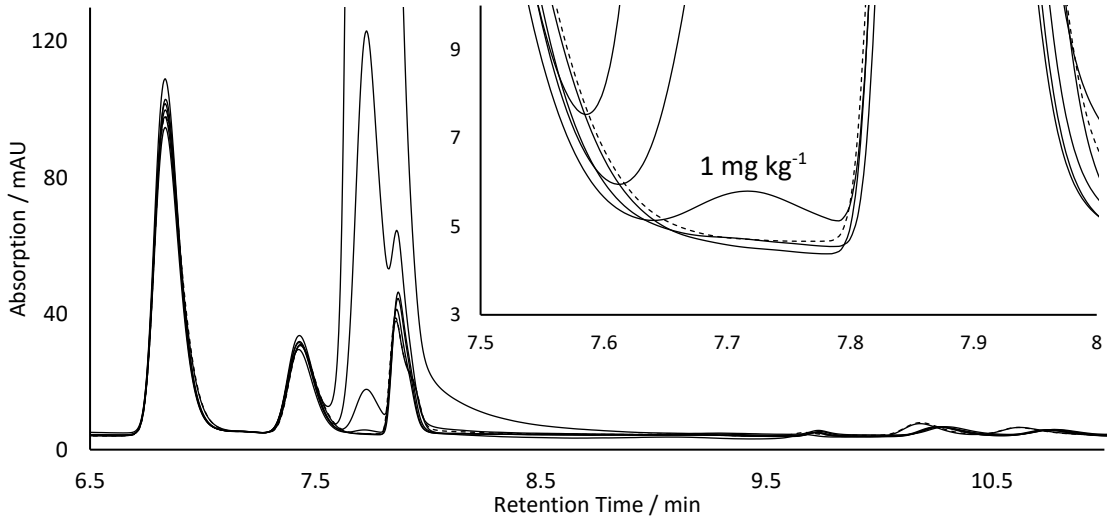

Figure 4. Exemplary chromatograms recorded at 258 nm for samples of residue spiked with various concentrations of EDTA, having undergone extraction and quantification using the optimised method (Method 2). Fe(III)-EDTA peak t_r ≈ 7.7 min, concentration of EDTA-spike decreases with decreasing intensity of Fe(III)-EDTA peak; 1000 (peak beyond *y*-axis scale), 100, 10, 1 (peak visible in inlay), 0.1 (peak not detected), 0.01 (peak not detected) mg kg^{-1}. Chromatogram represented by dashed line = 0 mg kg^{-1} EDTA-spike (chromatogram visible in inlay, peak not detected). Inlay: expansion of Fe(III)-EDTA t_r region.

The chromatogram plotted with a dashed line (Figure 4) shows the chromatographic response of an un-spiked sample of IX resin residue doped with EDTA prior to incineration. No Fe(III)-EDTA is detectable in the samples, confirming that the vast

majority (to below 0.32 mg kg^{-1}) of the EDTA was destroyed in the incinerator. Confidence in the destruction of EDTA to concentrations below this level is sufficient to satisfy the constraints agreed with LLW Repository Ltd at the outset of the project.

Figure 5 shows the various peaks that are detected over the chromatographic retention time range 0 - 30 min (absorption at 258 nm). The chromatogram was produced by analysis of a 100 mg kg^{-1} EDTA-spiked sample of IX resin doped with EDTA prior to incineration. The Fe(III)-EDTA peak is visible at $t_r \approx 7.7$ min; the peak was confirmed to be representative of Fe(III)-EDTA by comparison of the retention time, and UV-profiles extracted from the three-dimensional DAD data, to the single-species calibration data produced by analysis of crystalline Fe(III)-EDTA reference material ($t_r \approx$ 7.7 min, $\lambda_{max} = 258$ nm).

The other peaks visible in the chromatographic retention time range indicate the presence of EDTA thermal degradation products in the extractant solution (Figure 5a). The species are known to be EDTA products because they do not appear in the chromatograms produced in the analysis of blank IX resin residue (Figure 5b).

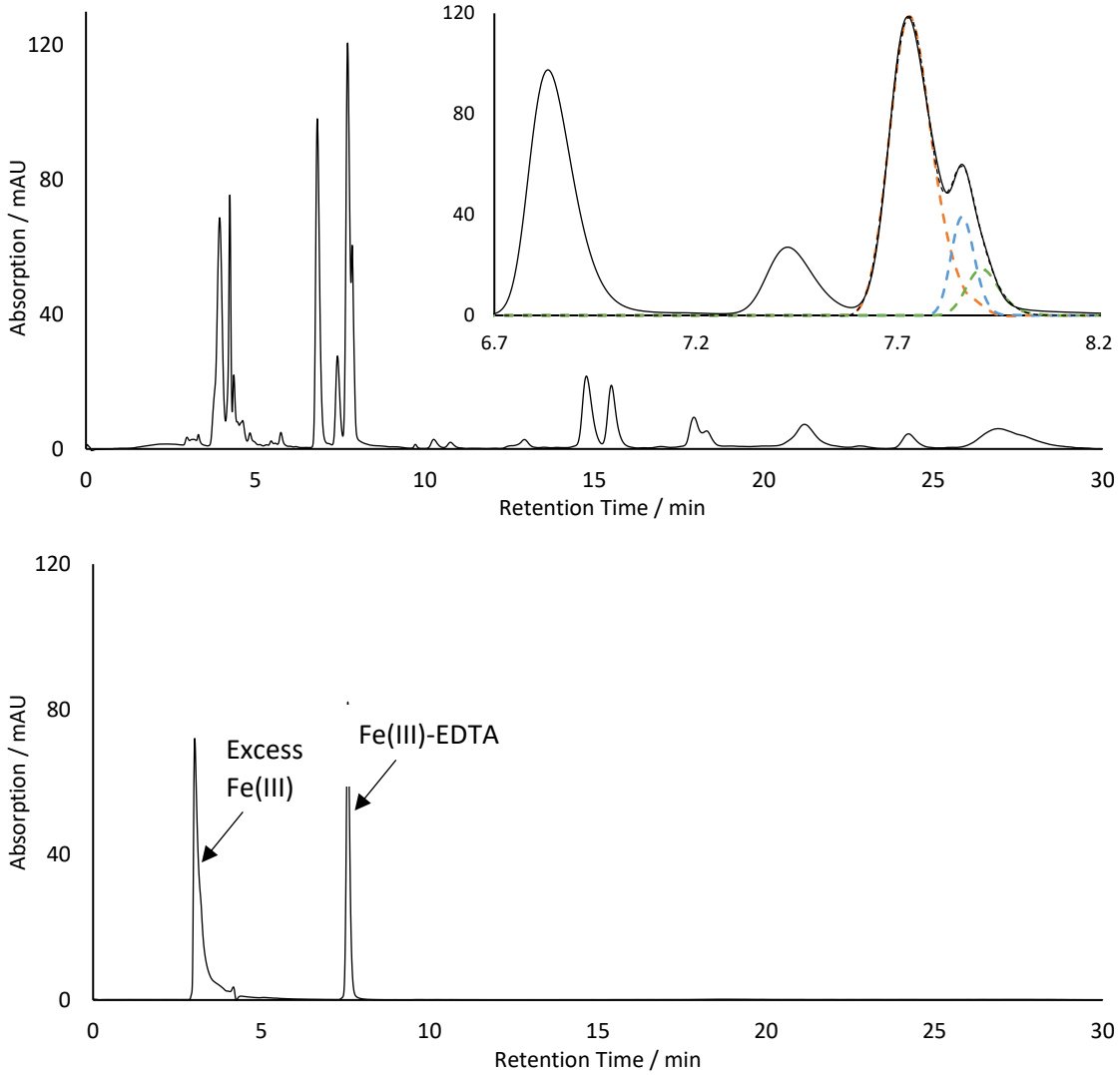

Figure 5. a) Example chromatogram recorded for sample of residue spiked with 100 mg kg^{-1} EDTA, having undergone extraction and quantification using the optimised method (Method 2). Inlay: expansion of Fe(III)-EDTA t_r region, peaks fitted according to LSF procedure: orange dashes = Fe(III)-EDTA fit results, blue/green dashes = interfering peak (EDTA-thermal degradation product) fit results, black dashes = overall fit, black line = experimental data. b) identical experimental parameters; extraction from EDTA-spiked blank residue.

The peaks of three of the EDTA-thermal degradation products interfere with the Fe(III)-EDTA peak ($t_r \approx 7.4$ and 7.9 min, Figure 5). The peak at $t_r \approx 7.9$ min is assumed to be composed of two individual peaks because of the apparent peak shoulder on the high t_r flank (best visualised in Figure 6). A LSF procedure was implemented to elucidate the actual peak area of the Fe(III)-EDTA peak; an exemplary fit has been displayed (Figure 5, inlay).

Identification of the interfering EDTA-thermal degradation products is speculative; the strongly absorbing UV-profiles suggest Fe(III)-complexation, and the similarity of the t_r to Fe(III)-EDTA suggests mononuclear complexation of polydentate degradation

products. Two possibilities are Fe(III) complexes of iminodiacetic acid (IDA) and 2,2'-[(2-hydroxyethyl)imino]diacetic acid (HIDA); the two species are reported thermal degradation products of EDTA, and are both polydentate complexants.[42]

The percent recovery results presented in Table 4 suggest that the quantity of EDTA recovered is dependent on whether or not EDTA is present in the pre-incineration matrix (mean recovery from pre-incineration EDTA-doped resin (ball-milled) = 78 ± 3.3%, mean recovery from blank incinerated resin (ball-milled) = 40 ± 7.0%). This implies that the percent recovery of the extraction procedure is a function of the concentration of EDTA present in the initial pre-incineration matrix.

It was assumed that, upon incineration, the 60 g kg^{-1} mass of EDTA added to the matrix pre-incineration thermally degrades to coat the combusting IX resin spheres in a chemically active surface layer (greater hydrophobicity observed for pre-incineration EDTA-doped IX resin residue than blank residue). It was also assumed that this coating layer would reduce the porosity of the residue structure. This assumption was supported by BET analysis (BET surface area of pre-incineration EDTA doped resin (ball-milled) = 1.4 ± 0.1 m^2 g^{-1}, BET surface area of blank incinerated resin (ball-milled) = 87 ± 2.7 m^2 g^{-1}) (Table 4). Therefore, it was concluded that both chemical and physical differences between the two samples of residue may contribute to the observed difference in EDTA recovery. This hypothesis was tested by performing the extraction and analysis procedure on a sample of pre-incineration EDTA-doped residue that had also been subject to an acetone wash targeted at removing a portion of the surface coating.

The chromatographic peaks in Figure 6a,b show the impact that the acetone wash has on the concentration of two of the EDTA-thermal degradation products at $t_r \approx 7.9$ min (convoluted with the Fe(III)-EDTA peak, $t_r \approx 7.7$ min).

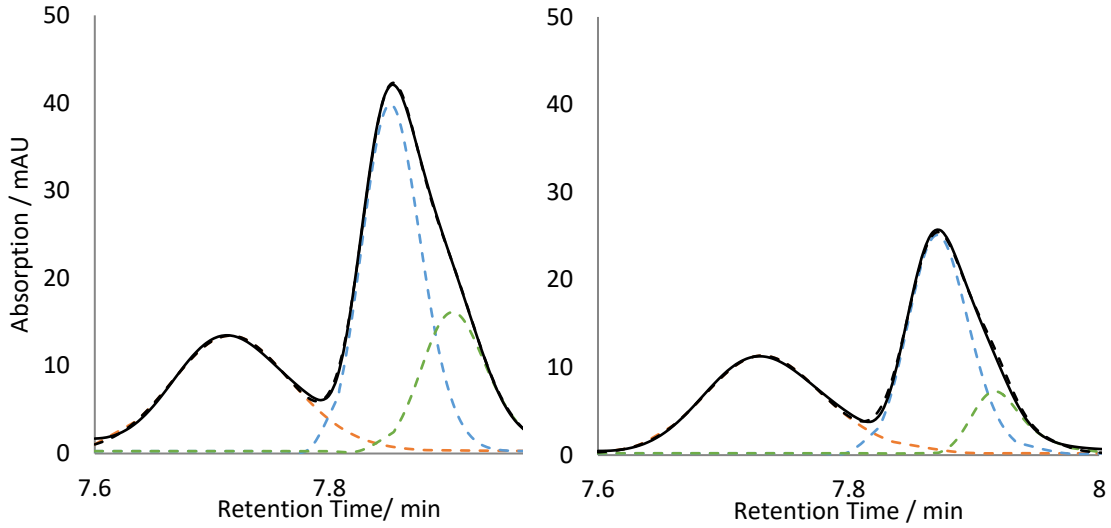

Figure 6. Chromatographic peaks in the Fe(III)-EDTA t_r region recorded for 10 mg kg^{-1} EDTA-spiked samples having undergone extraction and quantification using the optimised method (Method 2). a) Without acetone wash, b) with acetone wash. Orange dashes = Fe(III)-EDTA fit results, blue/green dashes = interfering peak (EDTA-thermal degradation product) fit results, black dashes = overall fit, black line = experimental data.

The results of the acetone wash experiment are presented in Table 5. The BET surface area was increased by almost a factor of 5 after a 24 h submersion in acetone (1.4 ± 0.1 to 6.7 ± 0.2 m^2/g). A similar result was obtained for the unground residue (0.1 ± 0.06 to 0.7 ± 0.1 m^2/g). The percent recovery of the EDTA was generally decreased (mean recovery without acetone = 78 ± 3.3%, with acetone = 73 ± 5.1%), and the decrease is on the order of magnitude that would be expected given the increase in BET surface area (solving the linear equation plotted for BET surface area vs. mean percent recovery predicts 75% recovery for 6.7 m^2/g).

Table 5. BET surface area, percent recovery and intra/inter-day precision results for IX resin residue washed with acetone and spiked with various concentrations of EDTA (to be compared with the first row of results in Table 4).

IX Resin Matrix	BET Surface Area / m^2 g^{-1}	EDTA Added to Residue / mg kg^{-1}	Recovery / %	Intra-day Precision / %RSD	Inter-day Precision / %RSD
EDTA doped, ball-milled, acetone wash	6.7 ± 0.2	1000	75 ± 1.4	1.08	1.91
		100	68 ± 3.4	2.47	4.99
		10	78 ± 2.1	1.25	2.71

The result provides further evidence for the relationship between the BET surface area and the observed recovery, which by proxy, supports the argument that the EDTA concentration in the pre-incineration matrix may affect the recovery.

3.4 Conclusion

A robust and simple method for the quantification of EDTA in an incinerated IX resin matrix has been developed and implemented. The method has been validated for its accuracy (mean recovery = 78 ± 3.3%), precision (%RSD ≤ 10%), sensitivity (procedural LOD = 0.32 mg kg^{-1}) and selectivity (LSF procedure used to determine EDTA peak area). The method is an order of magnitude more sensitive than a similar recently reported extraction and quantification technique for EDTA in feed and premix formulations (LOD = 5.5 mg kg^{-1}). No EDTA was detected in the residue produced in a preliminary trial phase MODIX resin incineration procedure. The method should also be applicable to residues obtained from incineration of other types of IX resin and other carbonaceous matrices from completely different sources. Currently, the method has not been tested on material containing radiological components. Competing ions may interfere with EDTA complexation to Fe(III); further work would be required to assess the impact of radiological contaminant ions on EDTA speciation and quantification.

Extraction of the EDTA-spike from samples of blank IX residue suggested that the procedural recovery may be a function of the EDTA concentration of the pre-incineration matrix. This was found to be a result of the presence of EDTA-thermal degradation products in the residue matrix. Extrapolating these findings to the real ILW resins, and the treatment process they are to undergo, has limited applicability as there are inherent differences to the locality of the EDTA in the simulant pre/post-incineration matrix used in this experimental approach, resulting in different physical and chemical interactions. For example, deposition of the EDTA-spike post-incineration by evaporation can only leave a surface layer of precipitated EDTA; the interactions of this surface layer may not be representative of the interactions of EDTA more thoroughly included in a real incineration residue. Furthermore, treatment of real waste by incineration is likely to involve higher temperatures and more forcing conditions, increasing the degree of oxidation of the interacting thermal degradation products, altering their quantities and properties.

The thermal degradation products have not been identified but results suggest they are polydentate complexing organic ligands (UV-active complex formation when

extracted into Fe^{III}-solution; complexes exhibit similar chromatographic behaviour to parent EDTA ligand). Their potential to mobilise radionuclides in the final wasteform, as known for EDTA, should be explored.

3.5 References

1. MOD, *Ion-Exchange Resin Information Pack*, RESIN IP101, Draft Final, 2015.
2. IAEA, *Classification of Radioactive Wastes,* IAEA Safety Standard Series No. GSG-1, Vienna, 2009.
3. LLWR, *Waste Acceptance Criteria – Low Level Waste Disposal*, WSC-WAC-LOW, V. 5.0, Issue 1, Cumbria, UK, 2016.
4. A. L. Rufus, S. Velmurugan, V. S. Sathyaseelan and S. V. Narasimhan, *Prog. Nucl. Energ.*, 2004, **44**, 1, 13-31.
5. M. Butcheli-Witschel and T. Elgi, *FEMS Microbiol. Rev.*, 2001, **25**, 1, 69-106.
6. J. L. Means and C. A. Alexander, *Nucl. Chem. Waste Man.*, 1981, **2**, 186-193.
7. Radioactive Waste Management (RWM), *Geological Disposal Behaviour of Radionuclides and Non-radiological Species in Groundwater Status Report*, NDA Report no. DSSC/456/01, RWM, Oxford, UK, 2016.
8. Norwegian Radiation Protection Authority (NRPA), *Study of Issues Affecting the Assessment of Impacts of Disposal of Radioactive and Hazardous Waste*, NRPA Report 2018:6, Østerås, Statens strålevern, 2018.
9. R. J. Serne, K. J. Cantrell, C. W. Lindenmeier, A. T. Owen, I. V. Kutnyakov, R. D. Orr and A. R. Felmy, *Radionuclide-Chelating Agent Complexes in Low-Level Radioactive Decontamination Waste; Stability, Adsorbtion and Transport Potential*, NUREG/CR-6758 PNNL- 13774, U.S. Nuclear Regulatory Commission (NRC), Washington D.C., 2002.
10. Environment Agency (EA), *Review of LLW Repository Ltd's 2011 Environmental Safety Case: Inventory and Near Field*, Issue 1, EA, Bristol, 2015.
11. M. Sillanpää, in *Rev. Environ. Contam. Toxicol.*, ed. G. W. Ware, 1997, **152**, 85-111, Springer, New York, NY.
12. P. Laine and R. Matilainen, Anal. Bioanal. Chem., 2005, **382**, 1601-1609.
13. B. Nowack, F. G. Kari, S. U. Hilger and L. Sigg, *Anal. Chem.,* 1996, **68**, 561-566.
14. LLWR, *Near Field*, The 2011 Environmental Safety Case, LLWR/ESC/R(11)10021, Holmrook, 2011.
15. British Nuclear Energy Society, *Radiation Dose Management in the Nuclear Industry*, Thomas Telford, London, 1995.
16. R. Torres, M. A. Blesa and E. Matijevic, *Journal of Colloid and Interface Science*, 1990, **134**, 2, 475-485.
17. LLWR, *Developments Since the 2011 ESC*, The LLWR Environmental Safety Case, LLWR/ESC/R(13)10058, Issue 1, 2013.
18. LLWR, *LLW Problematic Waste Technology Optioneering Summary Report*, The National Waste Program, NWP/REP/130, Issue 1, 2016.
19. NDA, *Upstream Optioneering Technical Feasibility of Mobile Plant for Higher Activity* Wastes, Geological Disposal, NDA/RWM/118, Didcot, 2014.
20. IAEA, *Application of Ion Exchange Processes for the Treatment of Radioactive Waste and Management of Spent Ion Exchangers*, Technical Report Series No. 408, Vienna, 2002.
21. M. Valkiainen and M. Nykyri, Nucl. Technol., 1982, **58**, 248-255.

22. T. Yahata and J. Abe, *The Effect of Controlled Oxygen on the Incineration of Radio Contaminated Organic Compounds*, Rep. JAERI-M-9974, Japan Atomic Energy Research Institute, Tokyo, 1982.
23. J. Neubauer, *Incineration of ion exchange resins: Operational experience*, Incineration and Thermal Treatment Technologies, Irvine, CA, 1996.
24. S. Halaszovich and M. Gomoll, *Incineration of ion exchange resins from NPP*, Waste Management, Arizona Board of Regents, Phoenix, AZ, 1991.
25. I. Bjerle, K. Hoglund and O. Svensson, *Incineration of Ion Exchange Resin in Fluidized Bed*, Technical University of Lund, 1980.
26. United States Department of Energy, *Summary of DOE Incineration Capabilities*, REP/DOE/ID-10651, US DOE, Washington, DC, 1998.
27. E. T. Glover and J. J. Fletcher, *National Waste Management Infrastructure for the Safe Management of Radioactive Waste in Ghana*, Waste Management Conference, Tucson, AZ, 2000.
28. LLWR, *Environmental Safety Case – Main Report*, LLWR/ESC/R(11)10016, LLWR, Cumbria, UK, 2011.
29. A. E. Martell, R. J. Motekaitis, A. R. Fried, J. S. Wilson and D. T. MacMillan, *Canadian Journal of Chemistry*, 1975, **53**, 22, 3471-3476.
30. C. Randt, R. Wittlinger and W. Merz, *Fresen. J. Anal. Chem.*, 1993, **346**, 6, 728-731.
31. M. Taddia, M. T. Lippolis and L. Pastorelli, *Microchem. J.*, 1979, **24**, 1, 102-106.
32. C. S. Bürgisser and A. T. Stone, *Environ. Sci. Technol.*, 1997, **31**, 9, 2656-2664.
33. M. Sillanpää and M-L. Sihvonen, *Talanta*, 1997, **44**, 8, 1487-1497.
34. Kemmeia, S. Kodamaa, A. Yamamotob, Y. Inouec and K. Hayakawad, *Food Chem.*, 2013, **138**, 2, 866-869.
35. J. De Jong, A. Van Polanen J. J. M. Driessen, *J. Chromatogr. A*, 1991, **553**, 243-248.
36. G. Wang and F. P. Tomasella, *J. Pharm. Anal.*, 2016, **6**, 3, 150-156.
37. J. A. O'Hanlon, R. D. Chapman, F. Taylor and M. A. Denecke, *J. Radioanal. Nucl. Chem.*, 2019, **322**, 1915-1929.
38. F. Dondi, A. Betti, G. Bio and C. Bighi, *Anal. Chem*., 1981, **53**, 496-504.
39. E. Grushka, *J. Phys. Chem.*, 1972, **76**, 18, 2586-2593.
40. S. J. Blott and K. Pye, *Earth Surf. Process. Landforms*, 2001, **26**, 1237-1248.
41. D. C. Harris, *Quantitative Chemical Analysis*, W. H. Freeman and Company, New York, 7th edn., 2007.
42. A. Napoli, *J. Inorg. Nucl. Chem.*, 1972, **34**, 3, 987-997.
43. F. Chiumiento, A. D'Aloise, F. Marchegiani and V. Melai, *Food Chem.*, 2015, **175**, 452-456.

Chapter Four: Study of the γ-Irradiation Stability of Fe(III)-Complexes of Common Aminopolycarboxylic Acids

James A. O'Hanlon[a†], Frank Taylor[b] and Melissa A. Denecke[c]

[a,c] The Chemistry Building, The University of Manchester, Oxford Road, Manchester, UK, M13 9PL.

[b]LLW Repository Ltd, Pelham House, Pelham Drive, Calderbridge, Seascale, Cumbria, UK, CA20 1DB.

[†]Corresponding Author e-mail: james.ohanlon@manchester.ac.uk.

Scope

The HPLC quantification method was applied to irradiated neutral aqueous samples of APCAs to quantify the degradation, elicit potential degradation mechanisms and identify radiolytic degradation products. The aim of this study was to establish the comparative radiation stabilities of the APCAs and their Fe(III)-complexes to provide relevant information for LLWR and the geochemical models they use to determine the fate of the ligands in the repository environment.

Although the complex conditions of the repository environment will factor into the specific speciation and reactivity of the ligands, it is anticipated that a large portion of contaminant APCAs will exist as their Fe(III)-complex because of the high abundance of the element in the LLWR near field. Therefore, the radiochemical behaviour of the Fe(III)-APCAs has been studied in neutral aqueous solution; the simple sample matrix allows greater mechanistic insight into the fundamental radiochemical behaviour of the analyte species.

G-values have been determined for EDTA, Fe(III)-EDTA and Fe(III)-DTPA under the given conditions and potential radiolytic mechanisms have been discussed by comparison of the results with the primary yield of water radiolysis. Fe(III)-EDTA was found to be more susceptible to radiolysis than was expected; further investigation

was designed to probe the degradation of the complex and relative formation of a potential radiolysis product in different dissolved O_2 environments.

The radiolytic stability of the ligands and their complexes in different environments are of interest to the assessment models used by LLWR to determine the fate of ligands in the repository environment, and to underpin the acceptance criteria of waste containing APCAs. Greater understanding of pathways that might remove contaminant APCAs from the environment under the specific conditions of the repository near field might eventually help LLWR to relax the WAC constraints and simplify waste acceptance procedures.

CRediT Author Statement:

J. A. O'Hanlon: Conceptualisation, Methodology, Validation, Formal analysis, Investigation, Data curation, Writing – original draft preparation, Visualisation. F. Taylor: Project administration, Funding acquisition. M. A. Denecke: Conceptualisation, Methodology, Writing – review and editing, Supervision, Project administration, Funding acquisition.

Abstract

Aminopolycarboxylic acids (APCAs), ethylenediaminetetraacetic acid (EDTA) and diethylenetriaminepentaacetic acid (DTPA), often arise in nuclear waste consignments to sites such as the Low Level Waste Repository (LLWR) because of their use in decontamination agents used in the decommissioning process. The complexants are potentially problematic in the final wasteform because of their capacity to bind and mobilise harmful species in the repository. Therefore, their acceptance is controlled according to safe limits determined by, for example, modelling studies. Geochemical modelling of the environmental impact of the ligands should take into account their potential degradation mechanisms, including radiolytic pathways. Experimental assessment of the comparative γ-irradiation stabilities of EDTA, Fe(III)-EDTA and Fe(III)-DTPA in neutral aqueous solution has been undertaken. *G*-values for each species have been calculated and compared with the primary yield of water radiolysis to allow speculation as to the radiolytic degradation mechanisms. $G(\text{-EDTA}) = 2.5 < G(\text{-Fe(III)-}$

EDTA) = 3.2 < *G*(-Fe(III)-DTPA) = 5.4 were determined. The entire primary yield of hydroxyl radical (G_{HO} 2.7) is thought to be scavenged by each APCA-species to initiate oxidative degradation of the compound. The excess degradation observed for the two Fe(III)-APCA species is thought to be initiated by hydroxyl radicals produced in secondary reactivity of H_2O_2, which can undergo catalytic conversion to $HO^{\cdot}$ by superoxide driven Fenton chemistry involving the Fe(II/III) metal-centre of the APCA-complexes. Irradiation of Fe(III)-EDTA in oxygen-saturated/nitrogenated solution suggested that secondary or inter-molecular reactions may be prevalent when the concentration of Fe(III)-EDTA and dissolved oxygen are high. Furthermore, analysis of the formation of a specific radiolytic degradation product, thought to be the Fe(III)-complex of ethylenediaminetriacetic acid (ED3A), in the different O_2-environments showed that the formation of the product was O_2-dependent, providing evidence to support the proposed oxidative degradation mechanism that proceeds through addition/elimination of O_2 to an APCA *C*-centred radical through a peroxyl intermediate.

Keywords

Gamma-irradiation stability, *G*-value, aminopolycarboxylic acids, ethylenediamintetraacetic acid, diethylenetriaminepentaacetic acid, reverse-phase, ion-pair, high-performance liquid-chromatography, low level radioactive waste.

4.1 Introduction

Aminopolycarboxylic acids (APCAs), such as ethylenediaminetetraacetic acid (EDTA) and diethylenetriaminepentaacetic acid (DTPA), are used throughout the nuclear industry in the decontamination agents used in decommissioning processes because of their capacity to bind and mobilise elements across the periodic table. As a result of such operations, there is an increased likelihood of the complexants arising in nuclear waste.[1-4]

The presence of APCAs in nuclear waste is of concern to disposal facilities, such as The Low Level Waste Repository (LLWR) near the village of Drigg, Cumbria, UK, because of

their potential to coordinate and solubilise otherwise surface-adsorbed or solid-state radiological or other chemo-toxic ions in the repository. APCA-complexation increases the mobility of the species, making them more susceptible to transportation out of the repository and into the geo/bio-sphere, leading to an array of negative environmental impacts.[3-7]

Though other complexants can arise in the wasteform through their use in decontamination agents (e.g. citric acid), degradation of waste material (e.g. isosaccharinic acid (ISA) evolved from cellulose degradation), or because they are naturally occurring (e.g. humic and fulvic materials), the risk associated with such species is considered to be lower than that of the APCAs because of their lower environmental persistence.[8,9] Compounds such as citric acid and ISA are readily consumed in the geomicrobiological environment of the repository[9], whereas the synthetic APCAs are known to be much more resistant to biodegradation (rate of EDTA biodegradation < DTPA).[10-14] Therefore, LLWR implement more stringent controls on the acceptance of APCA-containing wastes than on other complexant contaminants.[15]

In order to effectively allocate repository capacity for incoming APCA-containing wastes, and to monitor and manage the existing loadings, an understanding of the behaviour and fate of the ligands under the specific repository conditions is beneficial. Abiotic factors that can influence the rate of APCA-degradation include photolytic, chemical and radiolytic degradation pathways, many of which have been widely studied previously.[11]

Photochemical transformations are strongly dependent on natural conditions; sunlight intensity is attenuated through adsorption and scattering, and the specific photochemistry of each ligand is affected by complexation to different metal-centres (or if the ligand is uncomplexed). For example, the Fe(III)-EDTA complex is known to be highly photolabile, whereas, EDTA complexes of Na(I), Mg(I), Ca(II), Ni(II), Cu(II), Zn(II), Cd(II) and Hg(II) were not photodegraded in laboratory experiments.[11,16-19] A product study of Fe(III)-EDTA photodegradation found fragmented species such as iminodiacetic acid (IDA), ethylenediaminemonoacetic acid (EDMA), ethylenediaminediacetic acid (EDDA), ethylenediaminetriacetic acid (ED3A) and

glyoxylic acid (all of which have been identified as biodegradable).[16-20] Reports are conflicting on the pH-dependency of the rate of photolysis (pH-dependent[21,22], pH-independent[23]). Photolability has been reported for Fe(III)-DTPA[11,16], and free DTPA has been shown to be much more photodegradable than free EDTA.[24] Studies on APCA photochemistry are numerous as photolytic degradation is considered a remarkable pathway in the prevention of the environmental accumulation of the ligands in natural waters[11]; however, in an LLWR context, contaminant APCA-species contained in the final wasteform are unlikely to be exposed to direct sunlight.

APCA chemical degradation (e.g. hydrolysis) is not considered to be a significant contributor to the short-term fate of the ligands in natural environments because the conditions are typically mild.[11,22,23] However, the chemical conditions of the LLWR wasteform (pH 11, high ionic strength, reducing[9]) may facilitate more degradation pathways. Previous study on the chemo-degradation of EDTA reported 69% of the ligand destroyed after 175 days in an inorganic matrix designed to simulate the chemical composition of mixed nuclear waste from the Hanford Site (Washington, USA) and 89% of the ligand was destroyed when the matrix was exposed to ^{60}Co γ-rays (7.5×10^6 R). In both cases, a product study detected species such as IDA, ED3A and glyoxylic acid.[25]

G-values are used to quantify the radiolytic degradation (or formation) of a given species per 100 eV of absorbed dose, giving an indication of a compounds susceptibility to radiolytic damage and allowing mechanistic insight by comparison with the *G*-values determined for the primary yield of water radiolysis. Experiments usually involve exposure of purely APCA-containing aqueous solutions under variable conditions (e.g. pH, gas saturation) to an external radiation source.[25-30] Previous study of free EDTA indicated that radiolysis of the ligand is proportional to the formation of the hydroxyl radical ($HO^{\cdot}$) and proceeds through oxidative radical attack (most notably H-abstraction); similar mechanisms are likely to be available for uncomplexed DTPA.[26,30] Introduction of a coordinated Fe(III) metal-centre is reported to significantly affect the radiation chemistry of the APCAs because the variable oxidation state of the transition metal can facilitate charge transfer processes with the coordinating ligand

and the metal-centre can act as a site for reductive radical attack.[27-29] *G*(-Fe(III)-EDTA) = 0 has been previously reported for γ-irradiation experiments on an aerated, neutral (pH 6.1) aqueous because of charge transfer from the radically activated coordinating EDTA or direct reduction of the Fe(III)-centre to form Fe(II)-EDTA, followed by re-oxidation by dissolved O_2 back to Fe(III)-EDTA.[27]

APCAs arising in the near field of the LLWR site are likely to predominantly exist as Fe(III)-complexes given the abundance of the metal and the thermodynamic favourability of complexation. Therefore, a fundamental understanding of the behaviour of the APCA-Fe(III)-complexes in a radiation field is crucial to a complete understanding of the fate of the ligands in the repository. Identification of radiolytic degradation pathways that fragment the ligands to hinder their capacity for contaminant mobilisation could impact the models used to determine the APCA limits of acceptance. Additionally, potential radiolytic degradation products, such as ED3A, are themselves chelators, whose mode of action in the repository should be characterised.

Here, we present the results of a fundamental study into the comparative radiation stabilities of EDTA, Fe(III)-EDTA and Fe(III)-DTPA in neutral aqueous solution. Solutions were exposed to ^{60}Co γ-rays to deliver a maximum total absorbed does of 1 kGy (6.25×10^{18} eV g^{-1}) and analysed post-irradiation by reversed-phase high-performance liquid-chromatography (RP-HPLC) coupled with UV detection using a pre-optimised Fe(III)-APCA quantification method.[14,31] The HPLC method was chosen for its sensitivity, accuracy and selectivity; the chromatographic resolution was able to separate parent APCA-species from potential irradiation products to detect the species independently from one another.

4.2 Materials and Method

4.2.1 Chemicals and Reagents

EDTA disodium salt ($Na_2H_2EDTA{\cdot}2H_2O$), iron trichloride hexahydrate ($FeCl_3{\cdot}6H_2O$), iron-EDTA monosodium trihydrate (NaEDTA-Fe(III)$\cdot 3H_2O$), DTPA (protonated form), ethanol, tetrabutylammonium bromide (TBA-Br), sodium formate, sodium hydroxide,

acetonitrile (HPLC Grade, >99.9%) (Sigma-Aldrich, Merck KGaA, Darmstadt, Germany), formic acid (Fisher Scientific, Loughborough, UK) were obtained at ACS reagent grade or above. Deionised (DI) water (>18 MΩ/cm) used for all applications was obtained from a Millipore® system, fitted with a SimPak® 1 cartridge (Merck Chemicals Ltd, Nottingham, UK).

4.2.2 Preparation of Samples for Irradiation

4.2.2.1 Synthesis of Fe(III)-DTPA

Equimolar quantities of $FeCl_3 \cdot 6H_2O$ and protonated DTPA were dissolved in a minimal amount of mildly basic aqueous solution. The solution was heated under reflux for 1 h, before precipitation was allowed to occur during evaporation. The resulting solid was collected by vacuum filtration, washed with cold ethanol and dried in a vacuum desiccator. The Fe(III)-DTPA complex was characterised by MS, UV-Vis, TGA, ICP-MS and HPLC. The structure was found to be $H_3DTPA\text{-}Fe(III)Cl \cdot 3H_2O$.

4.2.2.2 Samples of EDTA, Fe(III)-EDTA and Fe-DTPA

Neutral, aqueous stock solutions (100 mL, 10 mM) of EDTA, Fe(III)-EDTA and Fe(III)-DTPA were each prepared by dissolving $Na_2H_2EDTA \cdot 2H_2O$ (3.722 g), $NaEDTA\text{-}Fe(III) \cdot 3H_2O$ (4.242 g) and $H_3DTPA\text{-}Fe(III)Cl \cdot 3H_2O$ (5.2021 g) in DI water (80 mL). The pH of each solution was adjusted to pH 6.1 by dropwise addition of NaOH solution. Finally, the pH balanced solutions were transferred to a volumetric flask and made up to 100 mL with DI water. Stock solutions were diluted in triplicate to yield numerous sample solutions over the concentration range 0.025 - 0.8 mM and transferred to 2 mL autosampler vials to undergo irradiation. When not in use, all samples and stock solutions were refrigerated at 4 °C and kept under darkness to limit thermal/photo-degradation.

4.2.2.3 Nitrogenation and Oxygenation of Samples

Nitrogenated Fe(III)-EDTA samples were produced by bubbling nitrogen through a neutralised stock solution for 3 h. The stock solution was then transferred to a glovebox (under nitrogen), where samples of various concentrations were made following the same procedure outlined previously but using a nitrogenated (bubbled

with N_2, 3 h) batch of DI water to perform the dilutions. Oxygenated samples were made by taking Fe(III)-EDTA samples that had been made under normal atmospheric conditions following the procedure described previously and bubbling oxygen through a needle piercing the septum of each 2 mL autosampler vial for 30 min.

4.2.3 Irradiation

Irradiations were carried out using ^{60}Co-γ rays (Model 812 γ-irradiator, Foss Therapy Services Inc., CA, USA). The dose rate (71 Gy/min) was determined by Fricke dosimetry. During irradiation, samples were loaded around the circumference of a rotating brass drum to ensure even exposure. 200, 400, 600, 800 or 1000 Gy doses were applied during the experiments- and were later converted to values in eV g^{-1} (1.25, 2.50, 3.75, 5.00 and 6.25 × 10^{18} eV g^{-1}, respectively). These doses were selected to allow direct comparison with results obtained by Kundu *et al*.[27]

4.2.4 Chromatography

4.2.4.1 Preparation of Samples for Chromatography

Chromatographic sample preparation was minimal as irradiated samples were already contained in 2 mL autosampler vials and aliquots could be transferred directly to the HPLC. The exception was irradiated samples of uncoordinated EDTA, to which equivalent volumes of aqueous $FeCl_3$ solution were added ([$FeCl_3$ solution] = [EDTA pre-irradiation]) to coordinate any undegraded EDTA for detection as Fe(III)-EDTA.

Generally, samples were analysed within 0-3 days after irradiation. Measures were implemented to limit thermal/photo-degradation of the samples and replicate samples were analysed at intervals spread evenly across the three days to limit systematic bias. Furthermore, the effect of the time elapsed between the initial irradiation and HPLC analysis was critically assessed by performing multiple full analyses on samples of Fe(III)-EDTA under atmospheric, nitrogenated and oxygenated conditions at an increasing number of days post-irradiation (0, 7, 13 and 18 days).

4.2.4.2 Chromatographic Equipment

HPLC analysis was performed on an Agilent 1260A system (Agilent Technologies, CA, USA) coupled to a diode-array detector (DAD). The DAD was programmed to record UV-absorption in the 190 - 400 nm wavelength range over the entire chromatographic retention time range. The system was fitted with a quaternary pump, online degasser, autosampler with 100 μL sample loop and thermostatted column oven. The column was a Phenomenex® HyperClone 5 μM BDS C_{18} (4.6 x 250 mm) fitted with a SecurityGuard© C_{18} guard cartridge (4.6 x 5 mm) (Phenomenex Ltd, Macclesfield, UK).

4.2.4.3 Chromatographic Conditions

All chromatography was carried out isocratically at 25 °C with a 1 mL/min flow-rate of buffered mobile phase (20 mM formate buffer, pH 3.3, prepared by dissolving 10 mM TBA-Br ion-pair agent, 5 mM sodium formate, 15 mM formic acid, and 8% acetonitrile in DI water), with the exception of the Fe(III)-DTPA elution parameters, which used a 90:10 ratio of formate buffer:acetonitrile mobile phase to raise the total composition of acetonitrile to 17.2%. The injection volume was 10 μL and always performed in duplicate. Elution was monitored at 258 nm (λ_{max} Fe(III)-EDTA) and 262 nm (λ_{max} Fe(III)-DTPA).

4.2.4.4 Calibration and Data Collection

Calibration data for APCA quantification was obtained by performing HPLC analysis on multiple aliquots of the same samples used in the irradiation experiments prior to irradiation (concentration range: 0.025 mM - 0.8 mM). The resulting plots of the chromatographic response (integrated peak area (mAU)) of the Fe(III)-APCA species against the APCA concentration was observed to be linear ($r^2 > 0.98$) over the concentration range investigated. Each set of data was also validated for precision (relative standard deviation, %RSD ≤ 10%), selectivity (no peak overlap) and sensitivity (LOD = 3.3(σ/S, where S is the slope of the linear trend and σ is the standard deviation of the peak intensities for samples of lowest, measurable concentration).

The amount of radiolytically degraded APCA (in mol g^{-1} or μmol g^{-1} (degraded)) was calculated from the difference in APCA concentration determined from HPLC analysis pre- versus post-irradiation.

4.2.5 Data Processing

All chromatograms were initially processed and integrated using Agilent's ChemStation OpenLAB software (V. A.01.02). *G*-values were calculated by two methods: 1) the amount of APCA-species degraded divided by the absorbed dose (*G* = Avagadro constant × Δ[APCA-species] (radiolytically degraded) / absorbed dose) (by calculation), or 2) from the slope of the linear trend of the plot of the amount of APCA-species degraded as a function of increasing absorbed dose (y / μmol g^{-1} = $m \cdot x$ / eV g^{-1} + c, dy/dx = m / μmol g^{-1}/eV g^{-1} (where y = Δ[APCA-species] and x = absorbed dose)) (by differentiation).

HPLC analysis of irradiated samples was performed 0, 7, 13 and 18 days after irradiation to measure the stability of the species responsible for chromatographic peaks (parent species/potential degradation products) as a function of time since irradiation. The chromatographic peak area (mAU) was plotted against time since irradiation to give a value of ΔmAU day^{-1} for each species. This was converted to a percentage of the original peak area (mAU on day 0) to simplify comparison between high and low concentration species.

4.2.6 Mass Spectrometry

Electrospray ionisation mass spectrometry (ESI-MS) analysis in positive and negative mode was performed on samples before and after irradiation. Samples were injected directly into the system without any pre-treatment. Significant peaks that appeared only in the mass spectrum of irradiated samples were assigned to potential radiolytic degradation products by comparison of their m/z values with that expected for APCA radiolytic fragmentation products.

4.3 Results and Discussion

4.3.1 Stability of EDTA vs. Fe(III)-EDTA

Degradation of low concentration organic solutes by ionising radiation is initiated by the primary yield of water radiolysis. The *G*-values of the primary yield (γ-irradiation) of pH neutral water are given below (in parentheses):[26,27,30,32,33]

$HO^{\cdot}$ (2.7), e_{aq}^{-} (2.6), $H^{\cdot}$ (0.6), H_2 (0.45), H_2O_2 (0.7), H_3O^{+} (2.6)

Approximately equal quantities of oxidising and reducing species are formed initially. In the presence of air, e_{aq}^{-} and $H^{\cdot}$ readily combine with dissolved O_2 to form O_2^{-} and the hydroperoxyl radical, HO_2 ($k = 1.9 \times 10^{10}$ and 2.1×10^{10} L mol^{-1} s^{-1}, respectively); HO_2 partially dissociates (pH-dependent) to form its conjugate base, O_2^{-} ($pK_a = 4.9$). The highly reductive superoxide radical, O_2^{-}, is known to have low reactivity with organic species such as phenols and aliphatic acids and, in the absence of metal ions, can disproportionate to form O_2 and H_2O_2.[32,33]

Radiolytically generated hydroxyl radicals are known to react rapidly with EDTA to form EDTA-derived radicals. The reactivity of $HO^{\cdot}$ Is unaffected by the presence of O_2, but the rate of reaction between the electrophile and EDTA in its various protonation states is pH-dependent (e.g. pK_a 6.2 (H_2EDTA^{2-}), $k = 4 \times 10^8$ L mol^{-1} s^{-1}; pK_a 10.3 ($EDTA^{4-}$), $k = 6 \times 10^9$ L mol^{-1} s^{-1}). The hydroxyl radical commonly attacks organic molecules by H-abstraction or addition to double bonds.[30]

A test to determine the difference in radiation stability between unbound EDTA and EDTA complexed to an Fe(III) metal centre in aqueous solution (pH 6.1) was performed under atmospheric conditions. Sample solutions containing an initial concentration of APCA over the range 0.025 - 5 mM were exposed to 6.25×10^{-18} eV g^{-1} and *G*-values were determined by calculation.

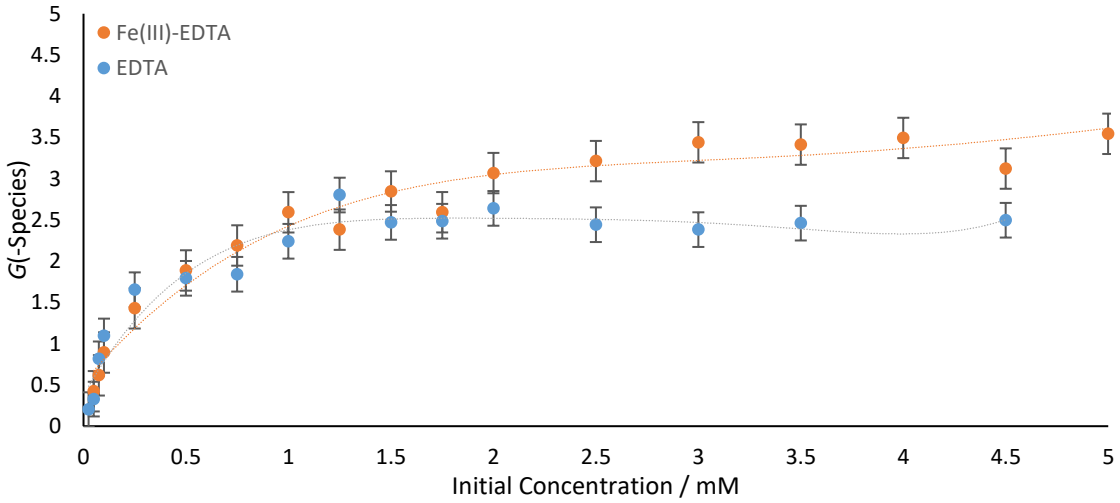

Figure 1. *G*-values determined for EDTA (blue) and Fe(III)-EDTA (orange) in neutral aqueous solution (pH 6.1) after γ-irradiation to a total dose of 6.25×10^{18} eV g^{-1} plotted against the initial concentration of each species. Lines are simple guides for the eye. Error bars = standard error.

Figure 1 shows the effect of initial EDTA solute concentration on the calculated *G*-value; the *G*-value initially increases with increasing concentration and then increases asymptotically towards a maximum limit. This pattern is observed because at low solute concentration the primary yield of water radiolysis is comparably high and reactions between the solutes and water radiolysis products can degrade the solute. At higher solute concentration, there is enough solute to effectively scavenge the entire primary yield and the *G*-values tend to a plateau, the asymptote (assuming degradation of solute molecules via direct radiolysis to be small). In contrast to previous reports, no significant difference between EDTA and Fe(III)-EDTA concentrations marking a transition between low to high concentration behaviour is observed.[26,27] What is observed is a higher *G*-value asymptote for the complex compared to that of the unbound EDTA.

G(-EDTA) calculated from the results in Figure 1 is 2.5 ± 0.1. Pulse radiolysis studies of uncoordinated EDTA have shown that reaction with primary yield hydroxyl radicals (G_{HO} (2.7)) produce *N*-centred radical cations, which are bridged to neighbouring nitrogen atoms, and *C*-radicals centred on carbon atoms in the ethylene bridge or carboxylate functionality, formed via H-abstraction at one of two locations on the ligand.[30] *N*-centred radical products disproportionate to form *C*-centred radicals, which undergo addition of O_2, followed by elimination of a superoxide radical anion, to produce a tertiary iminium Schiff-base through a peroxyl radical intermediate. The

Schiff-base can hydrolyse in water to form small organic molecules, such as formaldehyde, glyoxylic acid, formic acid and carbon dioxide, and the larger corresponding molecule fragments such as ED3A.[30] Similar UV-induced oxidative mechanisms have also been reported.[18,34,35]

The reported *G*-value (*G*(-EDTA = 2.5 ± 0.1) and its observed correlation with the pH-dependent value of G_{HO} (2.7) is in reasonably good agreement with previous work; *G*(-EDTA) = 1.9 ± 0.3 was reported when G_{HO} = 2.0 (lower energy X-irradiation).[26] *G*(-EDTA) is somewhat smaller than G_{HO}; an ideal asymptote would be the case where *G*(-EDTA) = G_{HO}, however, there are equilibria involved and not solely the degradation reactions.

Previous study on the effect of γ-irradiation on neutral, aerated solutions of Fe(III)-EDTA reported that *G*(Fe(III)-EDTA) = 0.[27] This was explained by e_{aq}^- and $H^{\cdot}$ combining with O_2 to form O_2^- and HO_2, which readily reduce the Fe(III)-centre to form Fe(II)-EDTA ($k = 3.1 \times 10^6$ L mol^{-1} s^{-1}). Oxidative chemistry initiated by hydroxyl radical attack at the ligand is followed by ligand-metal charge transfer (LMCT), to also form Fe(II) and an intact coordinating ligand. The Fe(II)-EDTA species are then oxidised back to Fe(III)-EDTA by the O_2 present in solution, hence *G*(Fe(III)-EDTA) = 0.

Our results (Figure 1), *G*(-Fe(III)-EDTA) = 3.2 ± 0.2 contrast this previous study; we observed significant decrease in Fe(III)-EDTA concentration post-irradiation, which was even greater for the complex compared to uncomplexed EDTA. Two reasons for the Fe(III)-EDTA lost during irradiation are imaginable: 1) the complex was converted to a stable reduced Fe(II)-EDTA complex, formed by the reduction at the metal centre by the O_2^- radical, and/or 2) radiolytic fragmentation of the complexing ligand occurred, most likely induced by oxidative H-abstraction by the hydroxyl radical.

We propose that the observed differences in the results between the two similar experiments are linked to the detection methods used; in the previous work, a simple photospectrometric analysis at a single wavelength was performed to assess the concentration of Fe(III)-EDTA before and after irradiation, implying that the method was not selective for Fe(III)-EDTA and that interferences from any UV-active irradiation products would have not been discernible. Our implementation of a chromatographic separation prior to UV-detection eliminates this problem, allowing for more accurate

determination of the susceptibility of Fe(III)-EDTA to radiolytic degradation and identification of potential radiolysis products.

The observed degradation is greater than the primary yield of hydroxyl radical (G(-Fe(III)-EDTA) = 3.2 ± 0.2 > G_{HO} (2.7)); the excess radiolytic decomposition of the ligand must be explained by another mechanism. The net result of the Haber-Weiss reaction (superoxide driven Fenton reaction) is to catalytically produce one equivalent of hydroxyl radical per H_2O_2 consumed (**1**&**2**).[29] At near-neutral pH, the rate limiting factor of the redox chemistry is usually the solubility of the ferric ion, which, in this case, is increased dramatically by the EDTA complexant. Therefore, the primary yield of H_2O_2 (G_{H2O2} (0.7)) may be consumed by catalytic conversion to an equivalent concentration of $HO^{\cdot}$, which can then initiate oxidative chemistry to decompose the ligand (**3**); the resultant G-value is in line with our observation (G_{HO} (2.7) + G_{H2O2} (0.7) = 3.4 ≈ G(-Fe(III)-EDTA) = 3.2). Pulse radiolysis studies have previously shown Fe(II)-EDTA complexes to be capable of participating in Fenton chemistry.[29,34,36]

(1) Fe(III)-EDTA + O_2^- → Fe(II)-EDTA + O_2 $k^{29} = 3.1 \times 10^6$ L mol^{-1} s^{-1}

(2) Fe(II)-EDTA + H_2O_2 → Fe(III)-EDTA + $HO^{\cdot}$ + HO^- $k^{36} = 3.2 \times 10^3$ L mol^{-1} s^{-1}

(3) Fe(III)-EDTA + $HO^{\cdot}$ → Fe(III)-(oxidised EDTA) + O_2^- $k^{36} = 5.2 \times 10^8$ L mol^{-1} s^{-1}

4.3.2 Stability of Fe(III)-EDTA vs. Fe(III)-DTPA

Further study was conducted to assess the comparative radiation stabilities of Fe(III)-complexes of two different APCAs, EDTA and DTPA. Though structurally similar, DTPA is larger than EDTA and has a greater affinity for Fe ($\log\beta_{Fe(II)/Fe(III)\text{-}EDTA}$ = 14.3/25.0 < $\log\beta_{Fe(II)/Fe(III)\text{-}DTPA}$ = 16.3/28.0).[37] Irradiation experiments were designed to probe the effect of initial concentration and increasing absorbed dose on neutral aqueous solutions of Fe(III)-APCA over the concentration range 0.1 - 8 mM. G-values were determined by calculation and differentiation (Table 1).

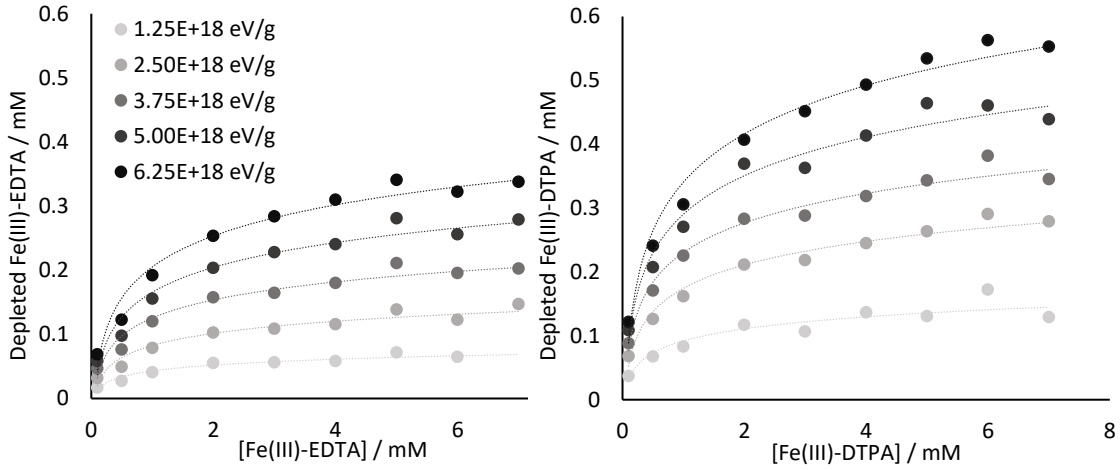

Figure 2. Plots of the change in concentration of Fe(III)-APCA after exposure to increasingly large γ-irradiation doses against the initial concentration of (left) Fe(III)-EDTA and (right) Fe(III)-DTPA, in neutral aqueous solution (pH 6.1).

The observed degradation is greater for Fe(III)-DTPA than Fe(III)-EDTA at all levels of absorbed dose (Figure 2). The data has been fitted with logarithmic curves to represent the trend of increasing degradation with increasing concentration. The degradation Fe(III)-DTPA appears to continue to steadily increase and not tend to plateau off, which could be the result of inter-molecular or secondary reactions in the irradiated matrix. The fact that the doubling, tripling and quadrupling the absorbed dose does not lead to doubling, tripling and quadrupling of the amount Fe(III)-DTPA degraded is another indication of other reactions playing a role. The *G*-values calculated from these data are displayed in Table 1. The *G*-values for Fe(III)-DTPA also are associated with large statistical error.

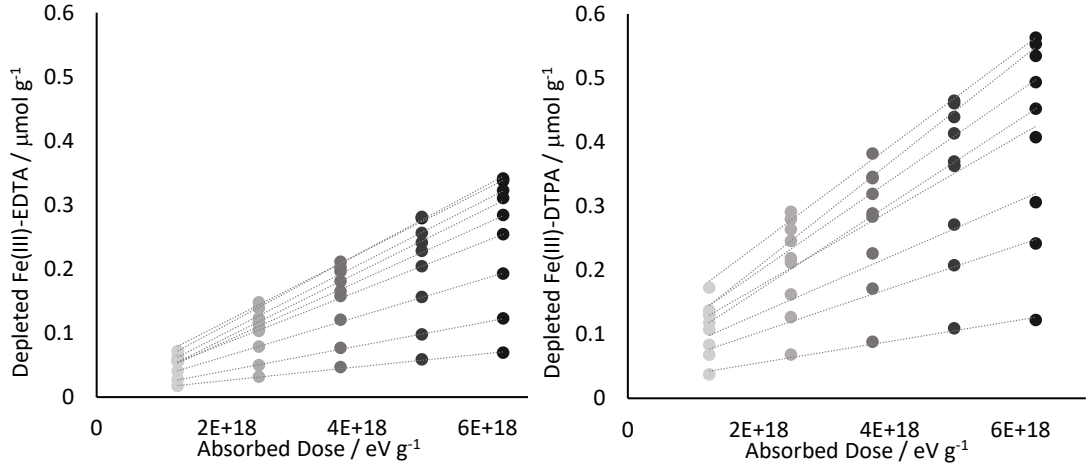

Figure 3. Plots of the change in concentration of Fe(III)-APCA after γ-irradiation at various initial concentrations (rearrangement of data shown in Figure 2; each linear trend represents one concentration level and shading of marker points corresponds; generally, shallower gradient = lower concentration) against the increasing absorbed dose applied to neutral aqueous solutions (pH 6.1) of (left) Fe(III)-EDTA and (right) Fe(III)-DTPA.

The data in Figure 2 can be replotted to show the linear proportional increase in degradation with increasing absorbed dose (Figure 3). The gradient of each trend (dy/dx = μmol g^{-1}/eV g^{-1}) can be used to calculate the *G*-value at each discrete concentration level (column *G*-Value by Differentiation, Table 1).

Table 1. *G*-values determined for Fe(III)-EDTA and Fe(III)-DTPA over a range of concentrations and by two methods: by calculation (the amount of APCA-species degraded divided by the absorbed dose) or by differentiation (the gradient of the linear trend of the plot of the amount of APCA-species degraded against increasing absorbed dose (Figure 3)).

		***G*-Value by Calculation**					
		Absorbed Dose / × 10^{18} eV g^{-1}					
	1.25	**2.50**	**3.75**	**5.00**	**6.25**	**Mean**	***G*-Value by Differentiation**
[Fe(III)-EDTA] / mM							
7	-	3.6	3.6	3.4	3.3	3.4 ± 0.14	3.1
6	3.1	3.0	3.1	3.1	3.1	3.1 ± 0.08	3.2
5	3.5	3.3	3.4	3.4	3.3	3.4 ± 0.06	3.3
4	2.8	2.8	2.9	2.9	3.0	2.9 ± 0.08	3.1
3	2.7	2.6	2.6	2.7	2.7	2.7 ± 0.06	2.8
2	2.7	2.5	2.5	2.5	2.4	2.5 ± 0.09	2.4
1	2.0	1.9	1.9	1.9	1.9	1.9 ± 0.04	1.8
0.5	1.3	1.2	1.2	1.2	1.2	1.2 ± 0.06	1.2
0.1	0.8	0.8	0.7	0.7	0.7	0.7 ± 0.05	0.6
[Fe(III)-DTPA] / mM							
7	6.2	6.7	5.6	5.3	5.7	5.8 ± 0.63	4.9
6	8.3	7.0	6.1	5.5	5.4	6.5 ± 1.19	4.6
5	6.3	6.3	5.5	5.6	5.2	5.8 ± 0.52	4.9
4	6.6	5.9	5.1	5.0	4.8	5.5 ± 0.76	4.3
3	5.1	5.3	4.6	4.4	4.4	4.8 ± 0.43	4.0
2	5.6	5.1	4.6	4.5	3.9	4.7 ± 0.66	3.6
1	4.0	3.9	3.6	3.3	2.9	3.5 ± 0.44	2.7
0.5	3.3	3.0	2.7	2.5	2.3	2.8 ± 0.38	2.1
0.1	1.8	1.6	1.4	1.3	1.2	1.5 ± 1.01	1.0

The *G*-values for Fe(III)-DTPA are found to be greater than those for Fe(III)-EDTA. Structural features of the DTPA complex could increase its propensity for oxidative radiological degradation. The ligand is potentially octa-dentate but can only coordinate to Fe(III) through six bonding modes, leaving up to two of its carboxylate groups un-coordinated and more prone to oxidative radical attack.

The calculated values of *G*(-Fe(III)-DTPA) are much larger than *G*(-Fe(III)-EDTA) (~5 versus ~3) which suggests that other significant reactive pathways are active that are not observed in the irradiation of Fe(III)-EDTA. A recently reported kinetic model showed that Fe(II)-DTPA can also drive Fenton chemistry to convert H_2O_2 to $HO^{\cdot}$(**7**), which could explain some, but not all, of the observed degradation of Fe(III)-DTPA (G_{HO} (2.7) + $G_{H_2O_2}$ (0.7) = 3.4 ≠ *G*(-Fe(III)-DTPA) = 5.4).[36]

Reduction of the Fe(III) metal-centre by the superoxide radical (**6**) is slower for DTPA than EDTA (k = < 1×10^4 (not detectable) < 3.1×10^6 L mol^{-1} s^{-1}, respectively), but Fe(II)-DTPA is found to be a more efficient Fenton catalyst than Fe(II)-EDTA (**7**).[29] The slower rate of reaction between the superoxide radical and the metal-centre could allow more time for radical recombination reactions to occur between its conjugate acid to produce a secondary yield of H_2O_2 ($HO_2 + HO_2 \rightarrow H_2O_2 + O_2$ (**2**), k = 8.3×10^5 L mol^{-1} s^{-1})[32,33,38], which could then be consumed in superoxide driven Fenton chemistry (**7**) to evolve $HO^{\cdot}$ that could initiate oxidative degradation (**8**) and explain some of the observed difference between (*G*(-Fe(III)-DTPA) and *G*(-Fe(III)-EDTA).

The pK_a of HO_2 is 4.9, meaning that the conjugate base is the dominant species at pH 6.1 ($O_2^- + O_2^-$ is too slow to consider; k < 0.3 L mol^{-1} s^{-1})[38]; however, the samples were not buffered so the irradiation may lower the pH, thus giving rise to an increased portion of HO_2 for recombination (**2**). The mechanism described earlier for the degradation of uncoordinated EDTA converts an equivalent of $HO^{\cdot}$ from the primary yield into O_2^- via a peroxyl intermediate formed by the reaction of molecular oxygen with the oxidised ligand.[30] If the conjugate acid of O_2^- can then combine with itself to produce H_2O_2 to further undergo Fenton catalytic conversion to $HO^{\cdot}$, then this cyclical process could explain the greater than expected value of *G*(-Fe(III)-DTPA).

(4) $O_2^- + H^+ \rightarrow HO_2$ $k^{33} = 4.5 \times 10^{10}$ L mol^{-1} s^{-1}

(5) $HO_2 + HO_2 \rightarrow H_2O_2 + O_2$ $k^{36} = 8.3 \times 10^5$ L mol^{-1} s^{-1}

(6) Fe(III)-DTPA + $O_2^- \rightarrow$ Fe(II)-DTPA + O_2 $k^{29} = < 1 \times 10^4$ L mol^{-1} s^{-1}

(7) Fe(II)-DTPA + $H_2O_2 \rightarrow$ Fe(III)-DTPA + $HO^\cdot$ + HO^- $k^{36} = 99$ L mol^{-1} s^{-1}

(8) Fe(III)-DTPA + $HO^\cdot \rightarrow$ Fe(III)-(oxidised DTPA) + O_2^- $k^{36} = 8.3 \times 10^5$ L mol^{-1} s^{-1}

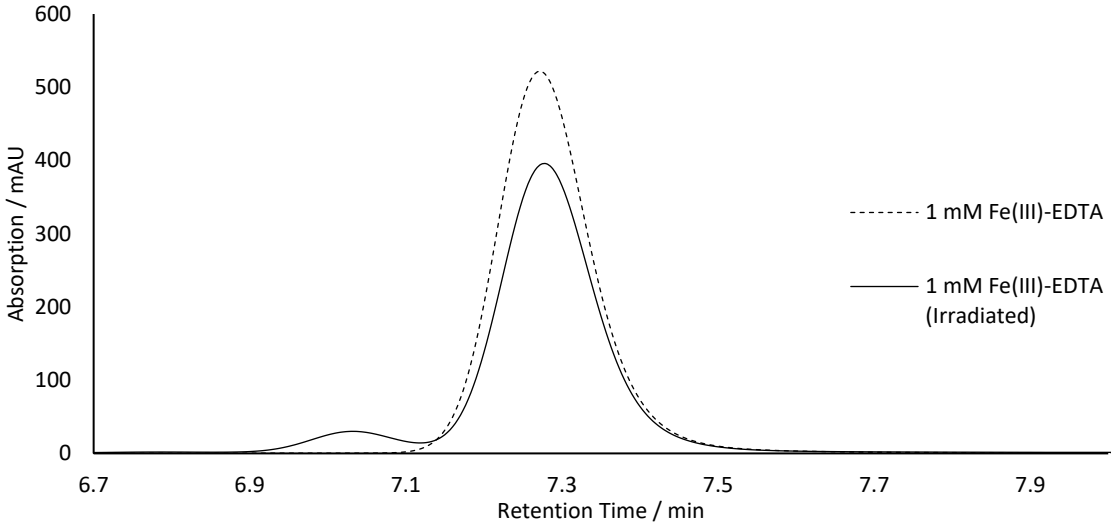

Figure 4. HPLC data from the Fe(III)-EDTA retention time region (detection via absorption of eluent at 258 nm). Dashed plot = 1 mM Fe(III)-EDTA calibration sample (un-irradiated), line plot = 1 mM Fe(III)-EDTA sample irradiated to 6.25×10^{18} eV g^{-1}). Fe(III)-EDTA $t_r \approx 7.3$ min, potential radiolytic product $t_r \approx 7.0$ min.

Comparison of the chromatograms recorded for the APCA-species calibration samples with those of the irradiated samples targeted identifying potential radiolytic degradation products by locating peaks that were present only in chromatograms recorded of samples post-irradiation. No significant peaks were discernible in the EDTA or Fe(III)-DTPA chromatograms; however, the analyses did reveal the consistent formation of a pre-peak on the low t_r flank of the Fe(III)-EDTA peak in the chromatographic data recorded for the irradiated complex (Figure 4).

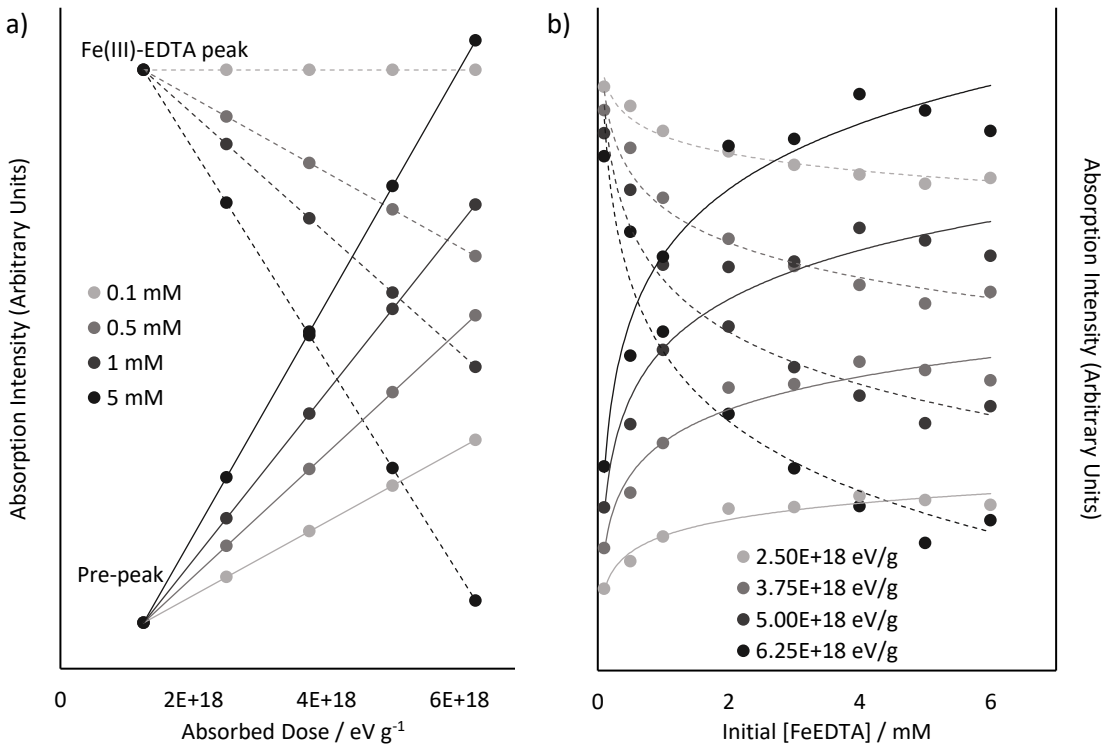

Figure 5. Plot of the chromatographic peak intensities recorded for the degradation of the Fe(III)-EDTA peak and the formation of the pre-peak. The data has been normalised and rescaled for visual clarity (arbitrary units on *y*-axes). Dashes = Fe(III)-EDTA peak (degradation), lines = pre-peak (formation). a) degradation/formation plotted against absorbed dose over a range of concentrations, and b) degradation/formation plotted against the initial concentration over a range of absorbed doses.

Quantitative analysis of the integrated area of the pre-peak revealed that its formation was proportional to the observed degradation of the Fe(III)-EDTA peak. Figure 5 shows the relationship between the absorption intensity of the pre-peak and the depleted absorption intensity of the Fe(III)-EDTA peak as a function of both increasing absorbed dose and initial concentration. This analysis provided strong evidence to suggest that the species responsible for the pre-peak observable in the Fe(III)-EDTA chromatographic data was a radiolytic degradation product.

The working hypothesis was that the peak could be caused by either a reduced Fe(II)-EDTA complex made by reduction of the metal-centre, principally, by O_2^- formed in the secondary yield, or a *bonafide* degradation product involving fragmented/decarboxylated EDTA components bound to an Fe(III)-centre. The radiolysis product was thought to involve an Fe(III)-centre and a coordinating ligand system because of the relatively strong UV-absorption profile (258 nm, Figure 4) exhibited by the species.

4.3.3 Stability of Fe(III)-EDTA in Varying p_{O_2} Environments

An experiment was designed to probe the identity of species responsible for the pre-peak. Neutral aqueous solutions of Fe(III)-EDTA over the concentration range 0.1 - 5 mM were irradiated to a total absorbed dose of 6.25×10^{-18} eV g^{-1}. Prior to irradiation, the samples were divided into three sets; one set was flushed with N_2 to create nitrogenated solutions free of dissolved O_2, another was flushed with O_2 to create an O_2-saturated environment, and a control group was left under atmospheric conditions. Should the pre-peak represent a reduced Fe(II)-EDTA structure, it was anticipated that its formation would be suppressed in the oxygenated environment (increased rate of re-oxidation back to Fe(III)-EDTA), whilst being amplified in the nitrogenated environment (limited re-oxidation available). Furthermore, each set of samples was measured at numerous time intervals extending over two weeks beyond the irradiation event, allowing the evolution of the pre- and Fe(III)-EDTA peak to be monitored for correlating changes in peak intensity over time.

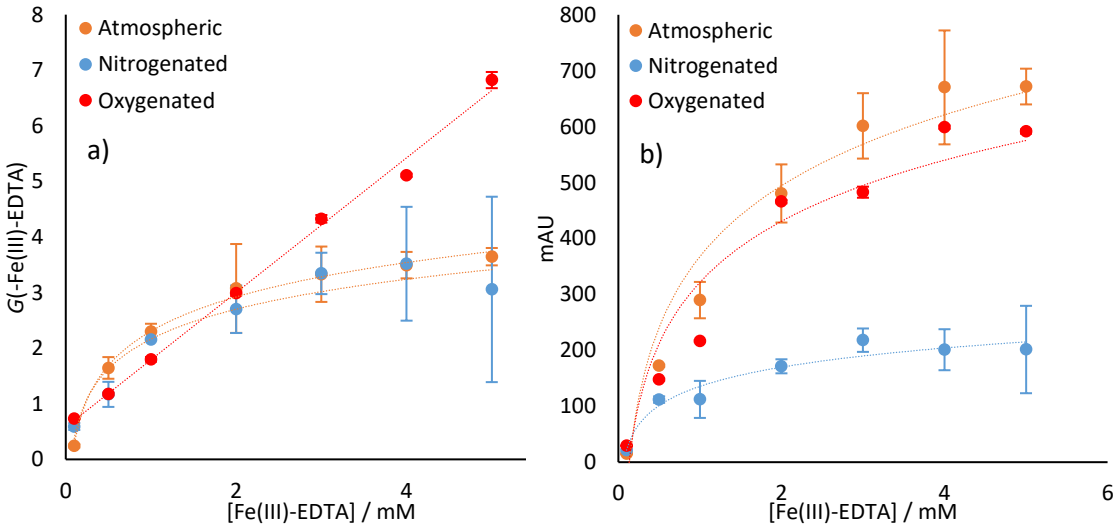

Figure 6. a) Plot of *G*(-Fe(III)-EDTA) against the initial concentration of the complex irradiated in neutral aqueous solution to a dose of 6.25×10^{-18} eV g^{-1} under various p_{O_2} environments (atmospheric = orange, nitrogenated = blue and oxygenated = red), b) corresponding formation of radiolytic degradation product pre-peak in various p_{O_2} environments.

Figure 6a shows the observed degradation of the Fe(III)-EDTA peak in the three irradiated matrices as a function of increasing initial concentration. The solutions flushed with N_2 show a similar pattern of degradation to those under atmospheric conditions. However, O_2-saturation of the samples appears to promote *G*-values that

increase linearly with the initial concentration across the entire tested range, which suggests that O_2 is directly involved in the degradation mechanism. The continued proportional increase of the trend beyond the concentration at which the primary yield of radicals is scavenged also suggests secondary reactivity in the irradiated matrix.

Figure 6b shows the corresponding intensity of the pre-peak that forms with the apparent radiolytic degradation of the Fe(III)-complex. The formation of the product is unaffected by the increased presence of O_2 in the irradiation matrix, but is significantly suppressed in the nitrogenated samples. This observation supports the argument that the species responsible for the pre-peak is not Fe(II)-EDTA, which would be expected to thrive under the more reducing conditions of an oxygen-free environment. Instead, the result suggests that O_2 is directly involved in the reaction needed to form the product, possibly through the addition-elimination reaction of a peroxyl intermediate (discussed previously).[30] This is supported by a mechanistic pulse-photolysis study, where it was found that the presence of O_2 played a crucial role in determining the fate of Fe(III)-EDTA in a photo-excited aqueous matrix; in deoxygenated media, reduced Fe(II)-species were formed (e.g. $[Fe(II)\text{-}EDTA]^{2-}$ and $Fe(II)_{aq.}$) along with uncoordinated EDTA oxidation products (e.g. $ED3A^{3-}$, CO_2 and formaldehyde); in oxygen saturated media, Fe(III)-complexes of EDTA and ED3A were detected, plus EDTA oxidation products.[17]

Table 2. Results of chromatographic analysis of irradiated Fe(III)-EDTA samples in various p_{O_2} environments as a function of time elapsed since irradiation.

	Fe(III)-EDTA Peak		**Pre-Peak**	
	ΔmAU day^{-1}	ΔmAU day^{-1} / % mAU of Original Peak	ΔmAU day^{-1}	ΔmAU day^{-1} / % mAU of Original Peak
Atmospheric	-28 ± 3	0.2 ± 0.1	-10 ± 2	1.8 ± 0.3
Nitrogenated	-33 ± 8	0.3 ± 0.2	-6 ± 1	3.3 ± 0.9
Oxygenated	-54 ± 6	0.4 ± 0.3	-18 ± 2	3.6 ± 0.5

Analysis of the evolution of the chromatographic peaks over time revealed that both species (Fe(III)-EDTA and the radiolytic degradation product) were relatively stable and no evidence of peak intensity shifts found, which could suggest re-oxidation of any

Fe(II)-EDTA back to Fe(III)-EDTA. Overall, the peak intensity associated with each species was found to decay over time (Table 2, all values of ΔmAU day^{-1} negative). The measured decay of the Fe(III)-EDTA peak intensity represented a very small fraction of the initial peak area (maximum change = 0.4 ± 0.3%), and a maximum change of 3.6 ± 0.5% was recorded for the pre-peak in oxygenated samples. This result suggests that the species is stable under all of the conditions tested.

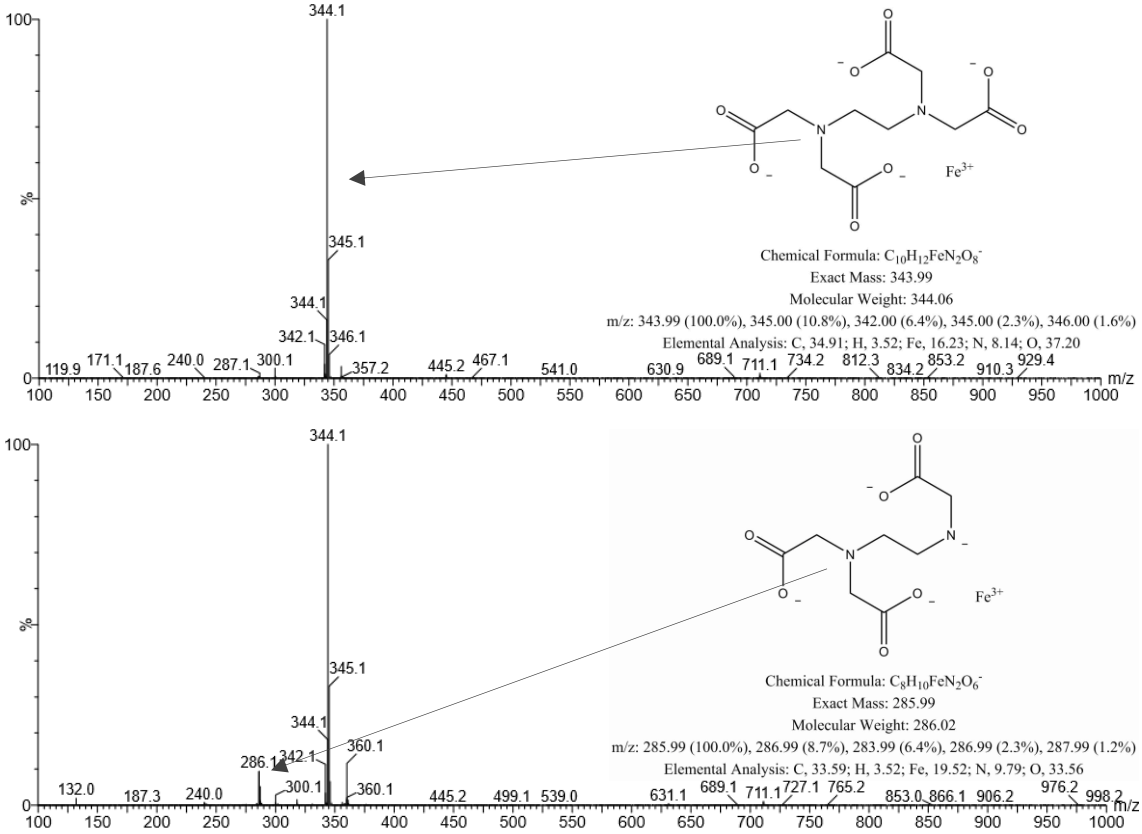

Figure 7. ESI$^-$ mass spectrometry data recorded for 1 mM solution of Fe(III)-EDTA (top) pre-irradiaition and (bottom) post-irradiation (6.25 × 10^{-18} eV g^{-1}, atmospheric conditions).

Mass spectrometric measurements recorded of samples of Fe(III)-EDTA pre/post-irradiation allow for some speculation as to the identity of the degradation product, as shown in Figure 7. The parent ion at m/z 344.1 corresponds with an [Fe(III)-EDTA]$^-$ species and is abundant in both spectra. A peak at m/z 286.1 is only visible in the mass spectrometric data recorded for irradiated samples and could correspond with the potential radiolytic degradation product, [Fe(III)-ED3A]$^-$ (Figure 7, bottom), formed by Schiff-base hydrolysis of a tertiary iminium. The similar charge distribution and hydrophobic radius of the Fe(III)-ED3A complex to Fe(III)-EDTA could also explain its

similar chromatographic retention time (Figure 4, Fe(III)-EDTA $t_r \approx 7.3$ min, pre-peak $t_r \approx 7.0$ min).

4.4 Conclusion

γ-Irradiation of neutral aqueous solutions of uncoordinated EDTA gave a *G*-value (2.5 ± 0.1), which corresponds well with the primary yield of $HO^{\cdot}$ (2.7), suggesting that degradation is initiated by the oxidative radical species, which is in good agreement with previous study.[26,30] In a similar experiment, irradiation of Fe(III)-EDTA gave a *G*-value (3.2) much greater than expected from a previously reported result: *G*(Fe(III)-EDTA) = 0).[27] This has been attributed to *bonafide* decomposition of the coordinating EDTA induced by the primary yield of the hydroxyl radical and the indirect involvement of hydrogen peroxide (G_{H2O2} (0.7)), which is thought to be catalytically converted (superoxide driven Fenton reaction) to an equivalent amount of $HO^{\cdot}$ by the Fe-centre of the EDTA-complex. It was also found that *G*(-Fe(III)-DTPA) = 5.4, suggesting that there are other significant reactive pathways available to the DTPA-complex that are not observed in the irradiation of Fe(III)-EDTA; structural, thermodynamic and kinetic factors are thought to play a role.

Study of the radiation stability of Fe(III)-EDTA in different p_{O_2} environments revealed that the concentration of dissolved O_2 has an impact on the observed degradation pattern of the complex. Results from the irradiation of high concentration (5 mM) oxygen-saturated solutions suggest that secondary or inter-molecular reactions are more prominent, causing the Fe(III)-EDTA to degrade to a greater extent than would be expected if only components from the primary yield were involved in the reactivity. Closer study of a Fe(III)-EDTA radiolytic degradation product, detectable in the chromatographic retention time range and thought to be Fe(III)-ED3A, showed that its formation was also influenced by the concentration of dissolved oxygen in the solutions; in a nitrogenated environment, formation of the product was significantly supressed, which suggests that oxygen is directly involved in the mechanism and provides supporting evidence for the degradation mechanisms that were proposed for the two Fe(III)-APCA complexes.

With respect to LLWR, the findings suggest that radiolysis of APCAs may be more likely than previously thought. Speciation of the APCAs in the LLWR near field is expected to give rise to a high portion of ligands existing as the Fe(III)-coordinated species. The results of this study suggests that coordination of the ligands to Fe(III) decreases their radiation stability, possibly by introducing Fenton chemistry to their immediate environment. The strength of the radiation field exerted by radionuclides in LLW is weak compared to a ^{60}Co γ-source, but the timescale on which the LLWR site and the associated geochemical modelling are very long (> 3000 y); inclusion of the potential for radiolytic decay of the ligands into the site models could ultimately allow LLWR to safely relax some of the constraints imposed on the APCA-species contained in waste consignments. Further study would be needed to determine the kinetics of such processes.

4.5 References

1. A. L. Rufus, S. Velmurugan, V. S. Sathyaseelan and S. V. Narasimhan, *Prog. Nucl. Energ.*, 2004, **44**, 1, 13-31.
2. M. Butcheli-Witschel and T. Elgi, *FEMS Microbiol. Rev.*, 2001, **25**, 1, 69-106.
3. J. L. Means and C. A. Alexander, *Nucl. Chem. Waste Man.*, 1981, **2**, 186-193.
4. Radioactive Waste Management (RWM), *Geological Disposal Behaviour of Radionuclides and Non-radiological Species in Groundwater Status Report*, NDA Report no. DSSC/456/01, RWM, Oxford, UK, 2016.
5. LLWR, *Environmental Safety Case – Main Report*, LLWR/ESC/R(11)10016, LLWR, Cumbria, UK, 2011.
6. Norwegian Radiation Protection Authority (NRPA), *Study of Issues Affecting the Assessment of Impacts of Disposal of Radioactive and Hazardous Waste*, NRPA Report 2018:6, Østerås, Statens strålevern, 2018.
7. R. J. Serne, K. J. Cantrell, C. W. Lindenmeier, A. T. Owen, I. V. Kutnyakov, R. D. Orr and A. R. Felmy, *Radionuclide-Chelating Agent Complexes in Low-Level Radioactive Decontamination Waste; Stability, Adsorbtion and Transport Potential*, NUREG/CR-6758 PNNL- 13774, U.S. Nuclear Regulatory Commission (NRC), Washington D.C., 2002.
8. LLWR, *Review of the Potential Effects of Complexants on Contaminant Transport at the LLWR*, LLWR/ESC/R(13)10054, LLWR, Cumbria, UK, 2013.
9. LLWR, *Near Field*, The 2011 Environmental Safety Case, LLWR/ESC/R(11)10021, Holmrook, 2011.
10. Environment Agency (EA), *Review of LLW Repository Ltd's 2011 Environmental Safety Case: Inventory and Near Field*, Issue 1, EA, Bristol, 2015.
11. M. Sillanpää, in *Rev. Environ. Contam. Toxicol.*, ed. G. W. Ware, 1997, **152**, 85-111, Springer, New York, NY.
12. P. Laine and R. Matilainen, *Anal. Bioanal. Chem.*, 2005, 382, 1601-1609.
13. V. Sýkora, P. Pitter, I. Bittnerová and T. Lederer, *Water Res.*, 2001, **35**, 8, 2010-2016.
14. B. Nowack, F. G. Kari, S. U. Hilger and L. Sigg, *Anal. Chem.,* 1996, **68**, 561-566.

15. LLWR, *Waste Acceptance Criteria – Low Level Waste Disposal*, WSC-WAC-LOW – Version 5.0, LLWR, Cumbria, UK, 2016.
16. A. Svenson, L. Kaj and H. Björndal, *Chemosphere*, 1989, **18**, 1805-1808.
17. P. Kocot, A. Karocki and Z. Stasicka, *J. Photochem. Photobiol. A: Chem.*, 2006, **179**, 176-183.
18. S. Metsärinne, T. Tuhkanen and R. Aksela, *Chemosphere*, 2001, **45**, 949-955.
19. H. B. Lockhart and R. V. Blakely, *Environ. Lett.*, 1975, **9**, 19-31.
20. R. T. Belly, J. J. Lauff and C. T. Goodhue, *Appl. Microbiol.*, 1975, **29**, 787-794.
21. H. B. Lockhart and R. V. Blakely, *Environ. Sci. Technol.*, 1975, **9**, 1035-1038.
22. R. Frank and H. Rau, *Ecotoxicol. Environ. Saf.*, 1990, **19**, 55-63.
23. F. G. Kari and W. Giger, *Environ. Sci. Technol.*, 1995, **29**, 2814-2827.
24. J. L. Means, T. Kucak and D. A. Crerar, *Environ. Pollut. B*, 1980, **1**, 1, 45-60.
25. A. P. Toste, K. J. Polach and T. Ohnuki, *J. Radioanal. Nucl. Chem.*, 2005, **263**, 559-565.
26. S. N. Bhattacharyya and K. P. Kundu, *Int. J. Radiat. Phys. Chem.*, 1972, **4**, 31-41.
27. K. P. Kundu and N. Matsuura, *Int. J. Radiat. Phys. Chem.*, 1975, **7**, 565-571.
28. Y. A. Ilan and G. Czapski, *Biochim. Biophys. Acta*, 1977, **498**, 386-394.
29. G. R. Buettner, T. P. Doherty and L. K. Patterson, *FEBS Lett.*, 1983, **158**, 143-146.
30. B. Höbel and C. von Sonntag, *J. Chem. Soc., Perkin Trans. 2*, 1998, 509-513.
31. J. A. O'Hanlon, R. D. Chapman, F. Taylor and M. A. Denecke, *J. Radioanal. Nucl. Chem.*, 2019, **322**, 1915-1929.
32. M. Sánchez-Polo, J. López-Peñalver, G. Prados-Joya, M. A. Ferro-García and J. Rivera-Utrilla, *Water Res.*, 2009, **43**, 4028-4036.
33. A. A. Basfar, H. M. Khan, A. A. Al-Shahrani and W. J. Cooper, *Water Res.*, 2005, **39**, 2085-2095.
34. G. Ghiselli, W. F. Jardim, M. I. Litter and H. D. Mansilla, *J. Photochem. Photobiol. A: Chem.*, 2004, **167**, 59-67.
35. A. F. Seliverstov, B. G. Ershov, Yu. O. Lagunova, P. A. Morozov, A. S. Kamrukov and S. G. Shashkovskii, *Radiochemistry*, 2008, **50**, 70-74.
36. C. J. Miller, A. L. Rose and T. D. Waite, *Front. Mar. Sci.*, 2016, **3**, 134.
37. R. M. Smith, A. E. Martell, *Critical Stability Constants*, 6, Plenum Press, New York, 1989.
38. H. A. Schwarz, *J. Chem. Educ.*, 1981, **58**, 101-105.

Blank page

Chapter Five: Conclusion

The aims of this project were to: i) develop, optimise and validate a suitable APCA detection method for use on samples relevant to LLWR, and ii) to apply the method to a range of real samples to collect useful information.

A robust and sensitive RP-HPLC-DAD procedure has been used to detect three common APCAs of interest to LLWR in complex aqueous matrices. A discussion of the steps taken to validate the method is presented in Chapter Two, with justification for each of the method parameters. The LODs for Fe(III)-EDTA, Fe(III)-DTPA and Fe(III)-NTA were found to be 0.31, 0.38 and 4.3 μM, respectively. The sensitivity for Fe(III)-EDTA and Fe(III)-DTPA was found to be suitably high for the purpose of environmental monitoring of leachate samples from LLWR. The LOD for Fe(III)-NTA is thought to be higher as result of the lower molar extinction coefficient of the complex and the poorer chromatographic resolution.

The monolithic silica stationary phase used in this analysis in place of a conventional particle-based C_{18} column was demonstrated to give rise to superior resolution; greater peak area per unit analyte (mAU μmol^{-1} L) resulted in higher sensitivity. Simultaneous determination of the three Fe(III)-APCA complexes with baseline resolution was achieved; a gradient elution was implemented to maintain peak sharpness. The column was proven to be robust (no signs of deterioration in the quality of results after nine-month period of frequent use), which has economical value as it helps to offset the greater investment associated with the polymeric stationary phase.

Method validation using purely aqueous samples of known standards demonstrated linearity of the chromatographic response ($r^2 > 0.98$), precision (intra/inter-day %RSD ≤ 10%) and accuracy (recovery = 100 ± 5%). To guard against the potential complications introduced to the procedure by competing ions or other interfering species, two peak deconvolution methods were successfully applied to the HPLC-DAD data recorded for various mixtures of Fe(III)- and Co(III)-EDTA. The accuracy of each method was comparable; most data points fell within the range 100 ± 10% (deconvoluted peak area

as a percentage of calibration sample peak area). Though more time consuming, the LSF procedure was found to be more reliable at low concentrations (LSF/PARAFAC Fe(III)-EDTA LOD = 0.35/2.3 μM), hence, was taken forward for application to real samples.

The HPLC procedure was applied to environmental samples of LLWR trench leachate. Analysis of EDTA-spiked samples of leachate determined a decrease in the recovery (55 ± 9% of a 7.82 μM EDTA-spike) which was attributed to the natural availability of Fe(III) for complexation amongst other matrix effects. A logarithmic trend was determined between EDTA concentration and recovery, which was used to introduce a correction factor to the results to account for decreased recovery. Without the correction factor, the result underestimates the amount of EDTA by approximately 15% at the concentration range of interest (~1 μM).

Of the six trench leachate samples that were tested, four were found to contain trace concentrations of EDTA, all of which fell below the LOQ of the method (1 μM). The total concentration of Fe(III)-EDTA found in the trench leachate samples ranges from 0.4 - 0.7 μM, which translates to an EDTA concentration range of 0.4 - 0.8 μM, should the correction factor be taken into account. These figures generally agree with those determined in a similar analysis of LLWR trench leachate in 2013.

The results further LLWR's understanding of the extent of APCA contamination in the repository near field and provide confidence to the Environment Agency that the levels used as reference concentrations in the biogeochemical modelling of the impact of APCAs in the environment were reasonable. The technique is considered to be robust and will be considered further in informing limits of acceptance on APCAs; the levels determined in this analysis are not considered sufficient to increase the risk of radionuclide mobilisation.

Use of the HPLC method was targeted at EDTA quantification in a potential wasteform under consideration for acceptance by LLWR. A trial incineration procedure designed to destroy spent ion-exchange resins designated for disposal in the repository produces a solid residue that must be tested to ensure complete destruction of the

ligand content (EDTA not detected above an acceptable LOD). Therefore, the quantification method was successfully extended to include a solid-liquid phase extraction to pre-treat samples of residue; it was necessary to optimise each parameter of the extraction method to maximise the quantity of analyte in solution to utilise the full potential of the liquid chromatographic detection technique. The results of this study are presented in Chapter Three.

The final procedure was validated for its accuracy (mean recovery = 78 ± 3.3%), precision (%RSD ≤ 10%), sensitivity (procedural LOD = 0.32 mg kg^{-1}) and selectivity (LSF procedure used to determine EDTA peak area). The target sensitivity of the overall extraction and quantification method was 1 mg kg^{-1}; in a recent study, a LOD of 5.5 mg kg^{-1} was reported for a similar extraction and HPLC quantification technique for EDTA in feed and premix formulations.[d] The simplicity of each method is comparable, as are the recoveries obtained from the solid-liquid phase extraction methods (> 70%), which suggests that it is the sensitivity of the HPLC detection method used in this analysis that make it overall more sensitive.

No EDTA was detected in the residue produced in a preliminary trial phase resin incineration procedure, which is a positive result for the development of thermal destructive techniques for the treatment of radioactive wastes prior to their disposal. The extraction and quantification technique could also be applicable to other solid sample matrices from completely different sources. The method is yet to be trialled on material containing a radiological component or other metallic elements that could interfere with the analysis; competing ions may interfere with EDTA complexation to Fe(III) which could necessitate further work to determine the speciation of the ligand for accurate quantification.

The EDTA-spike recovered from the residue matrix was co-extracted with a range of EDTA-thermal degradation products, the quantity and identity of which are thought to

[d] F. Chiumiento, A. D'Aloise, F. Marchegiani and V. Melai, *Food Chem.*, 2015, **175**, 452-456.

be a function of the concentration of EDTA present in the pre-incineration matrix and the incineration parameters. The surface chemistry of the suspected EDTA-thermal degradation products has been observed to influence the recovery of the ligand post-extraction. This could have implications for the application of the method to real IX residue samples as the specific recovery may be determined by a complex set of interactions between the physical state of the waste pre- and post-incineration. The thermal degradation products detected in this analysis have not been identified but results suggest that they are polydentate complexing organic ligands. Their potential to mobilise radionuclides in the final wasteform should also be explored.

Finally, the quantification technique was applied to irradiated neutral aqueous samples of APCAs to quantify the degradation, elicit potential degradation mechanisms and identify radiolytic degradation products. The results of a study into the comparative γ-irradiation stabilities of EDTA, Fe(III)-EDTA and Fe(III)-DTPA are presented in Chapter Four.

A *G*-value of 2.5 ± 0.1 was determined for uncoordinated EDTA and correlated with oxidative degradation initiated by the primary yield of hydroxyl radical ($G_{HO\cdot}$ = 2.7). Irradiation of Fe(III)-EDTA gave a *G*-value (3.2) much greater than expected from a previously reported result: *G*(Fe(III)-EDTA) = 0). This has been attributed to decomposition of the coordinating EDTA induced by the primary yield of the hydroxyl radical and the indirect involvement of hydrogen peroxide (G_{H2O2} (0.7)), which is thought to be catalytically converted (superoxide driven Fenton reaction) to an equivalent amount of $HO^{\cdot}$ by the Fe-centre of the EDTA-complex. It was also found that *G*(-Fe(III)-DTPA) = 5.4, suggesting that there are other significant reactive pathways available to the DTPA-complex that are not observed in the irradiation of Fe(III)-EDTA.

Study of the radiation stability of Fe(III)-EDTA in different p_{O_2} environments revealed that the concentration of dissolved O_2 has an impact on the observed degradation pattern of the complex. Closer study of a Fe(III)-EDTA radiolytic degradation product, detectable in the chromatographic retention time range and thought to be Fe(III)-ED3A, showed that its formation was also influenced by the concentration of dissolved

oxygen in the solutions; in a nitrogenated environment, formation of the product was significantly supressed, which suggests that oxygen is directly involved in the mechanism.

Some of these findings suggest that the APCAs may be more susceptible to radiolysis than was previously thought, particularly in the presence of Fe(II)/Fe(III), which decreases the radiation stability of the ligands by introducing Fenton chemistry to their immediate environment. From an LLWR perspective, this could be beneficial as a combination of a high abundance of Fe and the presence of radionuclides in the repository near field could facilitate degradation mechanisms to remove APCAs from the environment to reduce the risk of radionuclide mobilisation. The strength of the radiation field exerted by radionuclides in LLW is weak compared to a ^{60}Co γ-source, but the timescale on which the LLWR site and the associated geochemical modelling are very long (> 3000 y); inclusion of the potential for radiolytic decay of the ligands into the site models could ultimately allow LLWR to safely relax some of the constraints imposed on the APCA-species contained in waste consignments.

5.1 Future Work

To further develop the HPLC APCA quantification method, more work could be done to establish the effects of other competing ions that might be present in the repository environment. For example, the stability of the Cr(III)-EDTA complex is almost equivalent to that of Fe(III)-EDTA and could potentially interfere with the analysis ($\log\beta_{Cr(III)\text{-}EDTA} = 23.4 < \log\beta_{Fe(III)\text{-}EDTA} = 25.1$).[e] Furthermore, the detection profiles of other organic chelates known to occur in the repository (e.g. citric acid, ISA) have not been assessed under the HPLC elution conditions. Work to establish whether they interfere with the Fe(III)-APCA chromatographic peaks should be undertaken.

The trench leachate from the LLWR site was heterogenous. The solid phase was filtered from the sample matrix and discarded. For a more comprehensive analysis of

[e] R. M. Smith, A. E. Martell, *Critical Stability Constants*, Plenum Press, New York, 6th edn., 1989.

the APCA content of the leachate, an analysis should be developed to determine the quantity of ligand potentially adsorbed to the surface of the sediment. This could be achieved by extraction, or altering the surface chemistry of the precipitate by addition of surfactants, to bring adsorbed APCA into solution for analysis by HPLC.

With respect to the analysis of the incinerated ion-exchane resins, further work should be targeted at applying the method to resin residue obtained from incineration of real samples of the spent resin in storage, or at least spent resin that contains potentially interfering metallic ions. The presence of competing ions in the residue matrix is likely to complicate the extraction procedure and the quantitative conversion of the EDTA to Fe(III)-EDTA as the ligand can speciate to other metal ions. The effect of this potential interference should be quantified, and steps to develop and optimise the method should be taken accordingly.

The experimental approach used to assess the radiolytic stabilities of the APCAs and their complexes is very flexible and allows for investigation into the effects of many different variables (e.g. pH of solution, metal ion complexation, dose, dose rate, concentration). To make the results of the analysis more relevant for use in the LLWR geochemical models, an experimental irradiation matrix could be designed to mimic the specific conditions of the repository, or environments within the repository. Analysis of APCA degradation under these conditions could be more easily extrapolated to determine the ultimate environmental fate of the ligands in the repository.

Appendix: Supplementary Information

1. Co(III)-EDTA Synthesis

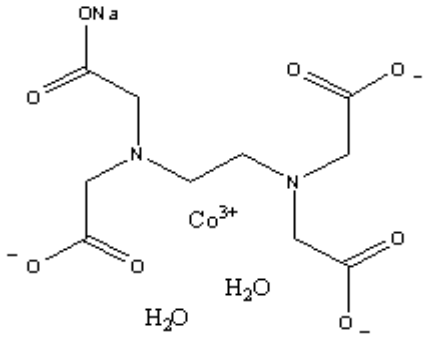

Chemical Formula: $C_{10}H_{16}CoN_2NaO_{10}$
Exact Mass: 406.00
Molecular Weight: 406.16
m/z: 406.00 (100.0%), 407.01 (10.8%), 408.01 (2.1%)
Elemental Analysis: C, 29.57; H, 3.97; Co, 14.51; N, 6.90; Na, 5.66; O, 39.39

Figure 1. Skeletal structure of the synthesised Co(III)-EDTA crystal (NaCoEDTA·2H_2O).

Table 1. ICP-MS results for the synthesised Co(III)-EDTA crystal (NaCoEDTA·2H_2O).

Element	Expected	Found
C	29.57	29.03
H	3.97	3.77
N	14.51	6.97
Co	6.90	14.57
Na	5.66	6.21
Fe	0.00	0.24
O	39.39	39.21 (remainder)

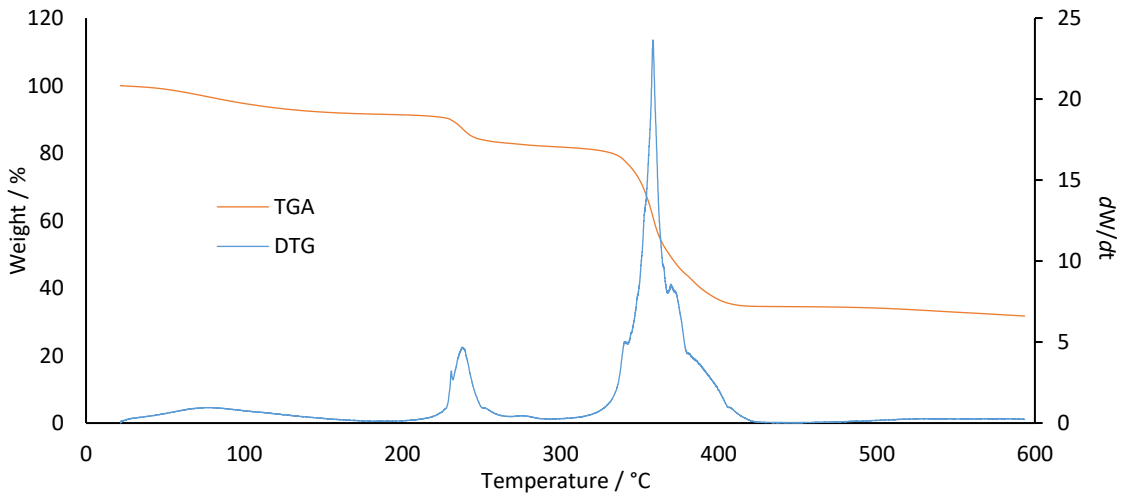

Figure 2. Results of TGA and DTG analysis of the Co(III)-EDTA crystal; TGA ran from 10 - 600 °C under air.

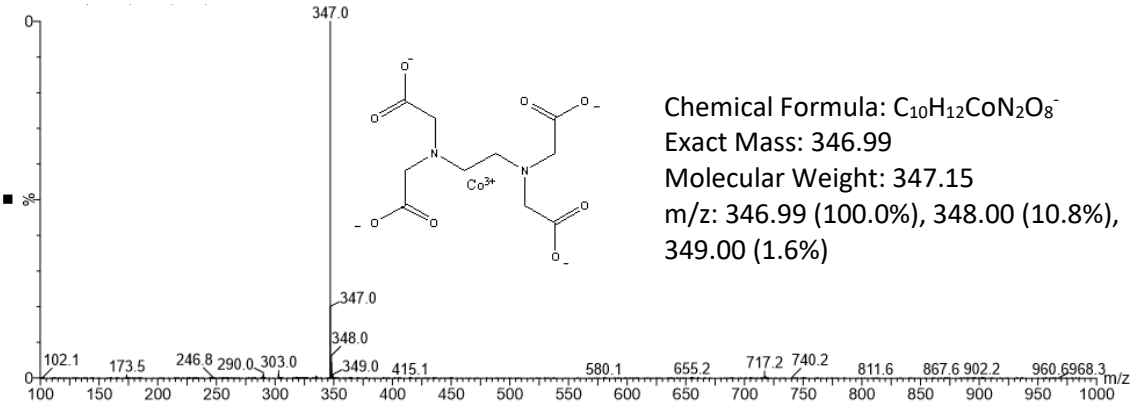

Figure 3. Results of mass spectrometric analysis of Co(III)-EDTA crystal. 0.01 mM aqueous solution, ESI negative.

2. HPLC Method Calibration

The Fe(III)-APCA HPLC quantification method was tested on a conventional particle-based C_{18} column (Column 2) as well as the monolithic silica column (Column 1) described previously. 100 μL injection volumes were also tested.

Table 2. Mean peak intensities of Fe(III)-APCA complexes over the concentration range (1000 – 0.1 μL) recorded using Columns 1 and 2 and two injection volumes (10 μL, 100 μL). σ and %RSD calculated from duplicate injections of samples prepared by sequential dilution of stock solutions in triplicate (n = 6). * = stock solutions made from crystalline material.

		Column 1 (Chromolith)				**Column 2 (Phenomenex C_{18})**			
		10 μL		**100 μL**		**10 μL**		**100 μL**	
M(III)-APCA	**Conc. / μM**	**Absorption ±σ / mAU**	**%RSD**	**Absorption ±σ / mAU**	**%RSD**	**Absorption ±σ / mAU**	**%RSD**	**Absorption ±σ / mAU**	**%RSD**
Fe-EDTA*	1000	9262 ±23	0.25	DS	DS	5082 ±78	1.53	DS	DS
	100	937.7 ±9.1	0.97	9290 ±66	0.72	339.4 ±7.8	2.29	5030 ±39	0.77
	10	94.96 ±3.22	3.39	930.40 ±10.0	1.07	21.24 ±0.92	4.31	354.9 ±9.3	2.62
	1	8.922 ±1.038	12.05	92.76 ±3.21	3.46	NQ	NQ	19.32 ±1.60	8.26
	0.1	ND	ND	8.68 ±0.930	10.72	ND	ND	NQ	NQ
Fe-EDTA	1000	9297 ±20	0.22	DS	DS	5098 ±16	0.31	DS	DS
	100	925.2 ±9.2	0.99	9248 ±49	0.53	350.2 ±12.2	3.49	5033 ±30	0.59
	10	93.82 ±2.80	2.98	914.9 ±10.1	1.11	19.63 ±1.56	7.94	352.6 ±8.3	2.36
	1	8.810 ±0.871	9.88	89.99 ±2.87	3.19	NQ	NQ	19.97 ±1.34	6.73
	0.1	ND	ND	8.332 ±0.897	14.56	ND	ND	NQ	NQ
Fe-DTPA	1000	9077 ±44	0.48	DS	DS	3996 ±129	3.23	DS	DS
	100	884.3 ±10.2	1.16	8925 ± 123	1.37	251.9 ±7.5	5.98	3904 ±103	2.63
	10	88.05 ±1.57	1.78	885.1 ± 13.5	1.53	16.99 ±0.89	5.27	270.4 +9.5	3.52
	1	8.471 ±1.035	23.43	87.304 ± 1.21	4.67	NQ	NQ	13.08 ±1.99	7.69
	0.1	ND	ND	NQ	NQ	ND	ND	NQ	NQ

Fe-NTA	10000	DS	DS	NT	NT	26364 ±411	1.56	NT	NT
	1000	5533 ±44	0.79	NT	NT	2178 ±86	3.95	NT	NT
	100	509.0 ±10.2	2.01	NT	NT	127.7 ± 11.5	9.04	NT	NT
	10	38.46 ± 1.57	4.09	NT	NT	ND	ND	NT	NT
	1	ND	ND	NT	NT	ND	ND	NT	NT
Co-EDTA	1000	16760 ±81	0.48	NT	NT	NT	NT	NT	NT
	100	1715 ±11	0.63	NT	NT	NT	NT	NT	NT
	10	171.8 ±1.85	1.08	NT	NT	NT	NT	NT	NT
	1	17.14 ±0.648	3.78	NT	NT	NT	NT	NT	NT

NQ = not quantifiable, ND = not detected and NT = not tested.

Table 3. Linearity, slope, LOD and LOQ values for the Fe(III)-APCA complexes detected under the various chromatographic conditions.

			Fe(III)-EDTA*	**Fe(III)-EDTA**	**Fe(III)-DTPA**	**Fe(III)-NTA**
Column 1	**10 µL**	Linearity / r^2	0.99999	0.99999	0.99999	0.99998
		Slope / mAU µmol^{-1} L	9.25478	9.29803	9.08401	5.56277
		LOD / µM	0.37	0.31	0.38	4.33
		LOQ / µM	1.12	0.94	1.14	13.14
	100 µL	Linearity / r^2	0.99999	0.99999	0.99999	NT
		Slope / mAU µmol^{-1} L	92.8954	92.5228	89.3115	NT
		LOD / µM	0.03	0.03	0.04	NT
		LOQ / µM	0.20	0.10	0.14	NT
Column 2	**10 µL**	Linearity / r^2	0.99932	0.99942	0.99912	0.99986
		Slope / mAU µmol^{-1} L	5.17559	5.18902	4.07652	2.66524
		LOD / µM	0.58	0.99	0.72	14.30
		LOQ / µM	1.77	3.00	2.19	43.32
	100 µL	Linearity / r^2	0.99950	0.99947	0.99947	NT
		Slope / mAU µmol^{-1} L	51.1524	51.1888	39.7358	NT
		LOD / µM	0.10	0.087	0.17	NT
		LOQ / µM	0.31	0.26	0.50	NT

Table 4. Mean peak intensity values obtained for Fe(III)-EDTA (formed in solution), expressed as a percentage of the mean peak intensity values obtained for Fe(III)-EDTA* (stock solution made from crystalline sample), recorded using Column 1 and 2 (10 µL and 100 µL injection volumes).

	Column 1		**Column 2**		
Conc. / µM	**10 µL**	**100 µL**	**10 µL**	**100 µL**	**Mean**
1000	100.38	DS	100.32	DS	100.35
100	98.67	99.56	103.18	100.06	100.36
10	98.8	98.34	92.39	99.33	97.21
1	96.1	97.02	NQ	103.34	98.82
0.1	ND	100.66	ND	NQ	100.66

Table 5. Mean peak intensities for Fe(III)-EDTA* (Column 1, 10 µL injection volume). Dataset 1 (Used): results displayed in Table 1. Dataset 2 (New): obtained from identical experiment performed nine months prior, when

column was new and unused. For σ of each individual dataset, n = 6. Inter-day precision σ and %RSD values calculated for all data from both datasets, n = 12.

	Dataset 1 (Used)		Dataset 2 (New)		Inter-Day Precision		
Conc. / mM	**Mean Absorption / mAU**	**σ**	**Mean Absorption / mAU**	**σ**	**Mean Absorption / mAU**	**σ**	**%RSD**
1000	92612	22	9344	24	9295	48	0.52
100	937.7	9.1	936.6	5.7	937.2	7.6	0.81
10	94.96	3.22	95.41	1.83	95.14	2.63	2.76
1	8.922	1.038	9.429	0.293	9.296	0.721	7.76

3. Calibration: LSF and PARAFAC

Table 6. Integrated peak areas for Fe(III)-EDTA and Co(III)-EDTA, recorded at their respective wavelengths of maximum absorption, obtained by application of comparative data analysis techniques. Table also shows σ, %RSD, gradient of linear trend and LOD.

		Fe(III)-EDTA (258 nm)					Co(III)-EDTA (228 nm)				
	[M(III)-EDTA] / μM	**Peak Area**	**σ**	**%RSD**	**Slope**	**LOD**	**Peak Area**	**σ**	**%RSD**	**Slope**	**LOD**
LSF	**1000**	150.23	0.57	0.38	0.15	0.35	287.34	1.50	0.52	0.29	0.13
	100	15.10	0.09	0.58			29.28	0.12	0.42		
	80	11.24	0.32	2.85			22.54	0.36	1.59		
	60	8.38	0.17	2.08			16.79	0.11	0.65		
	40	5.61	0.17	2.95			10.96	0.38	3.49		
	20	2.90	0.09	3.18			5.64	0.13	2.23		
	10	1.48	0.07	5.08			2.92	0.02	0.81		
	1	0.15	0.02	10.81			0.28	0.01	3.97		
PARAFAC	**1000**	101.43	1.91	1.89	0.10	2.34	146.54	3.61	2.47	0.15	4.38
	100	10.56	0.11	1.04			15.13	0.21	1.42		
	80	7.95	0.09	1.16			11.02	0.36	3.25		
	60	5.81	0.17	2.85			8.20	0.11	1.33		
	40	4.04	0.17	4.32			5.48	0.38	6.98		
	20	2.10	0.32	15.23			2.89	0.13	4.34		
	10	0.98	0.14	14.17			1.54	0.22	14.04		
	1	0.10	0.07	68.65			0.23	0.19	85.64		

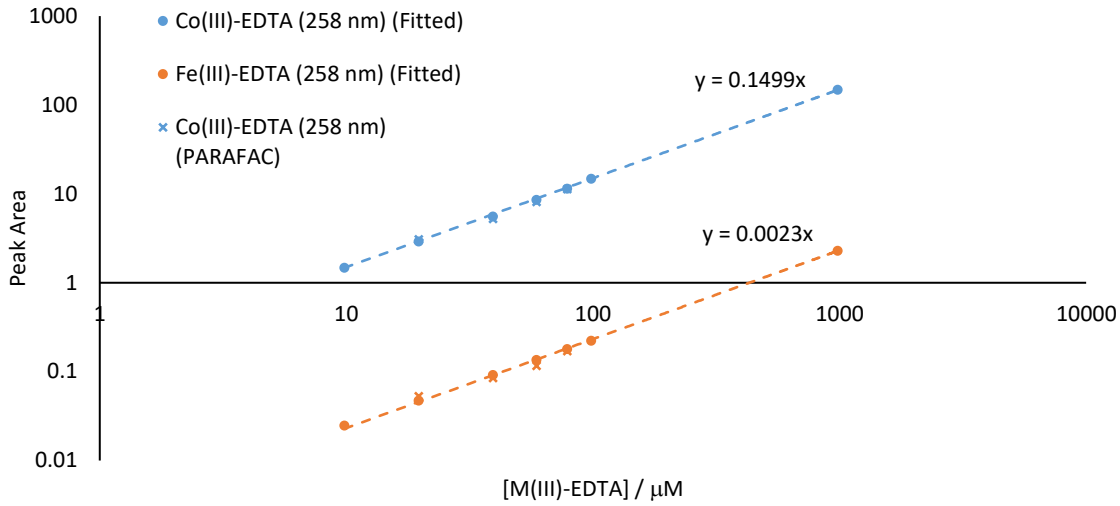

Figure 4. Plot of integrated peak areas of Co(III)-EDTA calibration samples, obtained from least-squares fitting and PARAFAC, showing the proportional Fe(III)-EDTA contamination present in each sample. Peak areas measured at 258 nm (Fe(III)-EDTA λ_{max}).

HPLC analysis of the Co(III)-EDTA solution prepared from the supposedly pure powdered synthesised crystalline product revealed evidence of Fe(III)-EDTA contamination in the sample. This was later confirmed by ICP-MS (Table 1). ICP-MS analysis of the starting materials indicated no significant Fe-contamination, suggesting that product contamination was procedural. The ratio of Fe(III)-EDTA impurity to Co(III)-EDTA determined by analysis of the HPLC data obtained from the Co(III)-EDTA calibration samples (Figure 4), and confirmed by concordant ICP-MS results, was found to be roughly 0.015:1. This contamination is accounted for in the analysis of the calibration data and in calculations of percent recovery.

4. Deconvolution: LSF and PARAFAC

Table 7. Deconvoluted chromatographic peak areas of various mixtures of Fe(III)- and Co(III)-EDTA obtained by least-squares fitting (LSF). Peak areas were converted to concentration using the slope determined by the calibration curve (Table 1), and are represented here as a percentage of the expected concentration. Values in **bold** and on the left of each column are for Fe(III)-EDTA, and values in normal font and on the right for Co(III)-EDTA. NQ = not quantified.

	[Co(III)-EDTA] / μM													
[Fe(III)-EDTA] / μM	**1000**		**100**		**80**		**60**		**40**		**20**		**10**	
1000	**98 ±5.8**	96 ±3.4	**98 ±1.8**	114 ±2.8	-	-	-	-	-	-	-	-	**98 ±1.0**	NQ
100	**103 ±13**	101 ±0.6	**100 ±5.6**	106 ±1.1	-	-	-	-	-	-	-	-	**100 ±1.6**	110 ±3.0
80	**-**	-	**-**	-	**102 ±2.7**	99 ±1.3	**102 ±2.2**	98 ±1.4	**100 ±2.4**	97 ±1.7	**99 ±1.9**	102 ±1.9	**-**	-
60	**-**	-	**-**	-	**104 ±3.2**	98 ±1.3	**103 ±2.3**	98 ±1.2	**101 ±2.1**	99 ±1.7	**98 ±2.2**	100 ±1.6	**-**	-
40	**-**	-	**-**	-	**105 ±5.0**	98 ±1.3	**103 ±4.2**	98 ±1.5	**102 ±3.1**	98 ±1.4	**100 ±1.8**	100 ±1.4	**-**	-
20	**-**	-	**-**	-	**113 ±9.1**	98 ±1.4	**112 ±6.5**	98 ±1.2	**108 ±5.2**	97 ±1.3	**105 ±2.9**	98 ±1.5	**-**	-
10	**NQ**	100 ±0.5	**107 ±16**	102 ±0.9	-	-	-	-	-	-	-	-	**100 ±6.5**	101 ±1.1

Table 8. Deconvoluted chromatographic peak areas of various mixtures of Fe(III)- and Co(III)-EDTA obtained from PARAFAC. Peak areas were converted to concentration using the slope determined by the calibration curve and are represented here as a percentage of the expected concentration of EDTA-complex in each sample of mixture. Values in **bold** and on the left of each column represent Fe(III)-EDTA, and values in normal font and on the right represent Co(III)-EDTA. NQ = not quantified.

	[Co(III)-EDTA] / μM													
[Fe(III)-EDTA] / μM	**1000**		**100**		**80**		**60**		**40**		**20**		**10**	
1000	**104 ±3.2**	105 ±1.5	**105 ±1.1**	119 ±13	-	-	-	-	-	-	-	-	**104 ±0.8**	NQ
100	**98 ±27**	105 ±0.5	**106 ±4.8**	111 ±2.3	-	-	-	-	-	-	-	-	**105 ±2.3**	127 ±13
80	**-**	-	**-**	-	**94 ±6.6**	106 ±3.8	**95 ±5.0**	106 ±3.9	**98 ±4.4**	105 ±4.9	**98 ±2.5**	106 ±4.3	**-**	-
60	**-**	-	**-**	-	**92 ±9.5**	105 ±1.9	**94 ±7.5**	105 ±3.0	**97 ±3.2**	103 ±4.3	**98 ±3.1**	104 ±1.8	**-**	-
40	**-**	-	**-**	-	**87 ±13**	104 ±0.9	**92 ±11**	104 ±2.0	**98 ±9.3**	103 ±2.1	**99 ±3.5**	107 ±3.1	**-**	-
20	**-**	-	**-**	-	**86 ±22**	103 ±1.6	**95 ±19**	103 ±2.2	**98 ±11**	102 ±1.7	**101 ±13**	104 ±4.9	**-**	-
10	**NQ**	104 ±0.8	**106 ±36**	107 ±0.9	-	-	-	-	-	-	-	-	**112 ±15**	111 ±6.9

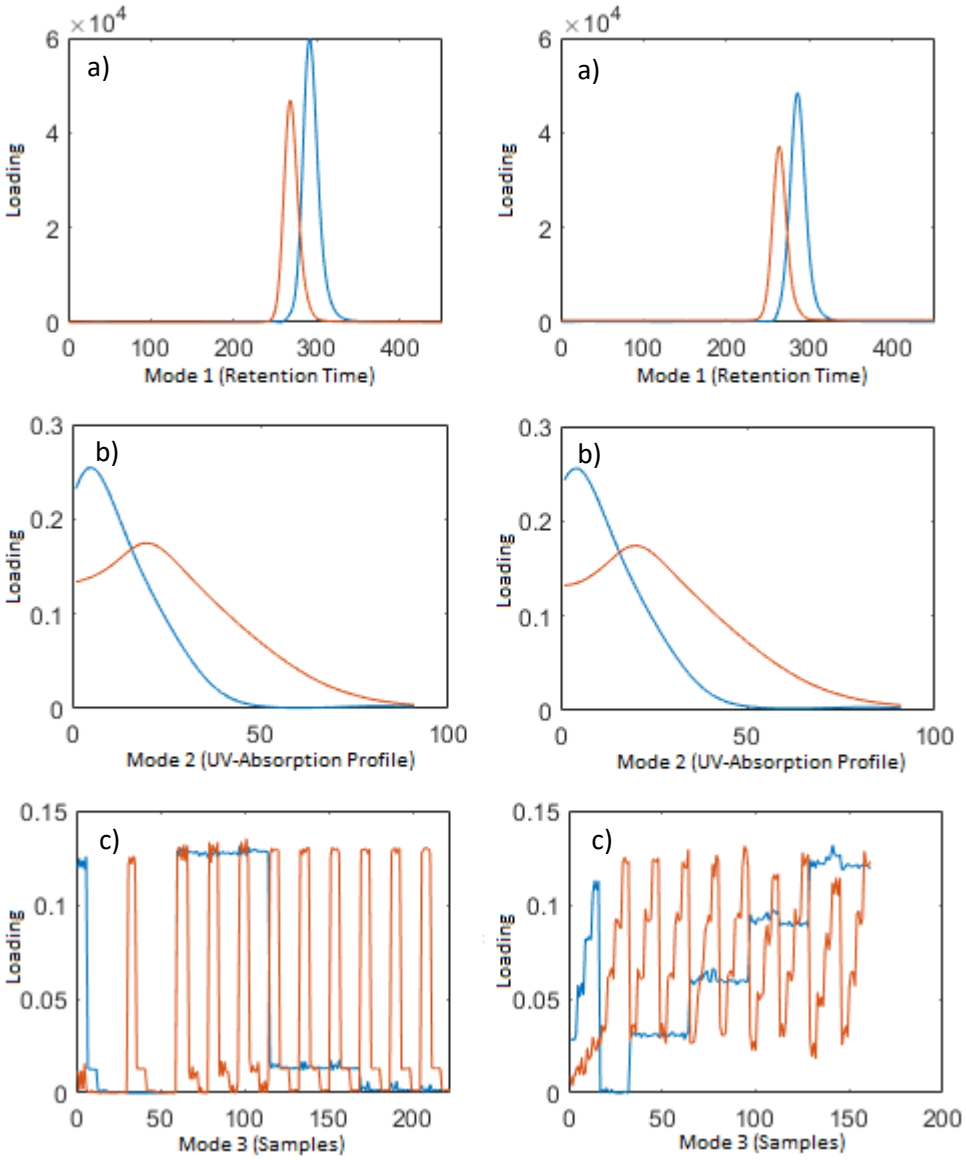

Figure 5. Loadings of Fe(III)-EDTA (orange) and Co(III)-EDTA (blue) in the three modes determined by PARAFAC. Columns: L) results of PARAFAC model of data obtained for mixtures containing 1000, 100 and 10 μM concentrations of M(III)-EDTA, R) results of PARAFAC model of data obtained for mixtures containing 80, 60, 40, 20 μM concentrations of M(III)-EDTA. Rows: a) chromatographic mode (retention time), b) spectral mode (UV-absorption), and c) chromatographic peak area.

5. Analysis of LLWR Trench Leachate

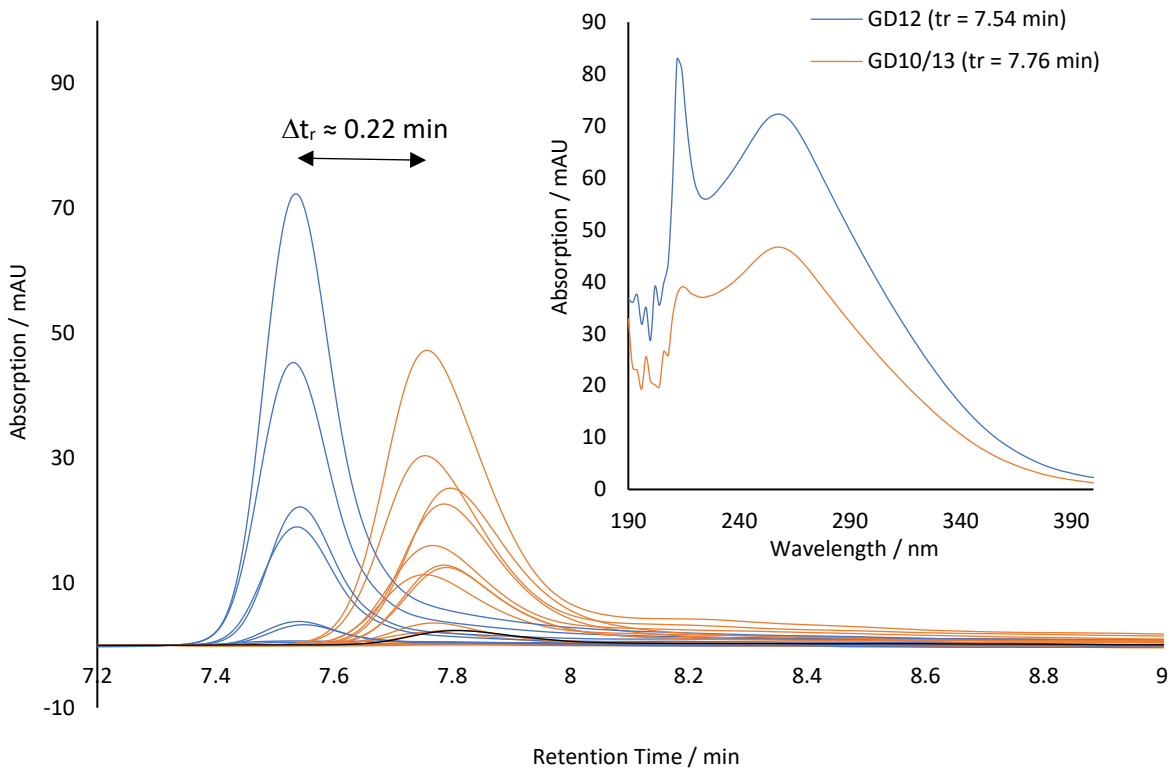

Figure 6. Peak shift observed in EDTA-spiked samples of GD12 trench leachate. Inlay: UV profiles extracted from diode-array detector data at both chromatographic peak maxima.

6. Fe(III)-DTPA Synthesis

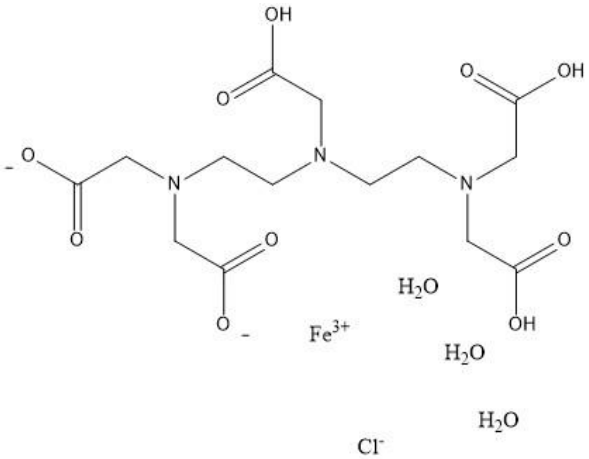

Chemical Formula: $C_{14}H_{27}ClFeN_3O_{13}$
Exact Mass: 536.06
Molecular Weight: 536.67
m/z: 536.06 (100.0%), 538.06 (32.0%), 537.06 (15.1%), 534.06 (6.4%), 539.06 (4.8%), 538.06 (2.7%), 537.06 (2.3%), 536.06 (2.0%), 537.06 (1.1%), 538.06 (1.1%)
Elemental Analysis: C, 31.33; H, 5.07; Cl, 6.61; Fe, 10.41; N, 7.83; O, 38.75

Figure 7. Skeletal structure of the synthesised Fe(III)-DTPA crystal (H_3DTPA-Fe(III)Cl·3H_2O).

Table 9. ICP-MS results for the synthesised Fe(III)-DTPA crystal (H_3DTPA-Fe(III)Cl·3H_2O).

Element	**Expected**	**Found**
C	31.33	31.48
H	5.07	4.88
N	7.83	7.73
Na	0.00	0.51
Fe	10.41	10.42
Cl	6.61	6.74
O	38.75	38.24 (remainder)

Mass spectrometric analysis of synthesised Fe(III)-DTPA shows m/z peak at 445 which corresponds with loss of the three water molecules and the Cl^- ion from the structure described above.